The University Of Sheffield.

Access to Electronic Thesis

Author:	John Plummer
Thesis title:	On the physical aspects that control mechanical deformation in bulk metallic glasses
Qualification:	PhD

If this electronic thesis has been edited by the author it will be indicated as such on the title page and in the text.

On the physical aspects that control mechanical deformation in bulk metallic glasses

John Douglas Plummer

A thesis submitted for the degree of Doctor of Philosophy

March 2012

Department of Materials Science and Engineering

The University of Sheffield

Abstract

In this thesis two analyses are performed to understand the intrinsic ability of bulk metallic glasses (BMGs) to deform plastically, based on their elastic properties. In the first of these, a Blackman diagram is utilised, which plots the ratios of second order elastic constants C_{12}/C_{11} and C_{44}/C_{11}. Two physically meaningful conditions are represented on such a plot: 1) proximity to the Born mechanical instability criterion, and 2) deviation from the zero Cauchy relationship ($C_{12}=C_{44}$), which indicates whether central or non-central forces govern material behaviour. Those alloys with greatest tendency for plastic strain are found closest to the Born condition, which is also found to correspond to BMGs with a large kinetic glass fragility index, m. Additionally, that plastic alloys exhibit the largest positive deviation from the Cauchy condition suggests that non-directional bonding is a feature of deformable BMGs.

In the second anaylsis, three isomechanical groups are found to exist when a representative group of 33 BMGs was studied, by plotting the Young's (E) and shear (G) moduli versus $k_b T_g/\Omega$ (Botlzmann constant, glass transition temperature and atomic volume respectively). An analysis of covariance reveals that the variation in the gradient between each group on such plots are statistically meaningful, indicating fundamental differences in both bonding and structure. These are rationalised as resulting from the extent of non-directional bonding and the ability for enhanced structure diversity in the potential energy landscapes (PELs) of fragile glass formers, in comparison to strong glass formers. This ability for structure variation in the liquid state can be translated to the solid state via the non-ergodicity parameter, α.

This ability for an enhancement in the variety of local minima in the PEL of fragile glass formers is further studied by comparing the ability of high, low and intermediate m BMGs to retain a low modulus and low surface hardness during suction casting in copper dies, observed by performing nanoindentation traverses across the cross-section of as-cast rods. The most fragile alloy ($Pd_{77.5}Si_{16.5}Cu_6$) is found to show the greatest propensity to retain a soft surface, while the effect is most limited in the strong composition ($Ce_{70}Al_{10}Cu_{10}Ni_{10}$). Finally, the extended x-ray absorption fine structure (EXAFS) method is used to understand the source of the mechanical homogeneity observed across the as-cast rods, which is found to potentially not be controlled by nearest neighbours. Instead, cluster rotation may control the variable mechanical properties (including plastic yield), and so length scales beyond the first atomic shell appear to be critical.

Acknowledgements

First and foremost I would like to express my sincere gratitude to Iain Todd for his limitless encouragement and enthusiasm in supervising this project, for believing in my abilities (when I often had my doubts), and for giving me the freedom to pursue my own ideas and interests. Without his support this thesis would be twice as long and not half as good.

Next, as anyone who has gone through the process will know, the success of a PhD candidate is often just as dependent on the people that are around them as it is on the candidate themself. At Sheffield, and in particular in the Innovative Metal Processing Centre - and even more specifically in the Rapid Solidification branch - there is a superb team of researchers and technical staff who have helped me in so many ways throughout both my undergraduate and postgraduate days. In particular I would like to mention Paul Hawksworth for providing good humour and honesty during the many dark days when the arc melter was caput. His technical knowledge, though often over looked, is second to none. Fellow rapid solidifiers - Paul, Andy, Shuang and Jake (all infamous in their own right) - are thanked for good humour and interesting discussions, as are all the members of the H-floor office (in no particular order: Jessie, Hassan, Magda, Fatos, Liz, Moi, Laily, Amir, Jake, Bin, Michelle, Darius, Amit, Sam etc.) throughout the last three years. We were even known to talk about materials!

Ignacio Figueroa (Nacho) is responsible for much of my enthusiasm for research and provided a guiding hand throughout my Masters project and the start of my PhD. He taught me a great deal about the practical and theoretical aspects of metals and always provided interesting and entertaining conversation, about everything from how to arc melt, through to the intricacies of life.

Finally, this thesis is dedicated to all my family and, in particular, my parents. They have, and continue to be, a constant source of support and guidance in my life and there can be no doubt that my achievements would have been small without their love.

John Douglas Plummer
March 2012

Table of Contents

1. Introduction

Metallic glasses rely on the simple principle that any material that displays both a high temperature amorphous melt and a low temperature crystalline phase can be forced to retain a disordered structure at room temperature if cooled fast enough. Because the free energy of the crystalline phase is often lower than that of the amorphous phase, glass formation is considered a kinetic phenomenon since it is the nucleation and growth of crystals that must be inhibited. For oxide glasses the kinetics of crystal nucleation are sluggish and slow cooling can be used to prevent residual stress build-up. For metallic alloys however, crystallisation occurs much more readily and rapid cooling must be applied to a metallic melt of suitable composition, if glass formation is to be realised.

In the time period from their discovery in 1960 through to the late 1990s, metallic glass research largely focused on understanding those alloying characteristics that can best impede crystal formation, typically by generating high viscosity melts where atomic rearrangement by diffusion is difficult. Through such an understanding, it became possible to manufacture metallic glasses with limiting dimensions of 1 mm or greater - termed bulk metallic glasses (BMGs) - with almost every metallic element in the periodic table now having been utilised in their manufacture. It has become apparent then that there are not just a handful of compositions capable of glass formation and, instead, thousands of chemically distinct alloys have been reported.

Since the turn of the millennium, interest in the BMG community has been most focused towards mechanical deformation and, in particular, the extent of plastic deformation that they show. This property is typically highly limited as a result of the unstable nature of shear bands, being the mechanism through which permanent deformation is accommodated in BMGs. Because of this limitation, the introduction of a chemically or structurally distinct second phase is often employed, so as to provide internal barriers to shear band propagation, as well as to initiate new ones at the low modulus interface. The empirical observation of large plasticity has been realised in BMGs however, which is most prolific in noble metal based alloys; a Pd-based composition has been exhibited as the best material yet developed in terms of a combination of fracture toughness and yield strength. It is thus possible to obtain BMGs with a large propensity for mechanical energy absorption without failure.

Although impressive plastic strain to failure has been demonstrated in some alloys - in some instances via a "bucket chemistry" type approach - the community is still trying to answer fundamental questions as to the mechanisms of plasticity, the factors that control it and techniques for its improvement. A number of unanswered questions remain therefore,

making BMGs an attractive research area for researchers of either a materials science or solid-state physics persuasion.

This research project focuses on the use of elastic moduli to indicate intrinsic deformability in monolithic BMGs, and to elucidate the physical origins of the behaviour and trends observed. This project therefore builds on the works of H.S. Chen in the 1970s and, more recently, a publication by J.J. Lewandowski *et al.* (Phil. Mag. Lett **85**, 2 (2007)). The following results and discussion chapters approach the project aim as follows:

- Chapter 4 uses a Blackman diagram (originally developed to find materials of constant Debye temperature) to determine the influence that proximity to the Born mechanical instability criterion and deviation from zero Cauchy pressure can have on plasticity reported from compression testing.

- Chapter 5 considers whether isomechanical groups exist in three classes of BMG, grouped according to their Poisson's ratio, and what this can tell us about variation in structure and bonding with intrinsic deformability in BMGs.

- Chapter 6 studies the tendency for mechanical inhomogeneity in as-cast BMGs as a function of cooling rate by performing nanoindentation traverses along the cross section of rods.

- Chapter 7 makes use of extended x-ray absorption fine structure (EXAFS) to determine the structure source of the variable mechanical response, performed at Diamond Light Source.

A summary of these findings ties together the individual conclusions of each chapter and suggested further work is considered in Chapters 8 and 9 respectively.

2. Literature review

2.1 Introduction

Bulk metallic glasses (BMGs) are multicomponent alloys that are capable of solidifying from the melt without the nucleation of crystals, over a limiting dimension of 1 mm. They rely on the simple principle that any substance that displays a) a high temperature amorphous melt, and b) a low temperature crystalline phase, can retain a disordered structure at room temperature if cooled at a fast enough rate. Glass formation is therefore a kinetic phenomenon since their free energy is often higher than that of the competing crystalline phase. The non-ergodicity parameter, α, is therefore a characteristic property of glasses, since it essentially quantifies how far the system is from equilibrium.

That glass formation can occur in metallic systems is hence surprising since there is a strong tendency to precipitate and grow crystals. Nevertheless, the first metallic glass that was produced by solidification from the melt was the binary $Au_{75}Si_{25}$ alloy in 1960, with a critical cooling rate of the order 10^6 K/s [1]. The first BMGs were later demonstrated in the Pd-Cu-Si, Pd-Ni-P and Pt-Ni-P [2-5] alloy series, where critical cooling rates of less than 1000 K/s were required. Through an understanding of those alloying characteristics that favoured glass formation (or rather impeded crystal precipitation) BMGs based on a huge range of elements have been demonstrated.

Turnbull's reduced glass transition temperature, T_{rg} ($T_{rg}=T_g/T_l$) [6] provides a useful post-mortem type analysis of glass formation. Maximising its value means that the extent of undercooling required from the liquid state, so to reach the glassy state at T_g, is limited. It is not surprising then that glass formation often correlates with compositions close to deep eutectics, such as in the binary Cu-Zr and Ni-Nb alloys [7]. The process of glass formation is summarised via the schematic time-temperature-transformation (TTT) diagram in Figure 2.1.
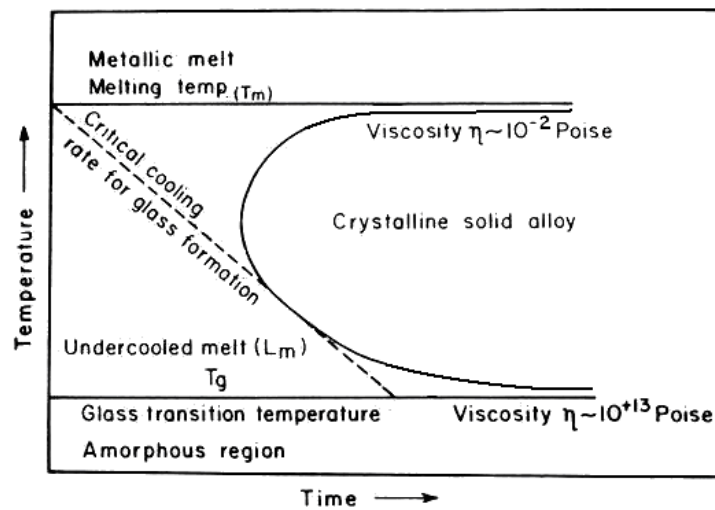
Figure 2.1. Time-temperature-transformation diagram for glass formation. The nose of the crystalline phase field must be avoided for glass formation to be realised, resulting in a critical cooling rate from the melt [8].

The critical cooling rate for glass formation is lowest in alloys where the nose of the crystalline phase field is pushed to the right. Inoue [9] and Donald *et al.* [10] are generally attributed to defining three rules to promote glass formation, which retard crystallisation and, in so doing, push the nose to the right:

1) Multi-component alloys composed of at least three elements,
2) Atomic mismatch between the constituents greater than 12% (and so violating the Hume-Rothery rules for solid solution formation),
3) Negative heats of mixing between the constituents.

Figure 2.2 presents an Angell diagram [11], plotting the dependence of melt viscosity on temperature for a range of amorphous materials. From this plot, the kinetic fragility index, *m*, quantifies the rate of change in viscosity as T_g is approached.
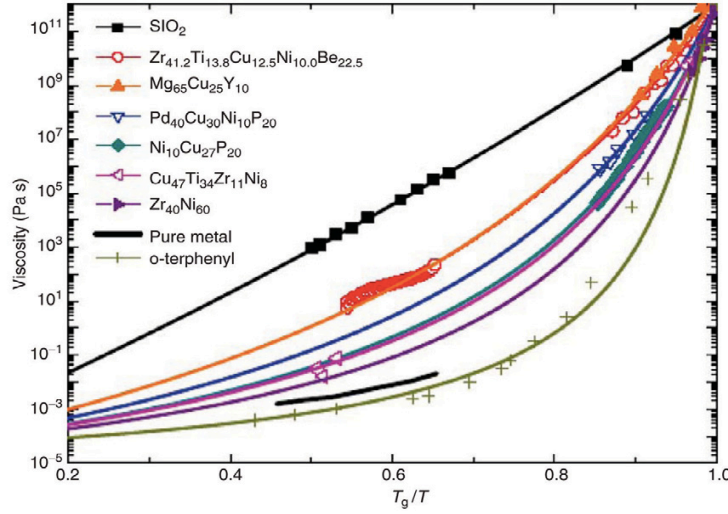
Figure 2.2. Angell diagram for various metallic and non-metallic glasses [12].

BMGs can be seen to have lower viscosity melts than SiO_2 (with organic glasses being the most fragile), indicating more rapid atomic diffusion and a stronger tendency for crystallisation. It is a general rule of thumb that fragile glass formers (with a large change in viscosity close to T_g) are difficult to vitrify because of enhanced atomic transport and vice versa [13,14]. Notable exceptions to this are the Pd-based BMGs where low critical cooling rates (e.g. 0.15 K/s for $Pd_{40}Cu_{25}Ni_{15}P_{20}$ [15]) combine with fragile behavior. m is often considered to indicate the liquid-like nature of glasses and is only applicable at temperatures above T_g, since at temperatures below it viscosity is fixed (10^{12} Pa s) and so m is a constant for all solids. Recent work by Scopigno *et al*. has linked m to the non-ergodicity parameter, α, where it was found that fragile glasses are the most non-ergodic, and could be linked by the empirical relationship $m=(135\pm10)\alpha$ [16]. Disorder, or a large departure from equilibrium, in the liquid state does transfer over to the solid state.

Senkov [10] considered the effects of both fragility index and T_{rg} in Equation 2.1 by quantifying a glass forming parameter, F_1, where m_{min} is the kinetic fragility of a glass that obeys an Arrhenius viscosity-temperature dependence ($m\approx16$), and so large m/m_{min} corresponds to a fragile glass former:

$$F_1 = 2\left[\frac{m}{m_{min}}\left(\frac{1}{T_{rg}}-1\right)+2\right]^{-1} \qquad (2.1)$$

This parameter was then related to the critical cooling rate for glass formation, R_c, by the fitting of F_1 to experimentally observed R_c, where $R_{co} = 2.7 \times 10^{11}$ K/s and $A \approx 48.7$:

$$R_c = R_{co} \exp(-AF_1) \tag{2.2}$$

These inter-relationships between m, T_{rg}, R_c and F_1 are shown in Figure 2.3, where the glass forming ability, as quantified by F_1, decreases with an increase in m.
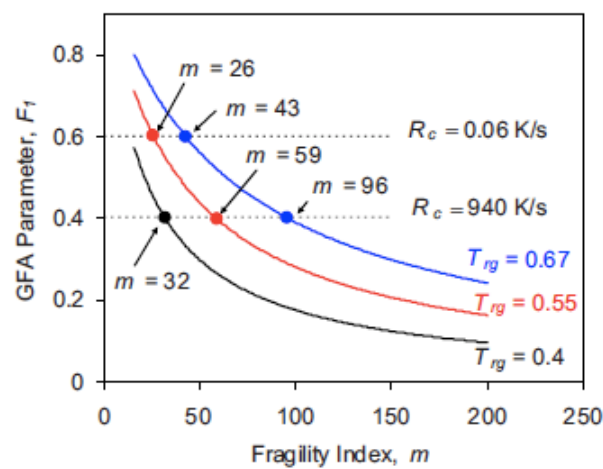
Figure 2.3. Effect of kinetic fragility index, m, critical cooling rate, R_c, and reduced glass transition temperature, T_{rg}, on glass formation parameter, F_1, as determined from Equation 2.1 and 2.2 [17].

This approach was able to predict well the critical cooling rates for both elemental metals (2.7×10^{11} K/s) and glasses that obey an almost Arrhenius viscosity-temperature dependence e.g. SiO_2 (2.3×10^6 K/s). Glass formation then is dependent on a number of physical parameters which can only be accurately quantified via a post-mortem type examination i.e. the glass has to be made first. Actually predicting alloys capable of forming glasses is therefore a difficult task, though attempts do exist, and which do so with a certain degree of success. One such approach is based on atomic and cluster packing and will be discussed later.

      This literature review will focus on aspects of BMGs that are most pertinent to the topic of this thesis. This includes: 1) atomic packing models of BMGs, 2) response under loading and techniques for improving plastic strain, and 3) the importance of elastic moduli and what they may help to reveal. Finally, a summary will be presented of unresolved issues and those that deserve further research attention.

2.2. Atomic structure

Understanding the structure of solids is a key driver in determining the effect that processing can have on mechanical properties. For crystalline metals the presence of an ordered periodic structure makes both studying - whether by experiment or simulation - and describing structure relatively simple, at least with respect to defining atomic positions. For amorphous materials structural studies are more involved and complex however, requiring the use of high energy diffraction for experimental observations and mathematical modelling (such as density functional theory, molecular dynamics and reverse monte carlo) to resolve atomic positioning. Determining the structure of BMGs is therefore non-trivial. A conceptual model that has gained acceptance is one in which atomic structure is created by the arrangement of atoms into short range ordered clusters, and their subsequent packing so as to generate global structure [18]. There has even been the suggestion of some form of long range order in a $Ce_{75}Al_{25}$ amorphous alloy [19]. In this study, pressure induced devitrification of a $50\mu m \times 40\mu m \times 15\mu m$ melt spun ribbon resulted in the [111] crystallographic direction in the crystalline phase aligning along the length of the ribbon, forming a single crystal. That a specific crystallographic direction aligned identically to a reference point (creating a single crystal) suggests some form of topological long range ordering in the amorphous state, which appears to be similar to that in the crystal. A range of length scales appear to exist then, including 1) nearest neighbour separation distances within a cluster, 2) how clusters subsequently fill space, potentially allowing for medium range order (MRO), and 3) the potential for some form of ordering over tens of microns.

The dense random packing (DRP) of hard spheres model of Bernal [20,21] aimed to understand the atomic structure of amorphous one component (unary) metallic systems based on the idea that separation must be equal to at least one atomic diameter. This was purely a geometric model with no consideration to interatomic potentials, enabling it to be simply studied via ball-bearing experiments. Five types of local coordination, or Bernal holes, were suggested as being present, which can be seen in Figure 2.4.
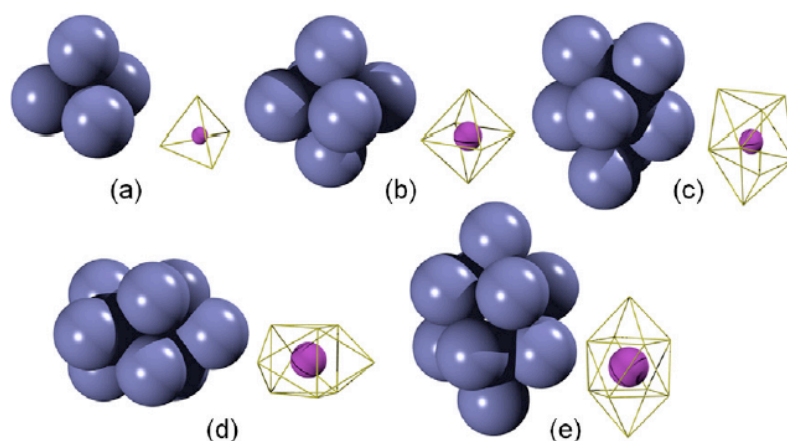
Figure 2.4. The Five Bernal hole environments in the DRP model: a) tetrahedron, b) octahedron, c) tetragonal dodecahedron, d) trigonal prism capped by three half octahedra, and e) Archimedean antiprism capped by two half octahedra. The size of the pink sphere indicates the relative size of the hole [22].

Tetrahedra have been found to be the most favoured of these holes and to result in the densest packing [22], though other holes must be present otherwise large frustration would exist, leading to structural instability. The DRP model calculates a packing density of 0.64 and an 11% volume change on crystallisation. However, a value of ~1% is typically observed in metallic glasses [23]. The DRP model then, while found to provide some accuracy for monatomic systems or alloys composed of elements of essentially equal size, cannot predict the dense packing that is actually present in BMGs. Moreover, in marginal glass formers, the density change on crystallisation is of the order of 2%. In BMGs this value is approximately 0.3-0.5% [24]. Efficient packing of BMGs, leading to dense structures, therefore appears to be a characteristic feature of good glass formers, an aspect of BMGs which the DRP model does not account for.

More efficient packing than that predicted by the DRP model can be expected as the multicomponent nature of BMGs means that atoms of different size are present, which is an inherent characteristic of Inoue's three rules [9]; smaller atoms can occupy interstices in the atomic structure, between larger atoms. Additionally, elements of different electronic structure will have a tendency to chemically interact, promoting atomic clustering and short range order (SRO). SRO, while predicted for many years, was only recently experimentally observed in the transmission electron microscope [25], where a highly focused electron beam was capable of resolving diffraction patterns from single SRO clusters. Frank [26] first suggested that icosahedral cluster order may be present as such coordination lacks translational periodicity and are difficult to grow, making them incompatible with the competing crystalline phase, retarding crystallisation. A range of local cluster types are

known to exist in any one BMG, as characterised by a range of radius ratios and Voronoi indices being known to exist [27]. Icosahedra have been determined as the favoured unit, confirming Frank's early thoughts however [28].

SRO results from chemical interactions between dissimilar elements, and is believed to be strongly promoted in BMGs containing metalloids, such as B, P, Si and C. The Efficient Cluster Packing (ECP) model of Miracle [18] allowed for some medium range order (MRO) through the packing of solute centered clusters in highly efficient face centered cubic (FCC) and hexagonal close packed (HCP) configurations. In this model, the following four topologically distinct atomic environments were believed to exist and which of these a certain sized atom occupied was dependent upon the ratio of solute to solvent atoms:

1) Ω, the solvent atoms,
2) α, the primary cluster forming solute species,
3) β, a secondary solute species, which occupies cluster-octahedral interstitial sites,
4) γ, a tertiary solute species, occupying cluster-tetrahedral sites.

Even multicomponent alloys then, with more than four constituents, were still described by the same model, meaning that only a few radius ratios exist in any one alloy, even when it contains a large number of components. This packing scheme can be seen in Figure 2.5.
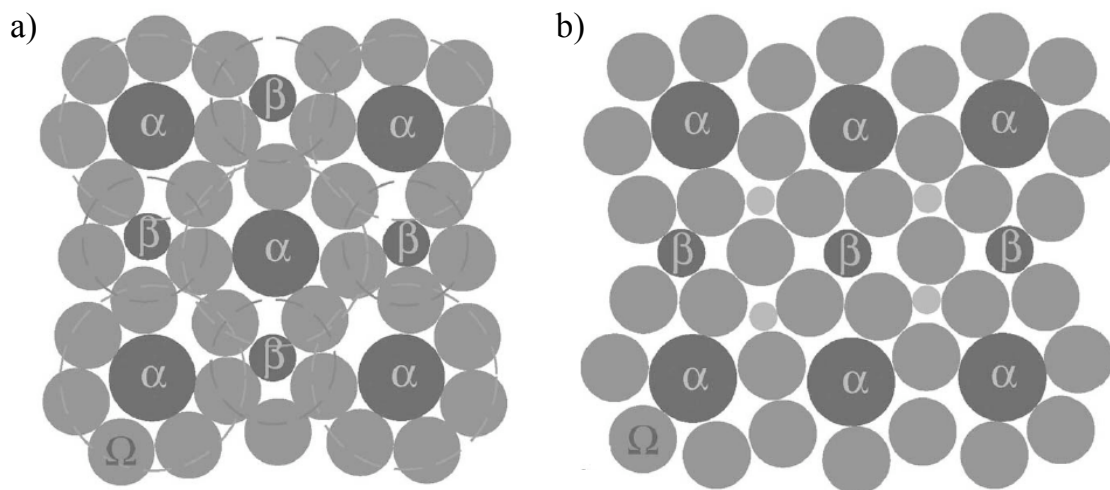
Figure 2.5. Representation of the efficient cluster packing model of glasses on the a) {100} plane and b) {110} plane of an FCC arrangement. Four distinct sites can be occupied: α, β, Ω and γ (the smallest sites in b) [18].

MRO has been observed in several binary metallic glasses through a combination of x-ray diffraction (XRD) and extended x-ray absorption fine structure (EXAFS) and then using reverse monte carlo to extrapolate the 3-D structure from pair distribution functions (PDFs) [27]. The high efficiency of cluster packing was confirmed in this experiment, in line with that predicted from FCC or HCP packing, though these exact configurations were not directly observed and dense icosahedral packing of clusters was found instead. The ECP model cannot account for the actual diversity of the metallic glass structure, while it considers atoms of equivalent size to occupy identical topological sites, despite chemical differences between them, which could potentially alter the SRO coordination. The casting cooling rate can also be expected to determine the number of defect atomic sites [29]. However, while the model is still being refined, it does provide an ideal reference state for the actual structure and is able to aid in the prediction of BMG compositions based on the relative sizes and proportions of elements used.

From attempts to extrapolate the 3-D structure from a combination of XRD and reverse monte carlo, a complex picture of the atomic structure of BMGs emerges [27]. Figure 2.6 presents results from such a study [30].

Figure 2.6. Reverse monte carlo generated 3-D atomistic structure of a model Zr_2Ni metallic glass. a) regions high and low in free volume are indicated by arrows and circles respectively, b) an MRO cluster, and c) a dense packed unit with an MRO cluster at the centre (circled region), where the red stars are free volume sites [30].

It can be seen that simple translation of either SRO clusters or packing of clusters, such as in the ECP model [18], cannot accurately represent atomic struc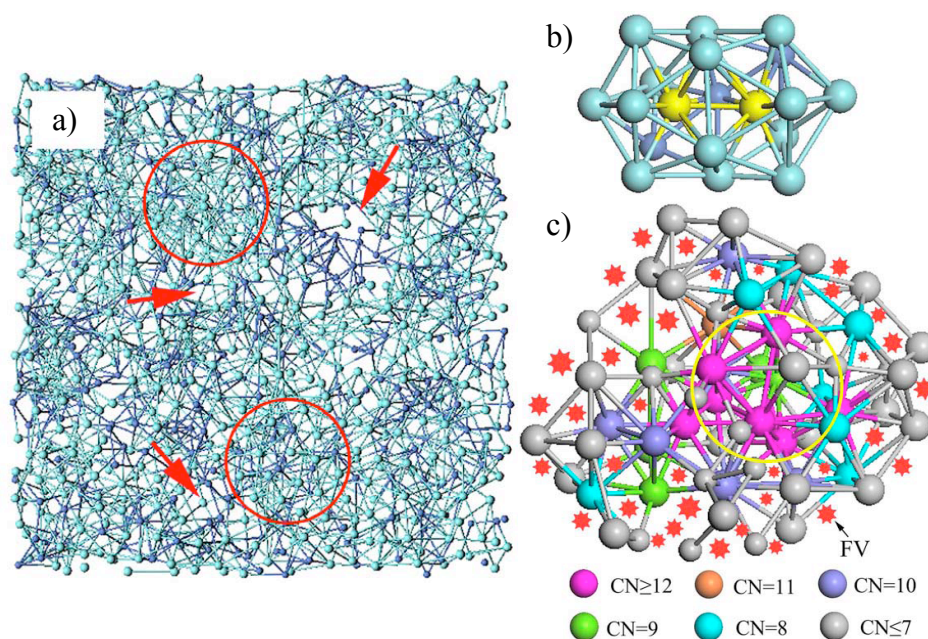ture as regions high and low in free volume are present. However, regions that do conform to this model were found, though they only extended over a limited distance; a dense cluster of atoms can be seen in Figure 2.6c with a diameter of approximately 1.5 nm which extends out from an MRO cluster in the centre (Figure 2.6b). A separate study suggested that free volume is accommodated between SRO clusters [31]. The efficient cluster packing model may indeed then be most useful for providing an idealised atomic structure.

This work lead to the tight-bond cluster model [31], where the structure is composed of three distinct parts: 1) tightly bound clusters with small atomic separation distances, 2) free volume regions between clusters, resulting in more slack bonding, and 3) interconnecting zones between the clusters. Free volume was considered as being accommodated between clusters, rather than within them i.e. not in the SRO. The core-shell model [32] went on to suggest that some clusters are more strongly interconnected, encasing a soft core region, where clusters are less well bonded. These structure features were believed to account for the hysteresis shown in load-displacement curves during the indentation of nanopillars. Schematics of the tight-bond cluster model and core-shell model can be seen in Figure 2.7.
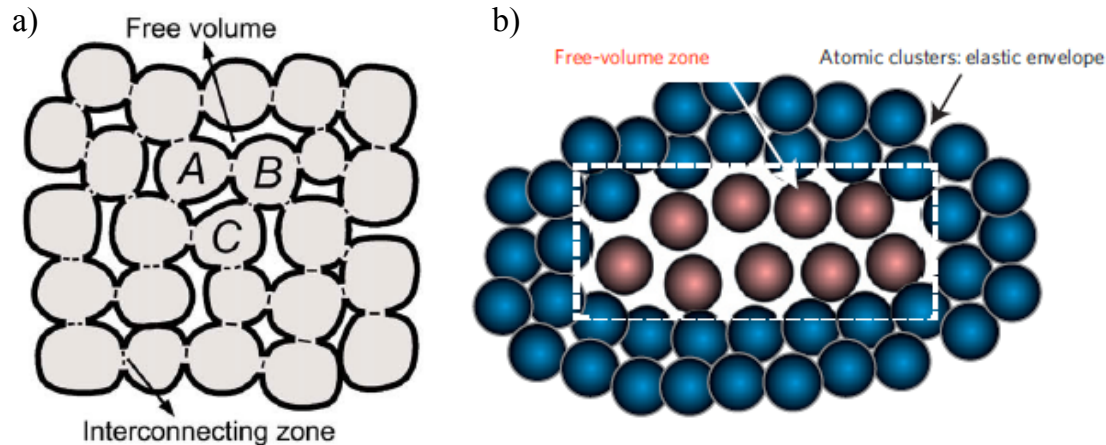
Figure 2.7. Schematic representation of cluster arrangement in a) the tight bound model, where clusters A, B and C are interconnected [31], and b), and the core-shell model [32].

A hierarchy of length scales may exist then in defining cluster formation (SRO) and their subsequent packing (MRO). Due to reduced connectivity between clusters, it was believed that shear band formation is controlled by the rotation of clusters rather than by the action of individual atoms [31, 32]. This approach, embodied in the tight bond and core-shell models, would appear to be supported by in-situ high energy x-ray studies where [33], in the elastic

portion of the loading regime, strain was more readily accommodated between clusters than within them. Moreover, an estimate of elastic moduli (which provide the activation barrier for yielding, as will be discussed later) by this approach over estimated their value in comparison to those experimentally measured, when considering nearest neighbours only to contribute to the elastic properties. To obtain more accurate values it was necessary to consider inter-cluster interactions, suggesting that bonding between clusters determines mechanical behaviour, rather than being dependent on short-range bond stiffness. Assuming icosahedral SRO, each cluster is composed of approximately 13 atoms and the number of atoms involved in a shear transformation zone (STZ) is believed to be approximately 100 [34]. The cooperative shearing of approximately 7 – 8 clusters would be predicted then as nucleating an STZ. The presence of MRO may extend up to 1 – 2 nm in BMGs [35]. This length scale broadly corresponds with the size of believed flow units, which control plastic deformation. The atomic scale structure may therefore have a large influence on deformation behaviour. Cluster and glue models have also been proposed [36] in which SRO clusters sit within a network of single atomic cores that act as a glue, holding the clusters together. The actual atomic structure of BMGs is therefore a diverse one and it can be expected that how clusters are formed and packed will show variation with alloy composition and cooling rate. Table 2.1 summarises the characteristic features some of the major structure models of metallic glasses that have been reported.

Table 2.1. A summary of some of the major structural models proposed for metallic glasses in the literature which attempt to explain atomic structure, glass formation and mechanical response.

FEATURES	LIMITATIONS	COMMENTS
Dense random packing of hard spheres – J.D. Bernal, 1960 [20,21]		
Identically sized hard spheres randomly arranged for maximum density. Shown to be applicable to monatomic metallic systems.	Results in packing fraction of 0.64, which is 14% different to that in close packed metals, when a 5% difference is typically observed for BMGs. Doesn't account for chemical interaction or soft interatomic potentials.	Provides a simple theoretical model for analysis of the amorphous state, without the need of complex interatomic potentials.
Icosahedral short-range ordering - Frank, 1952 [26]		
Short range ordered icosahedra form in the melt, and are retained below T_g, since icosahedra are: 1) close packed, 2) lack translational symmetry, and 3) are not structurally comparable with crystalline lattices, inhibiting crystal nucleation.	Only describes SRO, not the global atomic structure. Does therefore not consider MRO.	Icosahedra have been shown to be the favoured SRO co-ordination, proving Frank's theoretical ideas.
Stereochemical model – Gaskell, 1978 [37,38]		
Considers short range interactions in metal-metalloid glasses and crystals to be identical, resulting in approximately the same local environments. Difference in structure exists within the MRO rather than the SRO.	Has been proven true for some metal-metalloid glasses but is incorrect for metal-metal glasses.	While the basis of the model is limited to certain compositions only, it does consider SRO and MRO as being distinct. The ideas presented in it are not dissimilar from those of cluster packing suggested later.

FEATURES	LIMITATIONS	COMMENT
Efficient Cluster Packing – D. Miracle, 2004 [18]		
Topological model where SRO clusters are packed together in an HCP or FCC arrangement, as these configurations result in greatest packing density. Accounts for observation of MRO in some alloys.	Atomic size determines structure arrangement; no consideration is given to chemical interactions. Also considers atoms as hard spheres when soft interatomic potentials are known to exist.	Provides not just an ideal reference structure, but can also be used to predict glass forming compositions. The idea of packing clusters in efficient configurations has been proven experimentally.
Tight-bond cluster model – C. Fan *et al.*, 2009 [31,39]		
Mechanical deformation of BMGs is controlled by the rotation of SRO clusters, which are loosely bonded in comparison to strong bonds within a cluster. Free volume is thus considered as accommodated between clusters rather than within them.	A conceptual model that does not give specifics of cluster rearrangement under shear. Does also not simply allow for the sharing of atoms between clusters.	Rather than considering STZ activation being controlled by the co-operative shearing of individual atoms (see Figure 2.9), this model suggests that it is the rearrangement of clusters that is critical.
Core-shell model – J.C. Ye *et al.*, 2010 [32]		
"Cores" high in free volume (lower cluster density) are surrounded by an elastic "shell" (higher cluster density) which constrains the free volume rich core. Deformation is a summation of response from the soft core and hard shell.	Model was developed based on the observation of strain hysteresis during the compression of nanopillars – behaviour has not been observed during macroscopic tests and so may be a size effect.	Reverse monte carlo of pair distribution functions (e.g. Figure 2.6) suggest that regions high and low in free volume exist, and it is reasonable to expect that a region high in bond density would constrain a region with low bond density.

2.3. Deformation behaviour

Though BMGs are an interesting curiosity to the scientific community, providing an often more convenient way to investigate the glassy state, their favourable mechanical properties may offer up the potential of improving the performance of certain parts and components in critical applications. The topic currently most studied within the BMG field is therefore that of mechanical performance.

As with any material in the solid state, BMGs initially deform elastically to an applied load. There may be some local irreversible yielding within the bulk, but these events are spatially and temporally isolated and not widespread enough to trigger macroscopic yielding [40]. The elastic moduli of BMGs are, in all instances, lower than those of the competing crystalline phase [41]. As a result of the sensitivity of Young's modulus (E) and the shear modulus (G) to structure, they are approximately 30 % less than those of crystalline metals; in comparison the bulk modulus (B) is reduced by only 6 %. That moduli are lower in BMGs than their crystalline counterparts has been ascribed to a lower bond density associated with less efficient space filling [42]. BMGs may therefore be considered as suitable candidates in biomedical implants such as prosthetics, where their low E has the potential for mitigating bone degradation by stress shielding [43]. This, coupled with large elastic strains in the region of 2 %, make BMGs very "springy"; this property is exploited in the example of sporting goods, such as the well known golf club head example. Additionally, the strength of BMGs approaches Frenkel's predicted maximum theoretical value of a $0.1G$ [44], which is not typically obtainable in crystalline metals as defects inevitably exist in a crystalline lattice, causing yielding by dislocation activation, though strengths approaching the theoretical limit have been obtained in defect free Mo micropillars [45]. Some Co-based BMGs have exhibited compressive strengths of over 5 GPa [46] and, when comparing crystalline alloys to equivalent BMGs based on them, the glassy option will consistently show a tendency for higher strength.

However, the ability of BMGs to deform plastically continues to be the major limitation to broader application, as plasticity is most often restricted to less than 1%. On yielding, plastic deformation is accommodated inhomogeneously, within bands of reduced viscosity, which are unstable and can propagate through a specimen, causing failure. Analogies may be drawn here to the carriers of permanent deformation in crystalline metals, which are typically dislocations. Dislocations however can interact with each other and at interfaces within the microstructure, such as grain boundaries and at precipitates and inclusions. Thus, work hardening behaviour is observed, as a greater force is required to continue dislocation motion through or around an obstacle, or to activate new ones. As will be discussed shortly, permanent deformation of BMGs necessitates dilatation of the atomic

surroundings, causing the passage of a shear band, the material within which is at a vastly reduced viscosity, estimated to be close to that of the molten state [47]. Resultantly, BMGs are known to work soften during plastic deformation, leading to instability of plastic flow. Despite this, the $Pd_{79}Ag_{3.5}P_6Si_{9.5}Ge_2$ BMG has been reported as having the highest combination of strength and toughness of any material yet developed [48]. BMGs that are highly resistant to failure are possible then, and it can be stated that the successful development of this alloy (in part) originates from a greater understanding of plasticity and how it may be promoted.

2.3.1. Yielding and plastic flow

Two original theories pertaining to the mechanism of yielding of BMGs that are most widely cited are those of Spaepen [49] and Argon [50]. In the first of these, Speapen applied ideas related to the free volume theory of Cohen and Turnbull [51], originally developed to understand viscosity changes close to T_g in molecular glasses bonded by van der Waals interactions. They considered the movement, or diffusion, of a molecule from one atomic cage into another when a large enough gap exists for it to pass through. To do so, free volume associated with a single molecule was defined as "the volume within its cage less the volume of the molecule". Spaepen [49] adapted their ideas to the diffusion and mechanical yielding of BMGs, which was believed to occur when sufficient space existed for an atom to jump into a neighbouring cage. Because of the amorphous structure, such a jump requires the combination of shear and a dilatation event (a volume expansion) in the surroundings. This process is pictured schematically in Figure 2.8, taken from Spaepen's original paper.
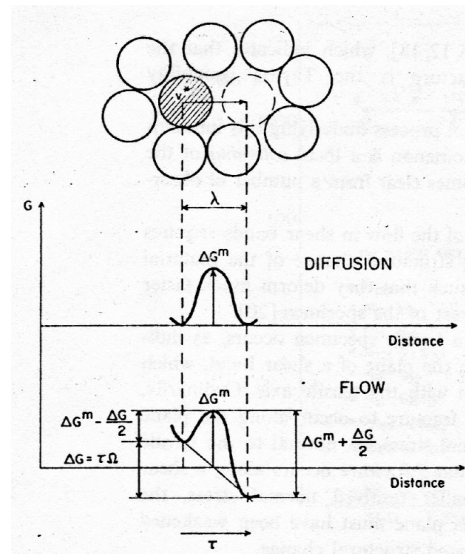
Figure 2.8. The jump of a single atom from one cage into another, across a distance, λ. ΔG^m is the activation energy of motion that must be overcome. Under a shear stress, τ, the shape of the energy landscape changes, reducing the barrier to $\Delta G^m - \Delta G/2$, where ΔG is the free energy of the atom and Ω is the atomic volume [49].

Certain limitations exist in the use of such free volume ideas however. Cohen and Turnbull developed the ideas for glasses with hard inter-atomic potentials, which are less compressible than for metallic systems, where the softer potential can allow an atom to move with relative ease through a narrower space. More will be commented on the implications of this shortly. As can be seen in Figure 2.8, Spaepen's model only considers the movement of a single atom, though yielding in BMGs is known to involve multiple atoms, and it had already been suggested [52] when this model was first proposed that the non-linear resistance of a solid to deformation (i.e. the presence of a defined yield point) was likely to originate from structural units larger than an atom.

Argon [50] subsequently developed the concept of a cooperative shear event, based on bubble raft experiments. Yielding occured by the instantaneous shearing of a group of atoms, believed to be five atoms in diameter, in a 2-dimensional plate configuration; this is depicted in Figure 2.9.
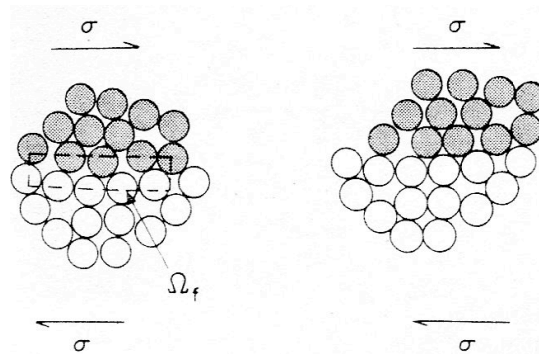
Figure 2.9. Schematic representation of an instantaneous shear event within a volume, Ω_f, under an applied stress, σ [50].

These sites are now popularly referred to as shear transformation zones (STZs). Because this process requires the cooperative displacement of a group of atoms, a pathway of STZs is created, propagating as a shear band.

Common to both Spaepen's and Argon's theories is the need for dilatation, accounting for the observed strain softening after yielding. Additionally, in both instances, yielding (either by atomic jumps or through the activation of an STZ) was expected to be favoured at sites high in free volume, where a lower local bond density reduces the activation barrier. Both theories are still well cited to this day and understanding STZs is still considered a key task for researchers in the field. With this in mind, Homer *et al.* [53,54] have used novel mesoscale modeling, coupled with finite element analysis, to consider STZ development spatially and temporally. At high temperatures STZs were found to nucleate non-preferentially throughout the system, accounting for the experimentally known homogeneous deformation of BMGs at a high enough homologous temperature of T_g, where Newtonian flow can occur (typically at $0.6T_g$). Under room temperature conditions, STZs were found to nucleate preferentially close to the plane of maximum shear stress. Interestingly, STZs, once activated, could also reverse and it was found that the creation of one STZ could trigger the nucleation and propagation of others in their vicinity. In this way shear bands formed throughout a whole body via continuous STZ generation. These results are summarised in Figure 2.10.
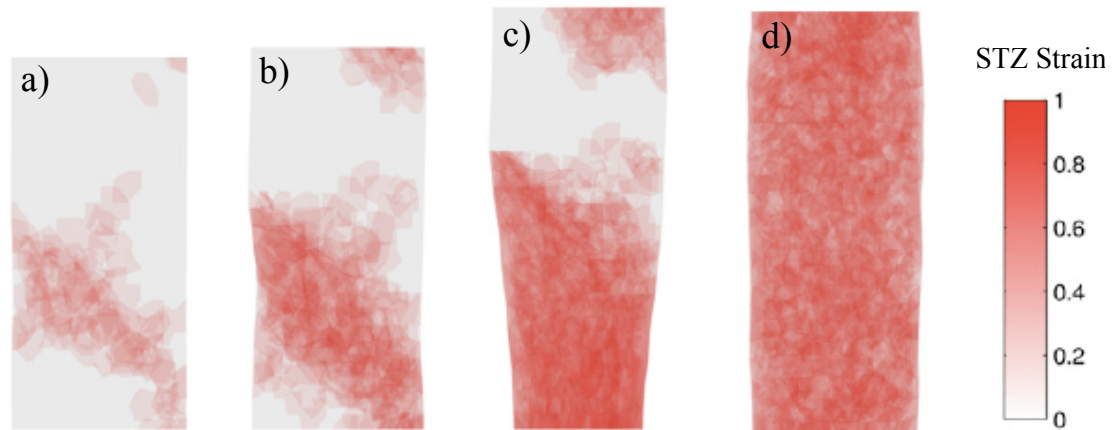
Figure 2.10. Spatial distribution of STZs in a model glass under tensile loading at 300K and an applied load of 3 GPa at 4% (a), 7% (b) and 18% (c) strain, and at 800 K with a load of 300 MPa at 15% strain [54].

The development of such a mescoscale model overcomes limitations associated with atomistic models, such as molecular dynamics (MD), where time scale limitations result from computer processing speed requiring faster cooling rates than are experimentally possible, even when considering melt spinning techniques (10^6 K/s). The resulting structures are therefore more similar to those in the liquid melt than to BMGs cast at experimental cooling rates [55], limiting any analysis that links such structures back to experimental observations. Mesoscale modeling may therefore be a very useful tool in future research.

The need for free volume is key in the considerations of both Spaepen [49] and Argon [50], in respect to yield. Because of the wide acceptance of this, only a very brief survey of the open literature is required for it to be surmised that enhancing free volume content is considered crucial to the promotion of plastic strain in compression, since more fertile sites for STZs are present and are more readily activated. Egami [55] has cautioned strongly on the use of such ideas however; to summarise the underlying issue in applying Cohen and Turnbull's [51] free volume ideas unmodified to BMGs, the softness of the interatomic potential of metallic systems means that they are in fact anything but hard spheres. In the instance of hard spheres (and an infinitely hard potential), simple geometry will determine whether an atom can move from one cage into another. The ratio of the critical value of free volume required for an atomic jump, v^*, to the atomic volume, v_a, (v^*/v_a) is approximately 0.8 for van der Waals molecular glasses; it has a value much closer to 0.1 in metallic glasses however [51]. Thus, a metal atom can move between cages even when the apparent space available is insufficient. An example of the limitation that this imposes is apparent from the pressure dependence of diffusivity; it would be expected that a large applied pressure would

contract the empty space, reducing diffusivity. In fact, diffusivity is only slightly reduced [56], as can be seen in Figure 2.11.
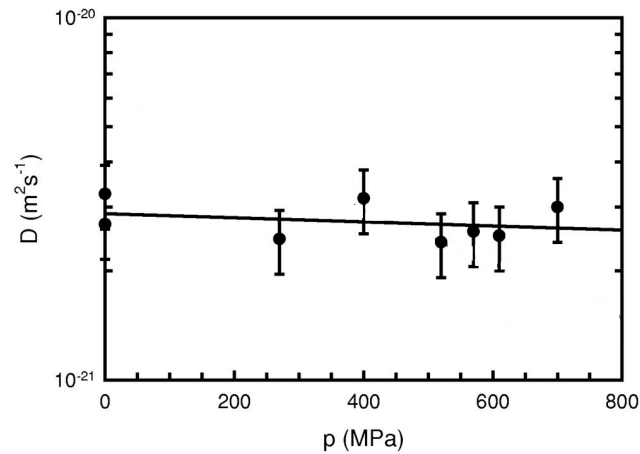
Figure 2.11. The effect of hydrostatic pressure, *p*, on the diffusion coefficient, *D*, of a ^{57}Co tracer in the $Co_{81}Zr_{19}$ metallic glass [56].

Egami has proposed a different model to that of free volume [55, 57, 58], based on there being a distribution in bond lengths, some of which are longer (free volume) and others which are shorter (anti-free volume) than the average, with a Gaussian distribution around the mean. This can be seen in Figure 2.12.
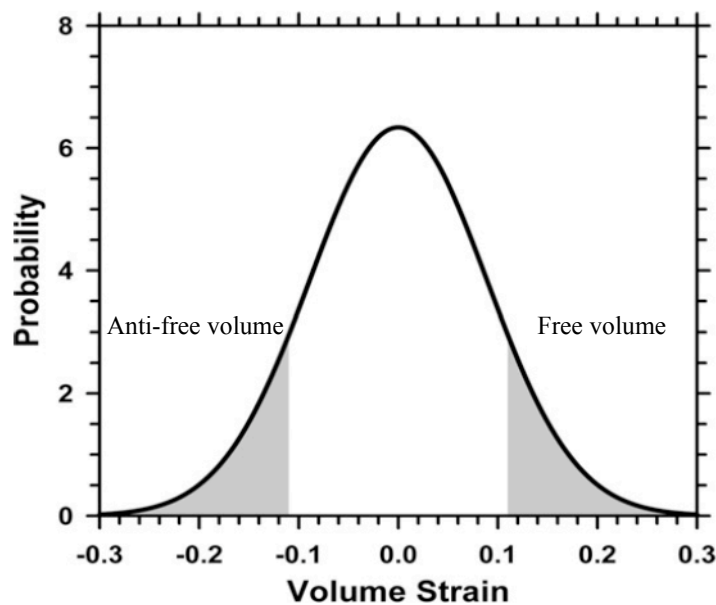
Figure 2.12. Distribution of local strain in a metallic glass, accounting for free volume (long bonds) and anti-free volume (short bonds) [55].

Then, as some atoms may be considered under tension (long bonds) and some in compression (short bonds) a variety of atomic level stresses and strains exist, resulting in atoms being positioned in various inherent states on the multidimensional potential energy landscape (PEL). X-ray diffraction experiments, from which partial distribution functions (PDFs) have been extracted, suggest that relaxation of Vitreloy 105 (a Zr-based BMG) results in a reduction in both short and long atomic bonds [59], which can be considered negative and positive density fluctuations respectively – this can be seen in Figure 2.13.
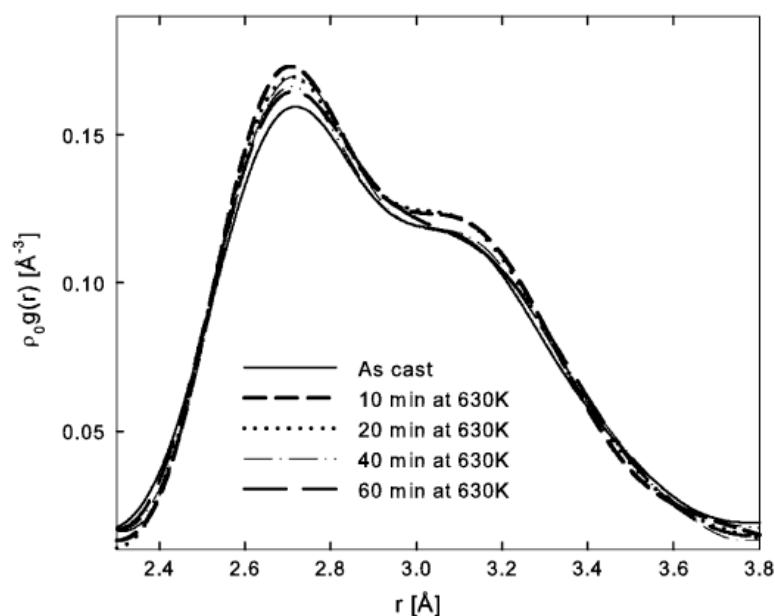
Figure 2.13. PDF for Vitreloy 105 as a function of annealing time (shown on graph). Annealing can be seen to not affect peak position but does sharpen the peaks, suggesting a reduction in long and short bonds [59].

If simple free volume theory were applied then it would be expected that bond length would globally decrease (i.e. there would only be a reduction in long bonds) under thermal treatment when, in fact, an increase in the average density of long bonds was observed. Though Egami appears to make a valid point with respect to the inappropriate citation of free volume theory, factors that would be expected to enhance free volume content do seem to favour increased plastic strains. Examples of this include more rapid cooling by casting in a more thermally conductive He environment (rather than Ar), increasing plasticity from approximately 0.1% to 2% in the $Cu_{45}Zr_{48}Al_7$ BMG [60] – an increase in free volume was determined from positron annihilation studies (during which positrons become trapped in

open cavities within the atomic structure and subsequently decay), where positron lifetime increased from 212 ps to 224 ps in the Ar and He casting environments respectively. The addition of 2 at% Ti was also sufficient to increase plasticity from 1.5% to 35% in the $Cu_{45}Zr_{46}Al_7Ti_2$ alloy [61] since Ti occupies Zr sites and, being a smaller element, creates lower density atomic sites where STZs could nucleate. Positron lifetime spectroscopy of a Zr-based BMG found that the lifetime of a positron is greater in a sample that has not undergone thermal relaxation, and this was related to the tendency for plastic strain [62]. Equally though, free volume can be expected to influence atomic level strain and the local topological environment. In summary then, the use of free volume theory, as mathematically defined by Cohen and Turnbull [51] and involving atomic hopping between cages, appears to not be valid for BMGs, when considering the evidence presented here. However, the fundamental concept of pushing the structure further from equilibrium by introducing non-uniform atomic strains does appear to promote STZ nucleation and plastic strain - this area is still under intense debate.

2.3.2. Promoting plasticity

Work hardening is a desirable property of any load-bearing material. Without it, a continuous increase in load above the yield point will result in premature failure, despite any ability for extensive plastic strain. Instead, work hardening allows for greater energy absorption and increasing retardation to deformation. In ductile crystalline metals, work hardening is permitted by the interaction of dislocations with themselves and at internal interfaces, requiring a progressively larger force to continue deformation. Thus, when necking occurs during tensile testing, hardening of the material in the thinned neck promotes deformation in the surrounding softer regions, a process by which large elongations can be obtained. The inherent lack of stable plastic deformation in BMGs results from work softening being an intrinsic characteristic of shear bands, despite large plasticity being possible. Pan *et al*. [63] successfully activated a single shear band in a BMG, by controlling sample size and machine stiffness, enabling the influence of a single shear band on the load bearing capabilities of a BMG to be studied. The engineering stress–strain curves in Figure 2.14 illustrates the issue of work softening, where a continuous stress drop-off occurred after yield.
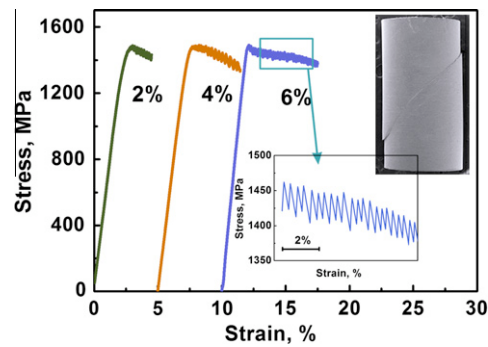
Figure 2.14. Engineering stress vs. strain in a $Zr_{69.5}Cu_{12}Ni_{11}Al_{7.5}$ BMG tested in compression to various plastic strains, exhibiting work softening. Inset shows serrations due to shear banding. Note that deformation was accommodated by a single shear band [63].

It is known in models for the deformation of granular materials (e.g. sand and soil) that shearing of grains causes dilatation of the surroundings [64]. This reduces local bond density, decreasing the activation energy for yielding. Such conceptual models for amorphous granular materials appear to hold for BMGs, as the typical fracture angle observed in compression is approximately 42 degrees, in agreement with the Mohr-Coulomb yield criterion [65]. Indentation studies of samples that have undergone plastic strain [66], and indenting shear bands themselves [63], both suggest reduced hardness in the deformed region, associated with free volume generation; one such study can be seen in Figure 2.15 where nanoindentation was performed across the sheared region (where the shear band was located), on the BMG deformed in Figure 2.15 [63]. The very nature of shear bands causing work softening therefore limits plasticity.
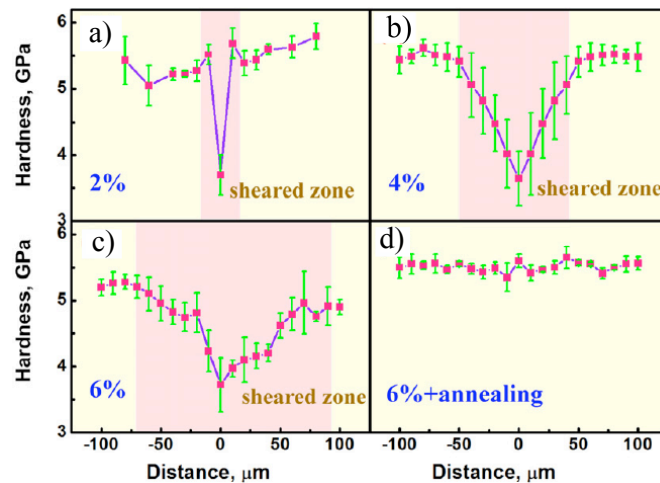
Figure 2.15. Nanoindentation across a sheared zone in the $Zr_{69.5}Cu_{12}Ni_{11}Al_{7.5}$ BMG deformed to plastic strains of a) 2%, b) 4%, c) 6% and, d) 6% and thermally annealed at 593 K for 1 hour [63].

Plastic strain enhancement in BMGs may be promoted by 1) varying alloy composition and intrinsic structure [67,68], 2) the inclusion of a second phase [69-71] and, 3) varying test conditions [72,73], including sample geometry [74]. With regard to point 1, this will be covered in detail in section 2.4, where relationships between elastic moduli and deformation will be reviewed. With regard to the second point, a range of techniques exist for introducing second phases into the amorphous matrix. These include, though are not limited to, precipitation of a ductile crystalline phase in-situ or by partial devitrification [69-71], the addition of inclusions that do not alloy with the liquid melt [75,76], glassy phase separation [77,78] and stress induced phase transformations [79-81].

In the instance of crystalline phase precipitation, the mechanism that is believed to favour the greatest plastic strains is that of enabling both dislocation motion within a ductile crystalline phase and by ensuring shear bands never reach an unstable condition in the amorphous matrix [70,71]. These are obtained by ensuring that *G* of the crystals is less than that of the matrix, encouraging permanent deformation to occur there first, and by the crystal separation distance not exceeding the plastic zone size, r_p. An alloy that conforms to these conditions can be seen in Figure 2.16.
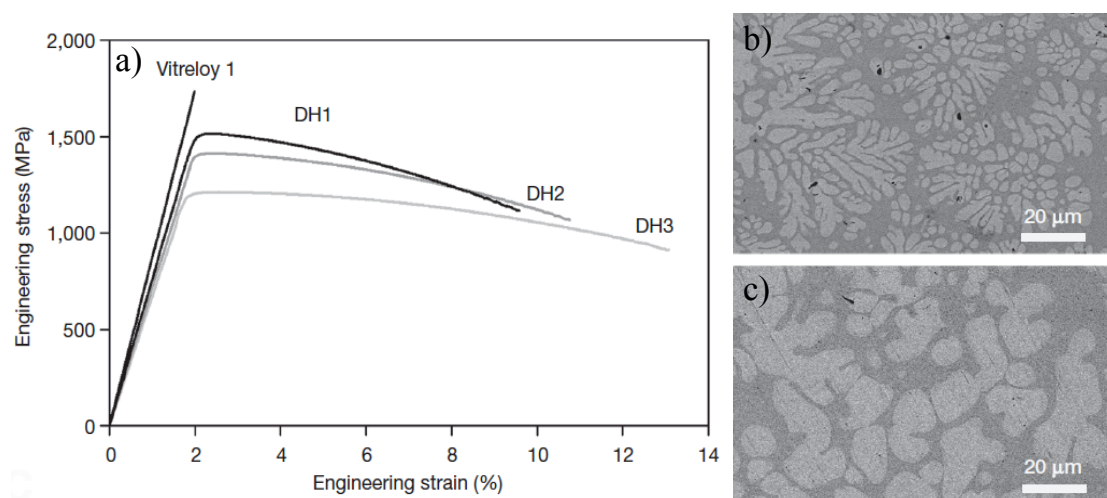
Figure 2.16. Tensile stress - strain curves comparing DH1 ($Zr_{36.6}Ti_{31.4}Nb_7Cu_{5.9}Be_{19.1}$), DH2 ($Zr_{38.3}Ti_{32.9}Nb_{7.3}Cu_{6.2}Be_{15.3}$) and DH3 ($Zr_{39.9}Ti_{33.9}Nb_{7.6}Cu_{6.4}Be_{12.5}$), a) and SEM micrographs of DH1and DH3 in b) and c) respectively. Note that r_p was calculated as 200 μm, which is less than the dendrite centre separation distance of 80-140 μm in DH1 and DH3. These composite structures were produced by quenching the microstructure from the two-phase semi-solid state (between the solidus and the liquidus) [69].

These length scale ideas were first presented in [70] where remarkable plasticity was realised in an La-based BMG composite (5% and 4% plastic strain in tension and compression respectively for $La_{74}Al_{14}Cu_6Ni_6$), containing an La solid solution in an amorphous matrix, which are highly brittle in monolithic form. It must be noted that the results in Figure 2.16 - impressive as these properties are, making them a benchmark against which others are compared – do not exhibit work hardening in tension and instead can be observed to work soften. Another composite type that does not work harden are glassy phase separated BMGs [82]. Spinodal decomposition, in which no additional energy input is needed to precipitate a second phase, results in a two phase glassy microstructure. Though it is believed that the interface between the chemically distinct phases can hinder shear bands [83], promoting irreversible strains, a complete understanding of the underpinning mechanism remains elusive, as some alloys show large plasticity while others do not. It may be that a small elastic modulus mismatch between phases is beneficial in this instance. However, inducing phase separation in BMGs can be achieved reasonably readily via the addition of an element with a small positive heat of mixing with the major alloy constituents (such as the atomic pair of Ta-Zr (+3 kJ/mol) in $Zr_{59}Ta_5Cu_{18}Ni_8Al_{10}$ [77] and Fe-Cu (+13 kJ/mol) in $Cu_{45}Zr_{47}Al_7Fe_1$ [78]). To date, no published data exists testing these materials in tension, though they would not be

anticipated to display the same levels of plasticity as in compression. This is because they remain a fully amorphous material and so will experience the same dilatation and work softening that limits all BMGs.

As mentioned earlier, work hardening is a critical trait for any load-bearing material. The DH series BMG composites of Hoffmann *et al.* [69], while a significant step forward, in terms of both processing and properties, do not exhibit this behaviour (see Figure 2.16). The actual use of this material may therefore be limited. A relatively new group of BMG composite has been reported however which do work harden in both compression and tension. These are based on martensitic forming systems (Cu-Zr or Ni-Ti) which can undergo a diffusionless transformation from a parent austenite phase to a martensite [79]. During mechanical testing the austenite then deforms in a similar manner to TRIP (transformation induced plasticity) steels, creating martensite. This has been demonstrated in Cu-Zr and Cu-Zr-Al BMGs [84]. Twinning has also been observed as an active mechanism [80], contributing to macroscopic deformation. Kim *et al* [81] reported the $Ti_{48}Zr_{27}Ni_6Be_{14}$ composition that was held between the solidus and liquidus temperatures, as per Hoffmann *et al* [69], generating a significant (though not quantified) crystalline volume fraction. 9.5 % plastic strain was found in tension with steady and continuous work hardening – see Figure 2.17.
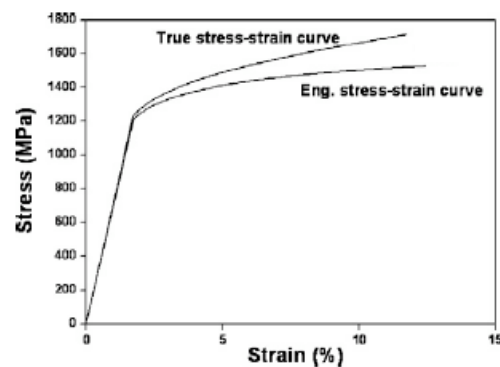
Figure 2.17. Tensile stress – strain curves for $Ti_{48}Zr_{27}Ni_6Be_{14}$, exhibiting work hardening and 9.5% plastic strain [81].

Recent work has demonstrated that by applying a mathematical analysis used for martensitic transformations in zirconia [85], the tough behaviour observed in these BMG composites cannot be caused by the transformation itself imposing compressive forces on the surrounding glassy matrix, preventing unstable shear banding, as had been previously proposed [86]. Instead, it is suggested that since maximum contribution to toughening is

observed over limited shear band propagation distance, when considering shape change associated with the transformation rather than only volume change (that would impose compression on the surroundings), a larger number of short shear bands could lead to maximum toughening. A number of research questions remain then as to exactly how these alloys operate. However, as alloys that undergo stress induced transformations, and that can twin, do not necessarily require the operation of shear bands, they have a strong potential to work harden which may not be possible in other BMG composites. Thus, these alloys are likely to receive increased attention in the future.

It is possible to tailor extrinsic factors to favour plasticity in BMGs. This includes reducing sample size, often referred to as the "smaller is softer" approach. For example, Huang *et al*. [74] showed that decreasing sample diameter, whilst retaining a constant length/width aspect ratio of 2, increases plastic strain from 1.2 % to 12.5 % for rod diameters of 6 mm and 1 mm respectively. Similar effects have been observed by others [87]. Whilst it was initially considered that this phenomenon originates from an enhanced free volume content, associated with more rapid cooling of a smaller diameter casting, Wu *et al*. [88] cast different sized rods of $Zr_{48}Cu_{45}Al_7$ and annealed them all at the same homologous temperature. Free volume content was then more similar in each sample, enabling a fairer comparison that only had rod size as the variable. Plasticity was again favoured in smaller rods suggesting that structural state is not the only factor controlling the smaller is softer response. They rationalise this result in two ways: 1) the number of defects (pores and surface irregularities), which could act as stress concentrators, will be reduced in a small sample, and 2) reducing the sample diameter will bring it closer to r_p, enabling stable shear banding. It should also be noted that compression of micro-pillars of BMGs causes homogeneous deformation rather than shear banding, allowing for extensive compression [89]. It is clear then that by reducing sample size, BMGs are more resilient to failure. This result is of practical importance when considering BMGs for mechanical applications, and they are considered a promising candidate for micro-electronic mechanical systems (MEMS) [12].

As well as sample size, machine stiffness [73] and the lubricant [72] used on the platen have been shown to be important parameters. With regard to machine stiffness, a mechanical tester will unload some of the deformation stored within it (the compliance) when a BMG yields, as it stops hardening. In the case of compression, this is unloaded onto the sample, potentially causing failure. Less energy will be stored in a stiffer rig however, reducing the chance of failure. In addition, the load applied to a larger diameter sample will be greater than a smaller one; on yielding more recovery occurs within the load frame of a larger sample, promoting failure. This may be contributing to the afore mentioned smaller is softer effect [74,87,88]. Finally, it has been demonstrated for Vitreloy 1

($Zr_{41.2}Ti_{13.8}Cu_{12.5}Ni_{10}Be_{22.5}$) that changing the lubricant used at the contact surfaces with the platen during compression testing influences the recorded plastic strain; changing from MoS_2 grease to Cu foil increased plastic strain from 0.15% to 8%, believed to result from a reduction in the build up of local frictional forces [72]. Test methodology therefore is another important factor, which, based on these results, may be almost just as important as alloy chemistry and thermal history.

Compression testing of BMGs appears to be an "anything goes" affair, where a lack of standards prevents a direct comparison of one alloy with another, and from different research groups, leading to difficulties in reproducing results in the literature. It can be expected that the plastic response of those alloys that are intrinsically plastic and brittle respectively should be less affected than those that are intermediate deformers, e.g. those that would show a yield event and approximately 1% plastic strain. These alloys could be more sensitive to test variables, resulting in them wrongly being reported as plastic or brittle. Fracture toughness measurements are a more reliable test and relate to the intrinsic ability of a sample to resist fracture. However, this test is less commonly performed than compression, with minimal data being present in the literature. It is apparent then that the BMG field suffers from a lack of standardization of compression testing and this could limit an analysis based on plastic strain if an insufficient or unreliable data set were to be used.

2.4. Correlation of elastic moduli with properties

2.4.1. Elastic moduli

Elastic response to an applied load is one of the basic properties of all solids and originates from the distortion of atomic bonds. The elastic properties that are most widely reported are *E*, *G* and *B*, corresponding to tensile, shear and hydrostatic loading respectively. Since *B* signifies the compressibility of a substance, it can be calculated from the partial derivative of volume (*V*) and pressure (*P*) at constant temperature (*T*), as per Equation 2.3.

$$K = \left(\frac{\partial V}{\partial P} \right)_T \qquad\qquad\qquad (2.3)$$

E measures the resistance to a change in atomic separation distance within the plane of the bond, and so can be determined from the linear portion of the interatomic potential. *G* quantifies the resistance to shear loading and *B*, since it corresponds to a volumetric dilatation, is dependent on the electronic properties of a solid i.e. the compressibility of the

electron gas. Elastic moduli are therefore controlled by interatomic interactions and so may be considered a fundamental property of condensed matter.

By excitation of longitudinal and transverse phone modes, E and G can respectively be calculated if the density (ρ) of the material is known. This is done via an ultrasonic probe which emits and measures the longitudinal (v_l) and transverse (v_t) sound waves velocities, from which E and G can be calculated via Equations 2.4 and 2.5:

$$E = \rho v_l^2 \tag{2.4}$$

$$G = \rho v_t^2 \tag{2.5}$$

E, G and B can also be calculated from C_{ij} elastic constants, which quantify the resistance to deformation on the i plane in the j direction of a crystalline material. For a material with cubic structure, the number of C_{ij} in the elastic tensor can be reduced from 36 to just 3, due to $C_{ij} = C_{ji}$ and there being strong symmetry in a cubic lattice. The resulting relevant C_{ij} are C_{11}, C_{12} and C_{44}.

$$C_{11} = B + \frac{4G}{3} \tag{2.6}$$

$$C_{12} = \frac{3B - C_{11}}{2} \tag{2.7}$$

$$C_{44} = G \tag{2.8}$$

$$C' = \frac{C_{11} - C_{12}}{2} \tag{2.9}$$

The tetragonal shear modulus, C', like C_{44}, corresponds to a specific phone vibration mode in the atomic structure, and is thus directional in nature. In comparison, B is non-directional as it relates to a volumetric effect.

2.4.2. Relationships in metallic glasses

Moduli show trends with a range of properties in BMGs including hardness, yield strength, toughness and fragility [67,90,91]. Correlation of T_g and T_m with E and G respectively [90] also suggests links with glass forming ability, via T_{rg}. This review will

concentrate on those relationships pertinent to the aims of this thesis viz. tendency for permanent deformation.

Returning to the models for yielding in BMGs discussed previously, the activation energy for a shear event in amorphous media is known to be proportional to G. The shoving model [92-94] considers the activation barrier for mechanical and thermal yielding (the glass transition) as being proportional to the instantaneous shear modulus, G_i and a temperature insensitive volume, V ($E_a \propto G_i V$). G can be used in place of G_i as, on very short time scales, liquids do not flow. Additionally, it is known from granular models for shear that dilatation of the surroundings is required [64] (accounting for free volume increase and work softening) and so B also contributes to the barrier. It was believed to provide 10% of the total activation energy and, in the instance of BMGs, a value of 9% was suggested [95]. Yielding in BMGs is therefore dominated by G, though it would be wrong to say that it is B independent. In Johnson and Samwer's co-operative shear model [34] the energy barrier is also purported as being proportional to G. Plastic strain does not simply correlate with a low G however as many BMGs with very low values are inherently brittle; Ce-based BMGs typically have low G but fail without yielding [96]. Other factors must therefore be involved and an apparent ability to readily yield is in itself insufficient to realise tough alloys.

Pugh suggested that the ratio G/B indicates the intrinsic ability of a crystalline metal to resist fracture and deform plastically [97]. This is because the force required to propagate a dislocation is proportional to Gb where b is the Burgers vector. Fracture strength is also proportional to Ba (a is the lattice constant) since B is related to surface energy, which indicates brittle fracture strength. Empirical observations implicate G/B as explaining well brittle or tough behaviour [98]. A similar trend was observed in BMGs by Lewandowski *et al*. [91], where fracture toughness and fracture energy (fracture toughness/E) increased with decreasing G/B or, equivalently, a high Poisson's ratio (v). Similar trends have been reported in Fe-based BMGs [67] and with plastic strain in a range of alloys [99]. The reasons for these trends are based around the same energetic considerations mentioned previously, as yielding in BMGs is proportional to G, while B correlates with fracture strength. Cheng *et al*. [100] considered G and B as consisting of a structural and an elemental (or composition dependent) component, the sum of which gives the global G and B ($G=G_e+G_c$ and $B=B_e+B_c$ where subscript e and c are elemental and configurational contributions respectively). It was shown using molecular dynamics simulations that increasing the cooling rate of the alloy increased the fraction of incomplete icosahedra (termed liquid-like sites) and, concurrently, the modeled plastic strain. Tying in with this, the effect of thermal history on G and B were reported in a separate study, where G was found to be more dependent than B [101] – this is shown in Figure 2.18.
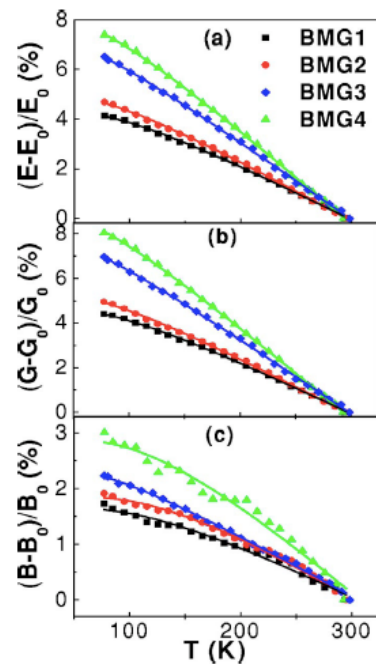
Figure 2.18. Change in *B*, *G* and *E* as a function of temperature for $Zr_{41}Ti_{14}Cu_{12.5}Ni_{10}Be_{22.5}$ (BMG1), $Cu_{47.5}Zr_{47.5}Al_5$ (BMG2), $La_{68}Al_{10}Cu_{20}Co_2$ (BMG3) and $Mg_{65}Cu_{25}Gd_{10}$ (BMG4) [101].

Thus, increased plastic strain was associated with faster cooling increasing the fraction of liquid-like sites, having a stronger reduction effect on *G* than on *B*, since *G* is more dependent on structure than *B* is. The ratio *G/B* would therefore be expected to decrease with increased cooling rate, since *G* would decrease proportionately more than *B*. Poon *et al.* suggest that local variation in structure may control deformation response [102]. They report that if the global *ν* is not conducive in itself to plasticity, multiple shear bands can still be activated if there are sites with a local *G* (termed *G**) less than that which would be measured in a macroscopic specimen. This behaviour is shown graphically in Figure 2.19.
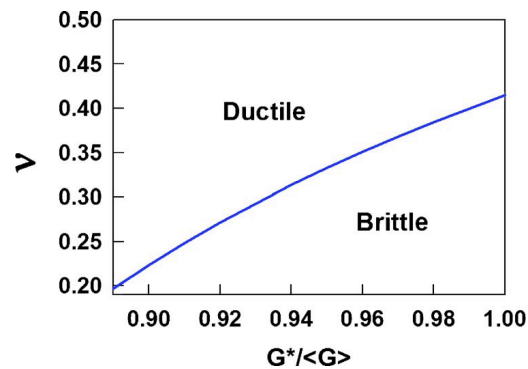
Figure 2.19. Ductile and brittle phase fields in metallic glasses, where *G** is the local modulus and *<G>* the global modulus. Decreasing the fraction of low *G* sites reduces the need for a globally low *v* [102].

It is local variation in structure that may control deformation response then and it can be anticipated that free volume is associated with such sites. Based on this model, experimentally measured moduli (by resonant ultrasound spectroscopy and ultrasonic time-of-flight measurements) may not be controlling macroscopic deformation since they are an average across the whole sample. A small *G** would be expected at sites with a high fraction of incomplete icosahedra, as defined by Cheng *et al*. [100], where, although *B* may only be slightly reduced, *G* is much smaller, favouring STZ nucleation.

Chen *et al*. published on this topic in the 1970s [103-107]. He suggested that elastic constants, packing densities and atomic configuration are all factors influencing a materials ability to plastically deform. Links were established between a high *v* and ease of "atomic regroupings" and plasticity is predicted as being higher in glasses with high *v*, where non-directional bonding was believed to prevail [103,104]. Figure 2.20 highlights part of this work.
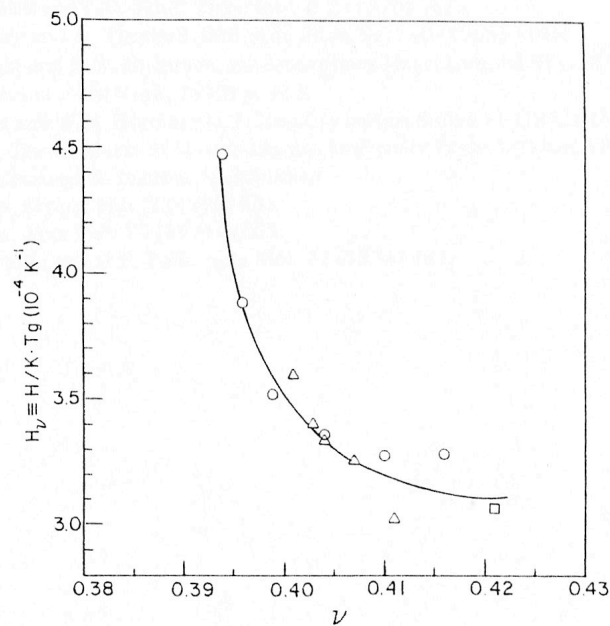
Figure 2.20. The resistance to shear strains, H_v, as a function of v in various Pd-based BMGs (H, and K are the hardness and Boltzmann constant respectively) [103].

In this figure a limited data set is used, as the range of v does not sample that which are obtainable now (approximately 0.3-0.42). This is because only Pd-based alloys are plotted, which are known to be malleable. However a link between elastic properties and plasticity is explicitly stated; "the high Poisson's ratio of metallic glasses, as indicative of the ease of atomic regroupings, is responsible for the ductile plastic deformation" [103]. These ideas have, and are being, borne out in the literature and it is apparent that Chen *et al.* were able to derive the general trends that researchers continue to study to this day.

The kinetic glass fragility index, *m*, is considered a fundamental property of amorphous media as it describes the temperature dependence of viscosity as T_g is approached (see Figure 2.2) [11]. It quantifies the slowing down dynamics of a system and is quantifiable from the gradient approaching T_g. G/B has been correlated with *m* by Novikov and Sokolov [108] for non-metallic glasses, where the relationship $m=29(B/G-0.41)$ was fitted. Park *et al.* [109] applied a similar analysis to BMGs, resulting in the empirical relationship $m=12(B/G+0.67)$. The less a glass can resist dilatation rather than a shear event then, the more fragile its behaviour becomes. Through this relationship, tendency for plastic strain can be linked to a high *m*; fragile glass formers based on Pd and Pt are known to be more deformable, while strong glass formers such as Mg-, Fe- and La-based are brittle. It is not immediately clear why this should be true though. One school of thought is that rapid viscosity decrease may encourage stress relaxation around a shear band, reducing its speed and enabling more controlled propagation [109]. Another study suggested that structural

heterogeneity is greater in fragile Mg-based glasses, permitting greater plastic strains [110], though the exact structural origin of this was not determined. No rigorous links beyond empirical findings have been established as to the effect *m* may have on permanent deformation. As fragility index reflects the rate of cluster formation and packing (causing an increase in viscosity) it may be anticipated that the atomistic structure of BMGs varies with *m*. Returning to the work of Cheng *et al*. [100], they correlate the fraction of liquid-like sites with plastic strain, resulting from non-perfect atomic packing. From the cluster packing models mentioned earlier, diversity may also exits in the arrangement of clusters, since free volume is suggested as being accommodated between them. This may provide a link as to why fragile glass formers appear to be the most plastic - this point will be considered in this thesis.

2.5. Summary and future challenges

The following bullet points summarise some of the main challenges facing the BMG community:

- BMGs containing most of the metallic elements in the periodic table have been found, and alloy development has moved beyond the bucket chemistry type approach used in the early days of BMG research. While a number of general guidelines exist for explaining glass formation (such as T_{rg} and Inoue's three rules), the Efficient Cluster Packing model of Miracle *et al*. [18] is the only one that goes beyond simply stating the chemical species that should be present, and their rough proportions, and instead gives exact atomic amounts.

- The SRO structure of BMGs has been extensively studied and is relatively simple to probe given the accessibility of central facilities and the quality of data that is obtainable. While the Efficient Cluster Packing model extends structure packing beyond nearest neighbours, it can only be considered an ideal model, preventing extrapolation over larger length scales. Attempts to reconstruct the 3-D atomistic configuration of a sizeable section of BMG (well beyond MRO) have been made [30] though it is currently not experimentally possible to verify their accuracy. Such data however suggests a complex structure with regions high and low in free volume.

- With it being suggested that it is the reorientation of clusters that controls yielding [31], modelling long-range structure could be advantageous and may further elucidate the geometric units and length scales involved in STZ nucleation. Determining direct links between structure and properties of BMGs, such as exist for crystalline metals, remains a challenge therefore.

- Defining what free volume is in terms of structure, and then being able to quantify it, is a difficult task in BMGs as metals are not possessed of hard interatomic potentials, permitting a large amount of atomic compressibility. Rather than quantifying the local environment around an atom in terms of free volume (which would be calculated based on the atomic cage approach of Cohen and Turnbull [51]), describing the atomic scale stresses and strains may be a more appropriate structure descriptor, and can be envisioned as the occupation of different inherent states in the potential energy landscape.

- The work softening of BMGs is an inevitable result of free volume increase by dilatation and so is likely to always be an issue when deformation is shear band mediated. Work hardening however is a necessary property for a material to be used in many critical applications, such as some of those that BMGs are believed to be suitable for. The introduction of a second phase that can undergo a diffusionless phase transformation, and that can twin, appears to be capable of alleviating this issue, whilst retaining the high yield strength of the amorphous phase.

- Elastic moduli can be correlated with a wide range of properties of BMGs, including tendency for plastic energy absorption under load. However, these are generally empirically based observations and theory to describe them is not as developed as other concepts in the BMG field.

- It is suggested that local moduli control STZ nucleation in BMGs. Given the results of the previous mentioned modelling of a whole 3-D element of BMG, where large variation in structure, and therefore bond density, were found, it can be expected that large local variation in elastic moduli can be expected on length scales similar to those of STZs.

- A low G/B ratio (or high v) should favour toughness but also indicates a fragile glass former, which are typically difficult to vitrify. Aside from Pd- and Pt-based alloys it may be difficult to fabricate large sections of inherently tough BMGs.

2.6. References

[1]   W. Klement, R. H. Willens and P. Duwez, Nature **187**, 869-870 (1960).

[2]   H. S. Chen, Acta Metallurgica **22**, 897-900 (1974).

[3]   H. S. Chen, Mater. Sci. Eng. **23**, 151-154 (1976).

[4]   A. L. Drehman, A. L. Greer and D. Turnbull, Appl. Phys. Lett. **41**, 716-717 (1982).

[5]   H. W. Kui, A. L. Greer and D. Turnbull, Appl. Phys. Lett. **45**, 615-616 (1984).

[6]   D. Turnbull, Contemp. Phys. **10**, 473-488 (1969).

[7]   D. Turnbull, J. Phys. Colloq. **35**, C4-1-C4-10 (1974).

[8]   T. R. Anantharaman and C. Suryanarayana, "Rapidly Solidified Metals, A Technological Overview", Trans. Tech. Publications-Switzerland, 1987, p101.

[9]   A. Inoue, Acta Mater. **48**, 279 (2000); B. C. Giessen, "Glass formation diagrams: A two parameter representation of readily glass forming binary alloys systems", Proc. 4th Int. Conf. on Rapidly Quenched Metals, Senday, Japan, 1981, pp. 213-224.

[10]   H. A. Davies, Phys. & Chem. of Glasses **17-5**, 159-173 (1976).

[11]   C. A. Angell, Science **267**, 1924-1935 (1995).

[12]   A. L. Greer, Mat. Today **12**, 1-2 (2009).

[13]   D. N. Perera, J. Phys. Condens. Matter **11**, 3807-3812 (1999).

[14]   Z. P. Lu, Y. Li and C. T. Liu, J. Appl. Phys. **93**, 286-290 (2003).

[15]   N. Nishiyama and A. Inoue, Mater. Trans. **43**, 1913-1917 (2002).

[16]   T. Scopigno, G. Ruocco, F. Sette and G. Monaco, Science **302**, 849 (2003).

[17]   O. N. Senkov, Phys. Rev. B **76**, 104202 (2007).

[18]   D. B. Miracle, Nature Mater. **3**, 697-702 (2004).

[19]   Q. Zeng, H. Sheng, Y. Ding, L. Wang, W. Yang, J. Jiang, W. L. Mao and H. Mao, Science **332**, 1404 (2011).

[20]   J. D. Bernal, Nature **185**, 68-70 (1960).

[21]   J. D. Bernal, Proc. Roy. Soc. London Ser. A **280**, 299-322 (1964).

[22]   Y. Q. Cheng and E. Ma, Prog. Mat. Sci. **56**, 379-473 (2011).

[23]   O. N. Senkov and D. B. Miracle, Mater. Res. Bull. **36**, 2183-2198 (2001).

[24]   A. Inoue, Acta Mater. **48**, 279-306 (2000).

[25]   A. Hirata, P. Guan, T. Fujita, Y. Hirotsu, A. Inoue, A. Yavari, T. Sakurai and M. Chen, Nature Mater. **10**, 28-33 (2011).

[26]   F. C. Frank, Proc. Roy. Soc. London Ser. A **215**, 33 (1952).

[27]   H. W. Sheng, W. K. Luo, F. M. Alamgir, J. M. Bai and E. Ma, Nature Mater. **439**, 419-424 (2006).

[28]   K. F. Kelton, G. W. Lee, A. K. Gangopadhyay, R. W. Hyers and T. J. Rathz, Phys. Rev. Lett. **90**, 195504 (2003).

[29]   Y. Liu, H. Bei, C.T. Liu and E. P. George, Appl. Phys. Lett. **90**, 071909 (2007).

[30]   X. J. Liu, G. L. Chen, X. Hui, T. Liu and Z. P. Lu, Appl. Phys. Lett. **93**, 011911 (2008).

[31]   C. Fan, P. K. Liaw and C. T. Liu, Intermet. **17**, 86-87 (2009).

[32]   J. C. Ye, C. T. Liu, Q. Wang and Y. Yang, Nature Mater. **9**, 619-623 (2010).

[33]   T. C. Hufnagel and R. T. Ott, Phys. Rev. B **73**, 064204 (2006).

[34]   W. L. Johnson and K. Samwer, Phys. Rev. Lett. **95**, 195501 (2005).

[35]   M. Chen, Annu. Rev. Mater. Res. **38**, 445-469 (2008).

[36]   C. Dong, Q. Wang, J. B. Qiang, Y. M. Wang, N. Jiang, G. Han, Y. H. Li, J. Wu and J.

H. Xia, J. Phys. D: Appl. Phys. **40**, 273-291 (2007).

[37]   P. H. Gaskell, Nature **276**, 484-485 (1978).

[38]   P. H. Gaskell, J. Non-Cryst. Sol. **32**, 207-224 (1979).

[39]   C. Fan, P. K. Liaw, V. Haas, J. J. Wall, H. Choo, A. Inoue and C. T. Liu, Phys. Rev. B **74**, 014205 (2006).

[40]   Egami T. Atomistic theory of metallic liquids and glasses. In: Miller M, Liaw P, editors. Bulk metallic glasses. Berlin: Springer-Verlag; 2008. p. 27–56.

[41]   C. A. Schuh, T. C. Hufnagel and U. Ramamurty, Acta Mater. **55**, 4067-4109 (2007).

[42]   H. S. Chen, J. Appl. Phys. **49**, 3289 (1978).

[43]   M. D. Demetriou, A. W. Weist, D. C. Hofmann, W. L. Johnson, B. Han, N. Wolfson, G. Wang and P. K. Liaw, JOM **62**, 83-91 (2010).

[44]   J. Frenkel, Z. Phys. 37, 572-609 (1926).

[45]   H. Bei, S. Shim, G. M. Pharr and E. P. George, Acta Mater. **56**, 4762-4770 (2008).

[46]   A. Inoue, B. Shen, H. Kato, A. R. Yavari, Nature Mater. **2**, 661 (2003).

[47]   F. Spaepen, Nature Mater. **5**, 7-8 (2006).

[48]   M. D. Demetriou, M. E. Launey, G. Garrett, J. P. Schramm, D. C. Hofmann, W. L. Johnson and R. O. Ritchie, Nature Mater. **10**, 123-128 (2011).

[49]   F. Spaepen, Acta Metall **25**, 407-415 (1977).

[50]   A. S. Argon, Acta Metall. **27**, 47-58 (1979).

[51]   M. H. Cohen and D. Turnbull, J. Chem. Phys. **31**, 1164-1169 (1959).

[52]   R. Becker, Z. Phys. 33, 185-213 (1925); E. Orowan, Z. Phys. **89**, 327-343 (1934).

[53]   E. R. Homer and C. A. Schuh, Acta Mater. **57**, 2823-2833 (2009).

[54]   E. R. Homer and C. A. Schuh, Modelling Simul. Mater. Sci. Eng. **18**, 065009 (2010).

[55]   T. Egami, JOM **62**, 70-75 (2010).

[56]   F. Faupel, W. Frank, M. Macht, H. Mehrer, V. Naundorf, K. Ratzke, H. R. Schober, S. Sharma and H. Teichler, Rev. Modern. Phys. **75**, 237-276 (2003).

[57]   T. Egami, Prog. Mat Sci. **56**, 637-653 (2011).

[58]   Egami T. Atomistic theory of metallic liquids and glasses. In: Miller M, Liaw P, editors. Bulk metallic glasses. Berlin: Springer-Verlag; 2008. p. 27–56.

[59]   W. Dmowski, W. Fan, M. L. Morrison, P. K. Liaw and T. Egami, Mat. Sci. Eng. A **471**, 125-129 (2007).

[60]   L. Y. Chen, A. D. Setyawan, H. Kato, A. Inoue, G. Q. Zhang, J. Saida, X. D. Wang, Q. P. Cao and J. Z. Jiang, Scripta Mater. **59**, 75-78 (2008).

[61]   L. Y. Chen, Z. D. Fu, G. Q. Zhang, X. P. Hao, Q. K. Jiang, X. D. Wang, Q. P. Cao, H. Franz, Y. G. Liu, H. S. Xie, S. L. Zhang, B. Y. Wang, Y. W. Zeng and J. Z. Jiang, Phys. Rev. Lett. **100**, 075501 (2008).

[62]   K. M. Flores, D. Suh, R. H. Dauskardt, P. Asoka-Kumar, P. A. Sterne and R. H.

Howell, J. Mater. Res. **17**, 5 (2002).

[63] J. Pan, Q. Chen, L. Liu and Y. Li, Acta. Mater. **59**, 5146-5158 (2011).

[64] O. Reynolds, Phil. Mag. **20**, 469-481 (1885).

[65] P. E. Donovan, Acta Metall. **37**, 445 (1989).

[66] R. Bhowmick, R. Raghavan, K. Chattopadhyay and U. Ramamurty, Acta Mater. **54**, 4221-4228 (2006).

[67] X. J. Gu, A. G. McDermott, S. J. Poon and G. J. Shiflet, Appl. Phys. Lett. **88**, 211905 (2006).

[68] X. J. Gu, S. J. Poon, G. J. Shiflet and J. J. Lewandowski, Acta Mater. **58**, 1708-1720 (2010).

[69] D. C. Hofmann, J. Suh, A. Wiest, G . Duan, M. Lind, M. D. Demetriou and W. L. Johnson, Nature Lett. **451**, 1085-1090 (2008).

[70] M . L. Lee, Y. Li and C. A. Schuh, Acta Mater. **52**, 4121-4131 (2004).

[71] X. Hui, W. Dong, G. L. Chen and K. F. Yao, Acta Mater. **55**, 907-920 (2007).

[72] S. Scudino, K. B. Surreddi, G. Wang and J. Eckert, Scripta Mater. **62**, 750-753 (2010).

[73] Z. Han, Y. Li and H. J. Gao, J. Mater. Res. **25**, 1958-1962 (2010).

[74] Y. J. Huang, J. Shen and J. F. Sun., Appl. Phys. Lett. **90**, 081919 (2007).

[75] R. D Conner, R. B. Dandliker and W. L. Johnson, J. Mater. Res. **13**, 2896 (1998).

[76] D. G. Pan, H. F. Zhang, A. M. Wang and Z. Q. Hu, Appl. Phys. Lett. **89**, 261904 (2006).

[77] L.Q. Xing, Y. Li, K.T. Ramesh, J. Li, T.C. Hufnagel, Phys. Rev. B. **64**, 180201 (2001).

[78] J. Pan, L. Liu, K.C. Chan, Scripta Mater. **60**, 822 (2009).

[79] J. Das, K. B. Kim, W. Xu, B. C. Wei, Z. F. Zhang, W. H. Wang, S. Yi and J. Eckert, Mater. Trans. **47**, 2606-2609 (2006).

[80] S. Pauly, G. Gorantla, G. Wang, U. Kuhn and J. Eckert, Nature Mater. **9**, 473-477 (2010).

[81] C. P. Kim, Y. S. Oh, S. Lee and N. J. Kim, Scripta Mater. **65**, 304-307 (2011).

[82] K. F. Yao, F. Ruan, Y. Q. Yang and N. Chen, Appl. Phys. Lett. 122106 (2006).

[83] E.S. Park, D.H. Kim, Acta Mater. **54**, 2597 (2006).

[84] S. Pauly, J. Das, C. Duhamel and J. Eckert, Adv. Eng. Mater. 9, 487-491 (2007).

[85] P. M. Kelly, L. R. Rose, Prog. Mat. Sci. **47**, 463-557 (2002).

[86] J. Corteen, M. Rainforth and I. Todd, Scripta Mater. **65**, 524-527 (2011).

[87] S. Xie and E. P. George, Intermet. **16**, 485-489 (2008).

[88] W. F. Wu, Z. Han and Y. Li, Appl. Phys. Lett. **93**, 061908 (2008).

[89] D. Jang and J. R. Greer, Nature Mater. **9**, 215-219 (2010).

[90]   W. H. Wang, J. Non-Crys. Sol. **351**, 1481-1485 (2005).

[91]   J. J. Lewandowski, W. H. Wang and A. L. Greer, Phil. Mag. Lett. **85**, 77-87 (2005).

[92]   J. C. Dyre, Rev. Moder. Phys. **78**, 953-972 (2006).

[93]   J. C. Dyre, T. Christensen and N. B. Olsen, J. Non-Crys. Sol. **352**, 4635-4642 (2006).

[94]   J. C. Dyre and N. B. Olsen, Phys. Rev. E **69** (2004).

[95]   M. Jiang and L. Dai, Phys. Rev. B **76**, 054204 (2007).

[96]   B. Zhang, R. J. Wang, D. Q. Zhao, M. X. Pan and W. H. Wang, Phys. Rev. B **70**, 224208 (2004).

[97]   S. F. Pugh, Phil. Mag. **45**, 834 (1954).

[98]   J. R. Thompson and J. R. Rice, Phil. Mag. Lett. **29** (1974).

[99]   Y. Liu, H. Wu, C. T. Liu, Z. Zhang and V. Keppens, Appl. Phys. Lett. **93**, 151915 (2008).

[100] Y. Q. Cheng, A. J. Cao and E. Ma, Acta Mater. **57**, 3253 (2009).

[101] P. Yu, R. J. Wang, D. Q. Zhao and H. Y. Bai, Appl. Phys. Lett. **90**, 251904 (2007).

[102] S. J. Poon, A. Zhu and G. J. Shiflet, Appl. Phys. Lett. **92**, 261902 (2008).

[103] H. S. Chen, J. T. Krause and E. Coleman, J. Non-Crys. Sol. **18**, 157-171 (1975).

[104] H. S. Chen, J. Appl. Phys. **49** (1978).

[105] H. S. Chen, H. J. Leamy and M. Barmatz, J. Non-Crys. Sol. **5**, 444-448 (1971).

[106] H. S. Chen, Scripta Metall. **7**, 931-936 (1973).

[107] H. S. Chen and B. K. Park, Acta Metall. **21**, 395-400 (1973).

[108] V. N. Novikov and A. P. Sokolov, Nature Lett. **431**, 961-963 (2004).

[109] E. S. Park, J. H. Na and D. H. Kim, Appl. Phys. Lett. **91**, 31907 (2007).

[110] E. S. Park, J. Y. Lee, D. H. Kim, A. Gerbert and L. Schultz, J. Appl. Phys. **104**, 23520 (2008).

3. Experimental methodology

3.1. Bulk metallic glass preparation

3.1.1. Argon arc melting

Samples for arc melting were weighed out from high purity elements with a Precisa XB120A precision electronic balance with an accuracy of ± 0.1 mg. Elements had a purity ≥ 99.8% and were either rolled from bar or used in lump form. Alloy pieces were first cleaned with wire wool to remove surface oxidation and dirt and, after weighing, were placed in isopropanol in an ultrasonic bath at room temperature for 2 minutes to dislodge any impurities from the surface. Cerium was stored in mineral oil and time between weighing it and placing it in the vacuum chamber was minimized so to limit reaction with the atmosphere.

Samples were placed on the copper hearth of an arc melter and pumped down to 5×10^{-3} Pa via a two-stage roughing and diffusion pump setup and was then backfilled with 1/3 atmosphere of argon. A titanium "getter" of approximately 20 g was melted prior to sample alloying, so to remove residual oxygen content from the chamber. Alloys were melted four times in total with the ingot flipped between each melt stage. After melting, samples were weighed again and if mass loss was > 0.1% then the ingot was rejected. Figure 3.1 shows the melting setup.

3.1.2. Suction casting

An *in-situ* suction casting setup was used to cast rods with a diameter of 1 mm – 4 mm. To minimize superheating of the alloy, which could otherwise impact on the critical diameter of glassy alloy observed, the current was set to a lower setting for casting than was used for melting.

Due to difficulties in casting 1 mm rod diameters with the existing setup, a larger secondary chamber was manufactured which could be attached to the existing suction chamber for the generation of the pressure differential. The larger chamber volume increased the suction force experienced by the molten alloy, permitting the casting of 1 mm rods with a length of up to 2 cm.
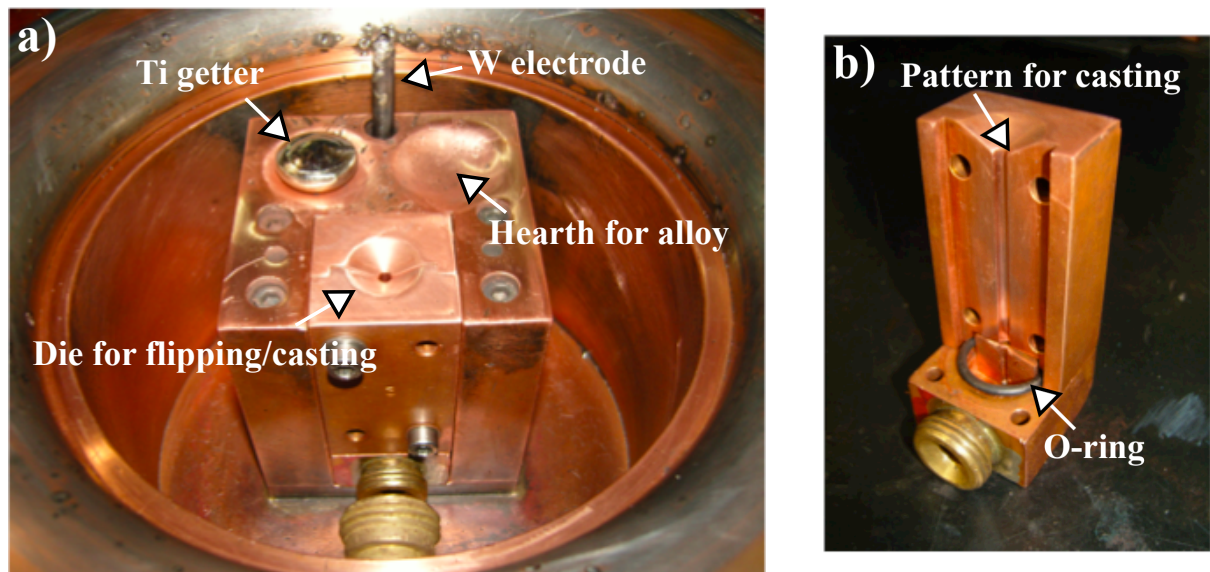
Figure 3.1. Photographs of a) the copper hearth for melting and casting alloys, and b) a 3 mm diameter pattern copper die for suction casting.

3.1.3. Melt spinning

To generate ribbons with a thickness of approximately 20 micron, a chill block melt spinner was used. Ingot pieces of the appropriate alloy were loaded into a quartz crucible with a 1 mm diameter hole ground into the nozzle at one end. The chamber was evacuated to a pressure of 5×10^{-3} Pa via a two-stage roughing and diffusion pump combination and then backfilled with 2/3 atmosphere of helium. An induction coil was used to heat the sample to above its melting point, after which an over-pressure of 40 KPa of helium was applied to the melt, forcing it out the crucible and into contact with the copper wheel, rotating at 45 ms^{-1}. With this setup, ribbon thicknesses of 15 microns were achieved.

3.1.4. Heat treatment

Samples for vacuum heat treatment were placed inside quartz tubing, loaded into a tube furnace and then evacuated to 5×10^{-4} Pa with a roughing – diffusion pump combined unit. Rather than backfilling the furnace, the valve between the chamber and the diffusion pump was left open throughout the heat treatments.

3.2. Sample characterisation

3.2.1. X-ray diffraction

Samples for study were sectioned into disks with a low speed cut-off saw fitted with a diamond blade, under continuous flow of a water based lubricant. As Ce-based BMGs react with water they were sectioned with oil used as the lubricant. Enough of each sample to cover an area of 1 cm^2 was mounted onto a glass slide with double-sided tape.

X-ray diffraction (XRD) was performed on a Philips D500 diffractometer fitted with a CuKα radiation source. Slow scan rates of 0.1 °/min were used to obtain maximum signal from the samples, between 20 - 80 2θ.

3.2.2. Differential scanning Calorimetry

Differential Scanning Calorimetry (DSC) was performed on a Perkin Elmer Diamond DSC at a heating rate of 20 °C/min in gold pans and under flowing argon gas. A baseline scan was run (with empty pans), which was subsequently subtracted from the data file to obtain the real signal. All transition temperatures were determined from the onset of the event.

3.2.3. Nanoindentation

Samples for nanoindentation were cut from suction cast rods and cold mounted in resin, before being ground and polished to a mirror finish by standard metallographic techniques. A final polish with colloidal silica suspension was used to ensure a high quality surface finish.

A Hysitron Nanomechanical tester was used for indentation tests, where the applied loading schedule could be adjusted with respect to force and load/unload time.

3.2.4. Extended x-ray absorption fine structure (EXAFS)

EXAFS experiments were performed on the I18 Microfocus beamline at the Diamond Light Source synchrotron. Figure 3.2 shows the experimental setup used to generate an incident beam of x-rays of a chosen energy of approximately 10 mircons diameter, which makes use of the following features:

1) Slits – reduce the size of the incident beam, creating a narrow beam diameter.
2) Mirrors – redirect and focus the beam.
3) Monochromator – a single crystal (Si(111)) that can be rotated. By varying its angle, only incident waves with a particular wavelength (and therefore energy) satisfy the Bragg diffraction condition, permitting selection of the desired beam energy.
4) Amplifier and computer – collect and process the energy of the incident (I_o) and transmitted (I_t) beams.
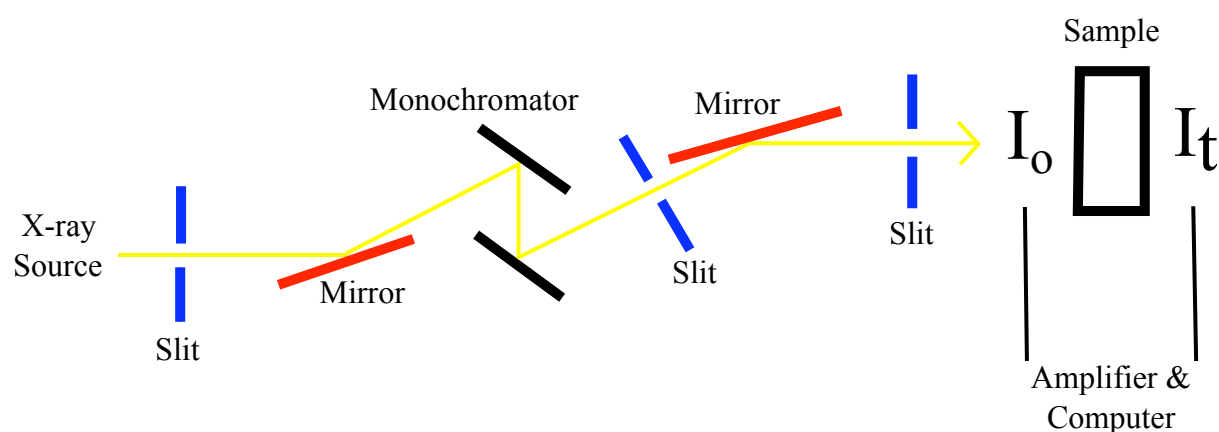
Figure 3.2. Experimental setup used at the I18 Microfocus beamline, Diamond light Source.

EXAFS refers to a specific part of the absorption spectra of an element, located approximately 50 eV after the absorption edge. During experiments, a beam of incident electrons is focused on a sample and, at the absorption edge, core electrons are emitted as photoelectrons via the photoelectric effect, overcoming their binding energy. A spectrum of pure copper can be seen in Figure 3.3.
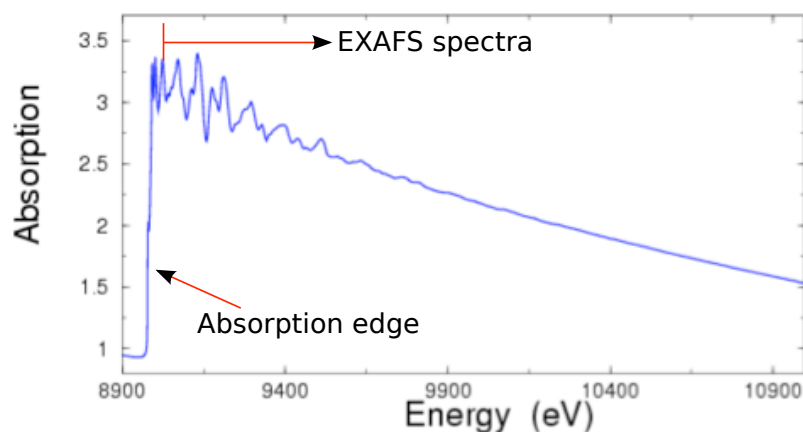
Figure 3.3. Absorption spectra of copper showing edge step and EXAFS oscillations. Absorption is calculated from I_o/I_t (see Figure (3.2)) [1].

The oscillatory signal straight after the absorption edge is the EXAFS spectrum and originates from emitted photoelectrons being backscattered by the nearest atoms, which subsequently interact with the wave vectors of the forward emitted photoelectrons. The EXAFS region thus contains information regarding the local atomic structure around a specific atom since the absorption edge is element specific. Information can be determined about local coordination number and atomic positioning. The EXAFS signal is subsequently extracted from Figure 3.3 by fitting a line to the pre- and post-edge regions, subtracting the pre-edge line from the entire data set and then dividing by the magnitude of the step height (i.e. the distance between the pre- and post-edges). The resulting spectrum can be seen in Figure 3.4.
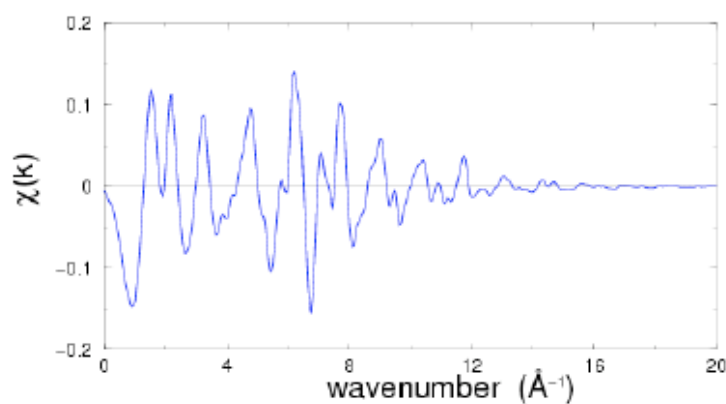
Figure 3.4. EXAFS spectrum in k-space after background removal from Figure 3.3 via Athena software [1].

By forward Fourier transform it is possible to obtain radial distribution functions (RDFs) from this data, giving information about nearest neighbour separation distances. The software Athena, developed by Professor B. Ravel, utilises the IFEFFIT processing package [2] to allow for the data handling and processing described here.

3.3. References

[1]   B. Ravel, Athena Users Guide, Version 1.5, July 2009.

[2]   http://cars9.uchicago.edu/ifeffit (Accessed 1/10/2011).

4. Physical factors controlling permanent deformation in bulk metallic glass

4.1 Introduction

Whether or not a material demonstrates brittle or ductile behaviour is of central importance as it has a direct influence on their applications range. If brittle crack propagation is favoured over controlled plastic deformation and stable crack growth, then practical uses for that material may be limited. Atomic interactions fundamentally determine which of these two conditions is theoretically observed and so it may be expected that many-body mathematical simulations would be necessary to elucidate the favoured mechanism of energy accommodation. Pugh [1] demonstrated in 1950 that the simple ratio of shear to bulk modulus (G/B) can indicate whether brittle or plastic fracture is to be expected in crystalline metals however, removing the need for complex theoretical studies since elastic properties are relatively simple to measure. That a low G/B was able to describe the intrinsic malleability of ductile face centered cubic (FCC) metals such as Au and Ag in comparison to brittle Be (with a hexagonal close packed (HCP) structure), with a high G/B, was confirmed in later studies [2]. This descriptor was additionally capable of justifying the intrinsically brittle nature of Ir (FCC) [3], which was originally believed to result from impurity segregation to grain boundaries, since FCC metals are typically resistant to fracture, when it can in fact be qualified by its low G/B.

Chen [4] was first to draw a link between the elastic properties of bulk metallic glasses (BMGs) and their tendency for ease of permanent deformation, where Poisson's ratio (v) was plotted against a parameter to quantify the resistance to shear strains, H_v ($\approx H/T_g k_b$, where H is hardness, T_g the glass transition temperature and k_b Boltzmann's constant); a small resistance to shear strain was favoured in high v alloys. Lewandowski *et al*. [5] made rigorous the connection between the elasticity of BMGs and their ability to resist fracture by returning to the work of Pugh [1]. They plotted G/B versus fracture toughness for a range of BMGs, where the correlation was found that a low G/B was capable of explaining the large toughness of Pd- and Pt-based BMGs, in comparison to brittle Mg-based alloys (e.g. G/B for $Pd_{77.5}Cu_6Si_{16.5}$ and $Mg_{65}Cu_{25}Tb_{10}$ are 0.189 and 0.439 respectively). The same trend was found when comparing the toughness of various Fe-based BMGs [6] and could be extended to account for the amount of plastic strain measured during uniaxial compression testing [33].

The underpinning reason as to why G/B can indicate the ability to resist fracture is identical in both crystalline and non-crystalline metals when considering energetics based ideas. In crystalline metals the force to propagate a dislocation is proportional to Gb (b is the

Burgers vector), while in BMGs the activation energy for yielding is proportional to *G* in both the Shoving model [7] and the Cooperative Shear model [8] – a low *G* therefore promotes the activation of the carriers of plastic deformation. Then, as *B* correlates with fracture strength, a low *G/B* represents ease of permanent deformation and concurrently large failure strengths, a combination of which is indicative of large energy absorption by irreversible deformation. While this simplistic analysis can justify the afore mentioned empirical observations, the use of elastic moduli to explain the tendency for toughness and plasticity in BMGs has not been significantly extended away from *G/B*, despite the ability of the elasticity of BMGs to explain their plastic properties well.

      Blackman diagrams plot the ratios of elastic constants C_{12}/C_{11} versus C_{44}/C_{11} [9]. This construction was first implemented to search for materials with constant Debye temperature. It can additionally be used to consider the following [10-12]: 1) the extent of elastic anisotropy, 2) proximity to Born's mechanical instability criterion [13] (where shear moduli C_{44} and C' tend to zero), 3) Poisson's ratio, and 4) similarity, or variation, in interatomic bonding through deviation from zero Cauchy pressure ($C_{12}=C_{44}$). A Blackman diagram can therefore allude to the physical state of a material, justifying its use in a study on the physical properties and interatomic bonding in FCC lanthanides-actinides, and has also been implemented to explain phase stability in the supercooled region (between T_g and the crystallisation temperature, T_x) in BMGs [12]. In this chapter a Blackman diagram will be constructed for a range of BMGs and this will be examined within the context of the mentioned physical conditions and whether these trend with a tendency for plastic strain.

4.2. Data collection and results

      Table 4.1 presents data collected from the literature for a wide range of BMGs. This is with respect to both composition and plastic strain, and so is intended to provide a characteristic sample of BMGs. A selection of non-metallic glasses have also been included to provide points for comparison. The kinetic glass fragility index, *m*, was calculated for each alloy in this table via the empirical relationship $m = 12(B/G + 0.67)$ [14]. This has been used rather than experimental values as it is difficult to find data for a large enough number of alloys that have had their m, elastic properties and compressive plasticity reported. Moreover, *m* can be measured by various techniques [15], which may not be compatible with one another, given that different systematic errors will be present in each method.

Table 4.1. Elastic property and plastic strain data for a range of BMGs in the literature. Glass fragility index m was calculated from $m=12(B/G+0.67)$. ($C_{44}=G$)

Alloy	E/GPa	G/GPa	B/GPa	C_{11}/GPa	C_{12}/GPa	C_{44}/C_{11}	C_{12}/C_{11}	m	ε_p/%	Ref.
Fused Silica	72.98	31.3	36.4	78.13	15.53	0.401	0.199	15	-	[16]
Window	67.13	27.7	38.8	75.73	20.33	0.366	0.269	17	-	[16]
Calcium Phosphate	49.99	19.56	37.53	63.61	24.49	0.307	0.385	24	-	[17]
ZBLAN	55.7	21.3	48	76.4	33.8	0.279	0.442	28	-	[18]
$Ce_{70}Al_{10}Ni_{10}Cu_{10}$	30.3	11.5	27	42.33	19.33	0.272	0.457	29	0	[19,20]
$La_{66}Al_{14}Cu_{10}Ni_{10}$	35.72	13.44	34.91	52.83	25.95	0.254	0.491	32	0	[19]
$Fe_{63}Mo_{14}C_{15}B_6Er_2$	202	77	177	293	119.75	0.263	0.409	28	0	[6]
$Mg_{58.8}Cu_{30.5}Y_{11}$	53.9	20.4	49.4	76.6	35.8	0.266	0.467	30	0.35	[21]
$Fe_{65}Mo_{14}C_{15}B_6$	104.4	73	195	280	146.33	0.250	0.501	33	0.8	[6]
$Zr_{57}Ti_5Cu_{20}Ni_8Al_{10}$	82	30.1	99.2	139.33	79.133	0.216	0.568	40	1.1	[21]
$Zr_{46.25}Cu_{46.25}Al_{7.5}$	93.81	34.3	116	161.73	93.13	0.212	0.576	49	1.2	[22]
$Mg_{57}Cu_{31}Y_{6.6}Nd_{5.4}$	54.4	20.7	48.3	75.9	34.5	0.273	0.455	29	1.2	[23]
$Hf_{50}Ni_{25}Al_{25}$	125.60	47	127.8	190.47	96.47	0.247	0.506	33	1.25[a]	[24]
$Cu_{47}Zr_{47}Al_6$	92.4	33.8	113.8	158.87	91.27	0.213	0.574	48	2.5	[25]
$Hf_{55}Ni_{25}Al_{20}$	117.63	43.7	127.2	185.47	98.07	0.236	0.529	36	2.5[a]	[24]
$Cu_{50}Zr_{50}$	87	32	103	145.67	81.67	0.220	0.561	39	4	[25]
$Zr_{45.25}Cu_{46.25}Al_{7.5}Sn_1$	97.3	35.7	118	165.6	94.2	0.216	0.569	40	4.1	[22]
$Zr_{64}Cu_{26}Al_{10}$	78.85	28.7	104	142.27	84.87	0.202	0.600	44	6.8[a]	[24]
$Pd_{77.5}Si_{16.5}Cu_6$	88.8	31.5	167	209	146	0.151	0.700	64	10.4	[26,27]
$Pt_{57.5}Cu_{14.7}Ni_{5.3}P_{22.5}$	94.6	33.3	198.7	243.1	176.5	0.137	0.726	72	20	[28]

[a]Average value

Figure 4.1 presents a Blackman diagram for the BMGs in Table 4.1, which have been spilt into three groups according to the extent of plastic strain they show: 1) plastic (>2%), intermediate (0.1 – 2%) and brittle (<0.1%). Non-metallic glasses, which are known to be brittle in comparison to BMGs, are shown also.
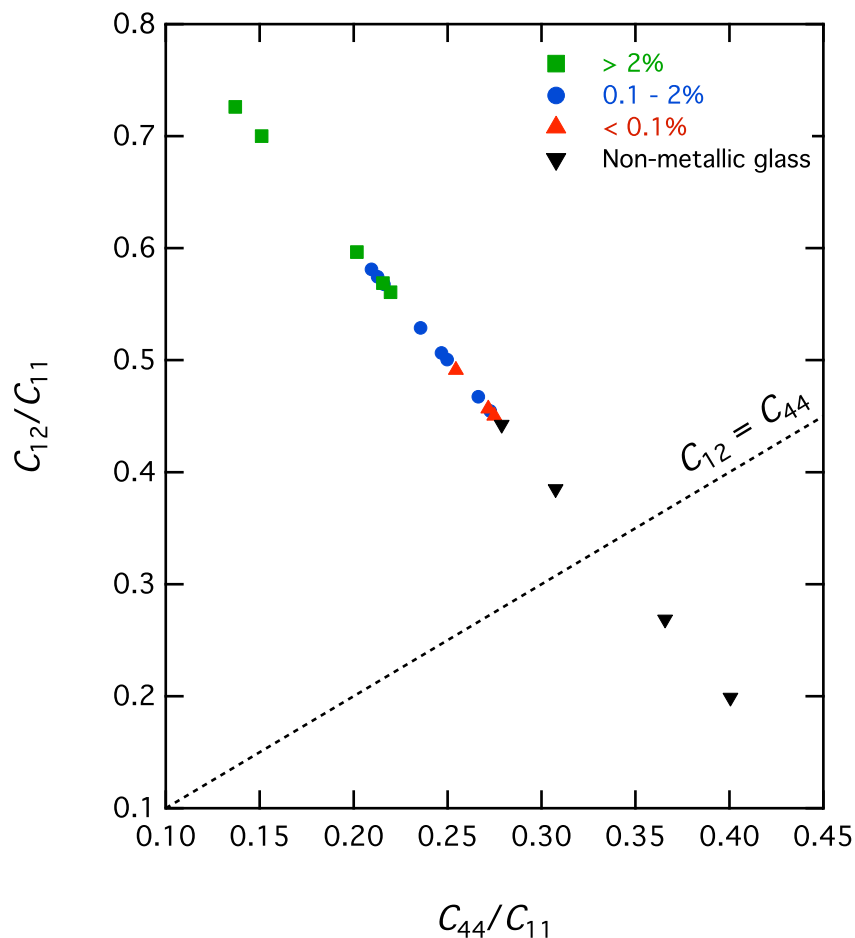
Figure 4.1. Blackman diagram plotted for the glasses in Table 4.1. Plastic strain for each group is indicated on the graph. Perforated line represents zero Cauchy pressure.

All glasses sit on a straight line because the anisotropy factor, *A*, is assumed to be equal to one i.e. they are perfectly isotropic. Though it has been demonstrated that some anisotropy may be induced in BMGs [29], this has been shown to be small, of the order of 5% in a $Pd_{40}Cu_{30}Ni_{10}P_{20}$ BMG and 3% in a melt spun ribbon of an Fe-based metallic glass, coming out of the plane of the ribbon [30] i.e. perpendicular to the melt spinning direction. Plastic alloys are found at large C_{12}/C_{11} and low C_{44}/C_{11} (and at large positive deviations from zero

Cauchy pressure, $C_{12}=C_{44}$), with the extreme point being a ductile Pt-based alloy. Brittle nonmetallic glasses lie at the opposite extreme, bounded at the lowest point by fused silica. Brittle BMGs are found to lie close to the nonmetallic glasses, and intermediate deformers congregate closer to the more ductile BMGs. A Blackman diagram is therefore capable of differentiating the plastic behavior of various glassy alloys.

In Figure 4.2 rather than grouping alloys according to plastic strain, they have been arbitrarily grouped according to their m value, by splitting them into "strong" ($m \leq 29$), "intermediate" ($m = 30$ to 50) and "fragile" ($m \geq 51$) classifications.
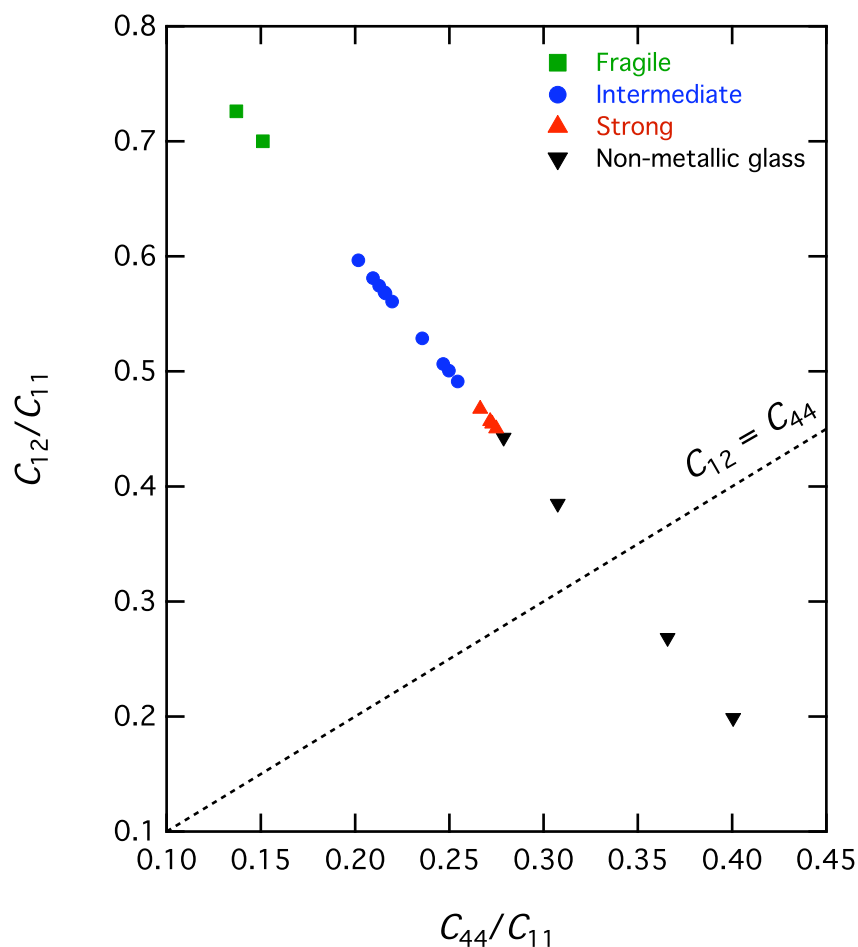
Figure 4.2. Blackman diagram plotted for the glasses in Table. 4.1. Compositions arbitrarily grouped according to their fragility index, m: "strong" ($m \leq 29$), "intermediate" ($m = 30$ to 50) and "fragile" ($m \geq 51$) glass formers. Perforated line represents zero Cauchy pressure.

It is seen here that fragile glasses congregate at large C_{12}/C_{11} and low C_{44}/C_{11} and the strong glass forming non-metallic glasses are at the opposite extremity; comparison of Figure 4.1 with 4.2 reveals that plastic strain is favoured in fragile glasses.

4.3. Discussion

Two limiting physical conditions are imposed on the Blackman diagram, being 1) proximity to the Born mechanical instability condition, and 2) deviation from zero Cauchy pressure. Born qualified melting of a substance [13]; "...there can be no ambiguity in the definition of, or the criterion for, melting. The difference between a solid and a liquid is that the solid has elastic resistance against shearing stress while the liquid has not." This condition is thus met when shear moduli drop off, as a liquid has little resistance to shearing, and so C' and C_{44} will tend to zero. When this occurs, as $C'=(C_{11}-C_{12})/2$, C_{12}/C_{11} will tend to 1 while C_{44}/C_{11} will approach zero; the Born instability is therefore met at the top left hand region of a Blackman diagram and materials present there may be considered the most liquid-like. The most fragile (and plastic) BMGs are present closest to this point and so are the most liquid-like with respect to Born's mechanical instability. Though these instability ideas cannot be simply extended to explain how atomic structure is affected, Cheng *et al*. [31] quantified the extent of liquid-like structure through the fraction of incomplete icosahedra in molecular dynamic studies of Cu-Zr BMGs. They found that plastic strain was highest in structures with the greatest number of incomplete icosahedra. The possible effects of liquid fragility on structure will be considered in subsequent chapters of this thesis, but, for the moment, it is sufficient to draw a link between fragile glass formers, ability for large plastic strain and mechanical instability.

The Cauchy relations (most commonly surmised as $C_{12}=C_{44}$) apply to atomic structures in which atoms are located at a centre of symmetry, such that they experience no net force from surrounding atoms. Central forces are present therefore with no angular bonding and so no internal stresses occur when deformed elastically. The Cauchy relations can only be applied under ideal circumstances and break down for covalently and metallically bonded materials. Even for ionic solids, where non-directional central forces dominate, some angular forces are likely, violating the $C_{12}=C_{44}$ condition. When $C_{12}>C_{44}$ negative deviation from zero Cauchy pressure is observed, indicative of a strong angular component to the bonds and directionality. Diamond shows one of the largest negative deviations from zero Cauchy pressure, owing to its covalent character generating strong directionality and an inability to resist bond bending. Under the opposite condition, when $C_{44}>C_{12}$, positive deviation occurs, such as in metallically bonded materials where an atom sits in the electron gas of the surrounding atoms – the more positive the deviation, the more non-directional the bonding.

In Figure 4.1, the most plastic BMGs are present at the largest positive deviations from $C_{12}=C_{44}$, while the covalently bonded oxide glasses lie much closer to it, and, in some cases, even deviate negatively from it, such as fused silica and window glass (which are the

strongest glass formers). This results from the non-metallic glasses being covalently bonded and suggests that those BMGs with the greatest tendency for plasticity exhibit the most non-directional bonding. In crystalline metals large plastic strains are possible because of the ease of instantaneous bond breaking and formation around a propagating dislocation, while plastic yielding is inhibited in oxide glasses through the inability for covalent bond rearrangement. In the instance of BMGs, more nondirectional metallic bonding will promote the cooperative collapse of groups of atoms, such as one that occurs during the activation of a shear transformation zone (STZ), encouraging stable shear banding and a concomitant improvement in ductility. Pettifor [32] suggests that the ratio C'/B describes the extent of bond angularity in intermetallics, where a low value suggests non-directionality; this is plotted for the metallic and non-metallic glasses from Table 4.1 in Figure 4.3.
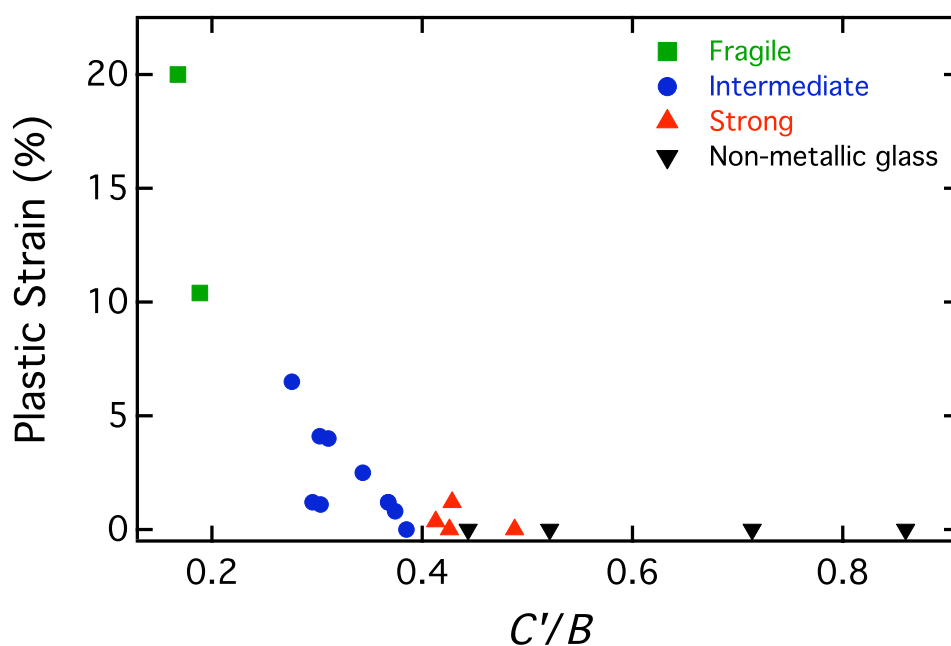
Figure 4.3. Plots of plastic strain versus C'/B for the glasses in Table 4.1.

Since C' quantifies the resistance to a shear strain, C'/B is of the same physical form as G/B, suggesting that bond directionality is also embodied by it, as well as the previously mentioned energetics based ideas. Those alloys with largest plasticity are generally metal-metalloid glasses, where it is considered that there is strong tendency for directional bonding due to the metalloid influence; this would appear to be at odds with what is being suggested here. Interestingly however, elemental Pd, Pt, and Au are all known to exhibit large positive deviations form zero Cauchy pressure [12], suggesting that non-directional bonding is a feature of the element on which the glass is based. Moreover, their noticeably large B in

comparison to BMGs in other groups would imply incompressibility of the electron gas, again suggesting a large number of delocalized electrons.

Finally, through communications with Prof. P. Dijema (Universite Paris 13), a Blackman diagram was constructed for a series of $Mo_{1-x}Si_x$ thin films, where, as the Si content was increased, the structure transformed from body centred cubic (BCC) to amorphous, with a concurrent decrease in coordination number and transition from conducting to insulating behaviour. This variation occurred going down the isotropic data line, with the insulating amorphous composition lying below zero Cauchy pressure and the BCC conducting composition lying well above it. It would appear then that Blackman diagrams may of use for studying a range of phenomena.

4.4. Conclusion

The major findings of Chapter 4 may be summarised as follows:

- A Blackman diagram facilitates the exploration of the generalities of elastic behavior in a particular material class, by incorporating important bounding conditions in its representation.

- It is capable of differentiating between plastic and brittle BMGs and non-metallic glasses, based on ratios of their elastic constants and proximity to the Born instability criterion and zero Cauchy pressure; this result suggests fundamental differences exist in the physical nature between different BMGs.

- Plasticity is highest in fragile BMGs, which are the most mechanically unstable and exhibit the most non-directional bonding, where angular forces are limited. This appears to be advantageous as it permits atomic movement and relaxation around a stress concentrator, while also permitting the possible blunting of shear bands and cracks.

- Blackman diagrams are of use for considering a range of phenomena, though are particularly advantageous in the study of amorphous materials since isotropy is generally assumed.

4.5. References

[1]   S. F. Pugh, Phil. Mag. **45**, 834 (1954).

[2]   A. Kelly, W. R. Tyson and A. H. Cottrell, Phil. Mag. **15**, 567 (1967)

[3]   J. R. Thompson and J. R. Rice, Phil. Mag. Lett. **29** (1974).

[4]   H. S. Chen, J. T. Krause and E. Coleman, J. Non-Crys. Sol. **18**, 157-171 (1975).

[5]   J. J. Lewandowski, W. H. Wang and A. L. Greer, Phil. Mag. Lett. **85**, 77 (2005).

[6]   X. J. Gu, A. G. McDermott, S. J. Poon and G. J. Shiflet, Appl. Phys. Lett. **88**, 211905 (2006).

[7]   J. C. Dyre, Rev. Moder. Phys. **78**, 953-972 (2006).

[8]   W. L. Johnson and K. Samwer, Phys. Rev. Lett. **95**, 195501 (2005).

[9]   M. Blackman, Proc. R. Soc. Lond. A **164**, 62 (1938).

[10]   H. Ledbetter and A. Migliori, Phys. Stat. Sol. (b) **245**, 44 (2008).

[11]   T. Paszkiewicz and S. Wolksi, J. Phys.: Con. Ser. **104**, 012038 (2008).

[12]   R. Tarumi, N. Hayama, M. Hirao, Y. Higo, H. Kimura and A. Inoue, Jap. J. Appl. Phys. **47**, 3807 (2008).

[13]   M. Born, J. Chem. Phys **7**, 591 (1939).

[14]   E. S. Park, J. H. Na and D. H. Kim, Appl. Phys. Lett. **91**, 31907 (2007).

[15]   A. Inoue, *Bulk Amorphous Alloys – Preparation and Fundamental Characteristics*, 1998, Trans Tech Publications, Uetikon-Zuerich.

[16]   R. J. Wang, F. Y. Li, J. F. Wang and W. H. Wang, Appl. Phys. Lett. **83**, 2814 (2003).

[17]   G. Li, Y. C. Li, Z. K. Jiang, T. Xu, L. Huang, J. Liu, T. Zhang and R. P. Liu, J. Non-Crys. Sol. **355**, 521 (2009).

[18]   S. Li, R. J. Wang, M. X. Pan, D. Q. Zhao and W. H. Wang, Scr. Mater. **53**, 1489 (2005).

[19]   W. L. Johnson and K. Samwer, Phys. Rev. Lett. **95**, 195501 (2005).

[20]   Q. Zheng, H. Ma, E. Ma and J. Xu, Scr. Mater. **55**, 541 (2006).

[21]   H. Men, X. K. Wang, J. Y. Fu, C. L. Ma and T. Zhang, Mater. Trans., JIM **47**, 194 (2006).

[22]   L. Zhang, Y. Q. Cheng, A. J. Cao, J. Xu and E. Ma, Acta Mater. **57**, 1154 (2009).

[23]   L. Q. Xing, Y. Li, K. T. Ramesh, J. Li, and T. C. Hufnagel, Phys. Rev. B **64**, 180201 (2001).

[24]   P. Yu and H. Y. Bai, Mater. Sci. Eng. A **485**, 1 (2008).

[25]   M. Jiang and L. Dai, Phys. Rev. B **76**, 054204 (2007).

[26]   A. V. Gayathri Devi, V. Rajendran and N. Rajendran, Int. Jour. Eng. Sci. & Tech. **2**, 2483 (2010).

[27]   M. Jiang and L. Dai, Phys. Rev. B **76**, 054204 (2007).

[28]   J. Schroers and W. L. Johnson, Phys. Rev. Lett. **93**, 255506 (2004).

[29]   A. Concustell, S. Godard-Desmarest, M. A. Carpenter, N. Nishiyama and A. L. Greer, Scripta Mater. **64**, 1091-1094 (2011).

[30]   R. Tarumi, A. Shibata, H. Ogi, M. Hirao, K. Takashima, Y. Higo, J. Appl. Phys. **101**, 053519 (2007).

[31]   Y. Q. Cheng, A. J. Cao and E. Ma, Acta Mater. **57**, 3253 (2009).

[32]   D. G. Pettifor, Mat. Sci & Tech. **8**, 354 (1992).

[33]   Y. Liu, H. Wu, C. T. Liu, Z. Zhang and V. Keppens, Appl. Phys. Lett. **93**, 151915 (2008).

5. Isomechanical groups in bulk metallic glass

5.1. Introduction

The use of C_{ij} elastic constants can elucidate the physical character of BMGs both individually and collectively, as demonstrated in Chapter 4 through the use of a Blackman diagram [4], which plots as its axis the ratios C_{12}/C_{11} and C_{44}/C_{11}. Inherent in such a plot are two limiting physical conditions, being 1) proximity to the Born mechanical instability condition [5], and 2) deviation from zero Cauchy pressure, where $C_{12}=C_{44}$. At the Born instability condition the resistance to an applied shear stress drops to zero, indicative of the liquid state, and so shear moduli C_{44} and C' ($C'=(C_{11}-C_{12})/2$) tend to zero. BMGs that exhibit a strong tendency for plastic strain in room temperature compression tests (termed malleability since ductility refers to tensile loading) congregate closest to the Born instability condition, indicating that they can be considered the most liquid-like within the concepts of Born. Concurrently, the kinetic glass fragility index, m, is highest (i.e. the most fragile glass formers) as the Born condition is approached, with strong glass formers furthest away. The relationship $C_{12}=C_{44}$ is only applicable when central forces exist between atomic cores, where bonding is non-directional and symmetrical; the Cauchy relationships are only suitable for ideal ionically bonded systems. When comparing metallically bonded BMGs with covalently bonded glasses however, directional bonding is enhanced at negative deviations from zero Cauchy pressure, while positive deviation is indicative of non-directional bonding, corresponding to the most plastic BMGs.

When considering the placement of BMGs on a Blackman diagram, the data range that is covered would suggest significant fundamental differences in the factors influencing their behavior. This is well embodied by the ratios of C_{12}/C_{11} and C_{44}/C_{11} of the most brittle BMGs, such as those based on La, Fe and Mg, being essentially equivalent to those of covalently bonded ZBLAN and calcium phosphate glasses [5]. Indeed, the fracture toughness of some Mg-based BMGs are known to be similar to those of oxide glasses [1] while, at the opposite extreme, a $Pd_{79}Ag_{3.5}P_6Si_{9.5}Ge_2$ BMG has been found to be the toughest material yet developed [6]. Despite this significant variation in the mechanical performance of BMGs however, they are generally considered to all be describable by the same universal rules and trends. Taking such an approach may mean that fundamental differences in their nature are being over-looked.

Brown and Ashby [7] and Frost and Ashby [8] have used the concept of the normalization of data to enable a fairer comparison of different material systems. By doing

so, it is possible to isolate both obvious and subtle physical trends between materials with non-identical structure and bonding. Such an approach was applied when considering the transport (diffusional) properties of various classes of materials via a temperature based normalization [7] and for comparing different semiconductor types [9]. Frost and Ashby [8] went on to define relationships between elastic moduli and the melting temperature, T_m, via the empirical relationship,

$$M = \frac{bk_bT_m}{\Omega}$$

(5.1)

where M is the modulus of interest, k_b the Boltzmann constant, Ω the atomic volume and b a constant of proportionality. The k_bT_m/Ω parameter used here originates from studies into the effect of phonon vibrations (and electrons at low temperatures) impeding the propagation of a dislocation through a crystal [10]. The resulting effect can be quantified by the drag coefficient, D, where ω_A is the atomic vibration frequency:

$$D \approx \frac{k_bT}{\Omega\omega_A}$$

(5.2)

Since k_bT_m/Ω will be constant for a certain material, it is the effect that phonon scattering has on atomic vibrations that determines D, and is a temperature based normalisation as dislocation movement will be highly dependent on temperature, through T itself in Equation 5.2 and the concurrent effect a temperature change will have on ω_A.

When M was taken as being the shear modulus, G, b was compared for different material classes with values ranging between 20 for highly deformable body centred cubic (BCC) alkali metals up to 95 for brittle simple oxides [8]. Hence, b was suggested as an appropriate parameter for separating out classes of materials with similar structure and bonding, causing similar mechanical and transport behavior. These material classes are termed isomechanical groups. In this chapter it is analysed whether it is possible to define classes of BMGs based on intrinsic toughness by considering: 1) proportionality between G and Young's modulus, E, and 2) the presence of distinct isomechanical groups, as per Frost and Ashby. The implications this may have on deviation in structure and bonding and the resulting deformation response will be discussed.

5.2. Data collection

Table 5.1 presents data for a range of metallic glasses reported in the open literature, representing a broad range of alloy chemistries. Much of this data has been sourced from tables in [11,12], though the original references are provided here. Alloys have been grouped according to their ability to resist fracture, via the use of Poisson's ratio, v, with three defined groups: I) $v \leq 0.33$, II) $v = 0.331 - 0.379$, and III) $v \geq 0.38$. v was chosen as the separating parameter for three reasons: 1) the intrinsic toughness of metallic glass is known to correlate with v, 2) elastic moduli of metallic glass can be determined with a high degree of accuracy via ultrasonic pulser-receiver methods and resonant ultrasound spectroscopy, and 3) elastic moduli are widely reported, allowing for a large data set to be used. To extend the study away from metallic glasses only, and provide a point of comparison, extensive data for a series of annealed Li borate glasses are also collated in Table 5.2 [13].

Table 5.1. Data for a range of BMGs in the literature.

	Alloy	M_m (g/mol)	ρ (g/cm^3)	T_g (K)	E (GPa)	G (GPa)	B (GPa)	ν	*Ref.*
Group I ($\nu \le 0.34$)	$Fe_{61}Mn_{10}Cr_4Mo_6Er_1C_{15}B_6$	51.52	6.89	870	193	75	146	0.280	30,39
	$Fe_{70}P_{10}C_5B_5Si_3Al_5Ga_2$	46.9	6.24	736	149.7	58.5	113.4	0.280	31
	$Mg_{65}Cu_{25}Y_{10}$	40.6	3.978	402	51.3	19.6	44.71	0.309	32-34
	$Mg_{65}Cu_{25}Tb_{10}$	47.4	3.98	414	51.3	19.6	44.7	0.309	31,35
	$Ce_{70}Al_{10}Ni_{10}Cu_{10}$	113.00	6.67	359	30.3	11.5	27	0.313	36
	$Nd_{60}Fe_{20}Co_{10}Al_{10}$	106.31	7.0	493	51.2	19.44	46.54	0.317	31,35,37
	$Ho_{39}Al_{25}Co_{20}Y_{16}$	97.08	6.5	630	69.1	26.2	63.6	0.319	31
	$Mg_{65}Gd_{10}Cu_{25}$	47.41	4.04	428	49.1	18.6	46.3	0.320	39
	$Fe_{53}Cr_{15}Mo_{14}Er_1C_{15}B_6$	54.95	6.92	860	195	75	180	0.320	39
Group II ($\nu = 0.341 - 0.379$)	$Ni_{40}Ti_{17}Zr_{28}Al_{10}Cu_5$	63.04	6.48	862	127.6	47.3	140.7	0.349	38
	$Zr_{55}Al_{19}Co_{19}Cu_7$	70.95	6.2	733	101.7	37.6	114.9	0.352	39
	$Zr_{41.2}Ti_{13.8}Ni_{10}Cu_{12.5}Be_{22.5}$	60.03	5.9	618	95	34.1	114.1	0.352	39-41
	$Zr_{41}Ti_{14}Cu_{12.5}Ni_{10}Be_{22.5}$	59.9	6.12	627	101.2	37.4	114.7	0.353	32,33,35
	$Cu_{57.5}Hf_{27.5}Ti_{15}$	92.80	9.91	729	103	37.3	117.5	0.356	39
	$Cu_{50}Hf_{43}Al_7$	110.41	11.0	774	113	42	132.8	0.358	39
	$Zr_{46.75}Ti_{8.25}Cu_{7.5}Ni_{10}Be_{27.5}$	59.5	6.01	590	95.7	35.2	113.38	0.359	31,37,42
	$Ni_{45}Ti_{20}Zr_{25}Al_{10}$	61.49	6.4	791	109.3	40.2	129.6	0.359	38
	$Cu_{46}Zr_{46}Al_8$	73.3	7.23	701	93.7	34.3	116.4	0.366	31
	$Zr_{48}Nb_8Ni_{12}Cu_{14}Be_{18}$	68.78	6.7	620	93.9	34.3	118	0.367	41
	$Zr_{65}Al_{10}Ni_{10}Cu_{15}$	77.4	6.75	653	83.0	30.27	106.65	0.370	31,37
	$Zr_{55}Ti_5Cu_{20}Ni_{10}Al_{10}$	73.84	6.62	625	85	31	118	0.375	43
	$Zr_{57.5}Nb_5Cu_{15.4}Ni_{12}Al_{10}$	76.63	6.5	663	84.7	30.8	117.6	0.379	39
Group III ($\nu \ge 0.38$)	$Ni_{64}Pd_{16}P_{20}$	61.3	8.75	587	105.8	37.9	169.8	0.396	31,35
	$Pd_{39.1}Ni_{10.1}Cu_{29.9}P_{20.9}$	73	9.2	576	98.3	35.2	158.7	0.397	39
	$Pd_{39}Ni_{10}Cu_{30}P_{21}$	72.9	9.152	586	98.1	35.1	159.1	0.397	31,35
	$Pd_{40}Cu_{40}P_{20}$	74.18	9.3	548	93	33.2	158	0.402	41
	$Pd_{48}Ni_{32}P_{20}$	76	9.83	590	101.7	36.2	176.7	0.404	31,35
	$Pd_{64}Ni_{16}P_{20}$	83.69	10.1	452	91.9	32.7	166	0.405	44
	$Au_{49.5}Ag_{5.5}Pd_{2.3}Cu_{26.9}Si_{16.3}$	127.55	11.6	405	74.4	26.5	132.3	0.406	45
	$Pd_{77.5}Cu_6Si_{16.5}$	90.92	10.4	635	89.7	31.8	166	0.409	44
	$Au_{55}Cu_{25}Si_{20}$	129.84	12.2	348	69.8	24.6	139.8	0.417	45
	$Pt_{60}Ni_{15}P_{25}$	133.60	15.7	488	96.1	33.8	202	0.422	46
	$Pt_{57.5}Cu_{14.7}Ni_{5.3}P_{22.5}$	131.59	15.02	49	94.8	33.3	198.7	0.423	47

Table 5.2. Molar mass, M_m, density, ρ, glass transition temperature, T_g, Young's modulus, E, shear modulus, G, bulk modulus, B, and Poisson's ratio, v, for Li borate glasses xLiO$_2$(1-x)B$_2$O$_3$ (all data from [13]).

x	M_m (g/mol)	ρ (g/cm^3)	T_g (K)	E (GPa)	G (GPa)	B (GPa)	v
0	69.62	1.84	520	16.9	6.6	12.8	0.281
0.02	68.79	1.87	526	20.2	7.9	15.3	0.280
0.04	67.96	1.90	535	23.1	9.0	17.6	0.281
0.06	67.15	1.92	557	26.5	10.4	19.5	0.274
0.08	66.34	1.95	600	30.5	11.9	23.2	0.280
0.10	65.53	1.99	617	35.1	13.8	26.3	0.277
0.12	64.70	2.02	639	39.7	15.5	29.5	0.276
0.14	63.94	2.05	672	44.0	17.2	32.8	0.277
0.16	63.16	2.07	694	48.4	19.0	35.9	0.275
0.18	62.38	2.10	719	52.8	20.6	40.0	0.280
0.20	61.63	2.13	745	57.8	22.6	43.1	0.277
0.22	60.85	2.15	758	63.0	24.7	46.7	0.275
0.24	60.04	2.18	763	68.4	26.9	50.1	0.272
0.262	59.20	2.20	768	73.5	28.91	53.4	0.271
0.28	58.45	2.23	769	77.9	30.7	56.2	0.269

To consider the apparent equivalence of plastic strain and v, Figure 5.1 presents a Blackman diagram for the metallic glasses in Table 5.1 and Li borates in Table 5.2, using the groupings presented here.
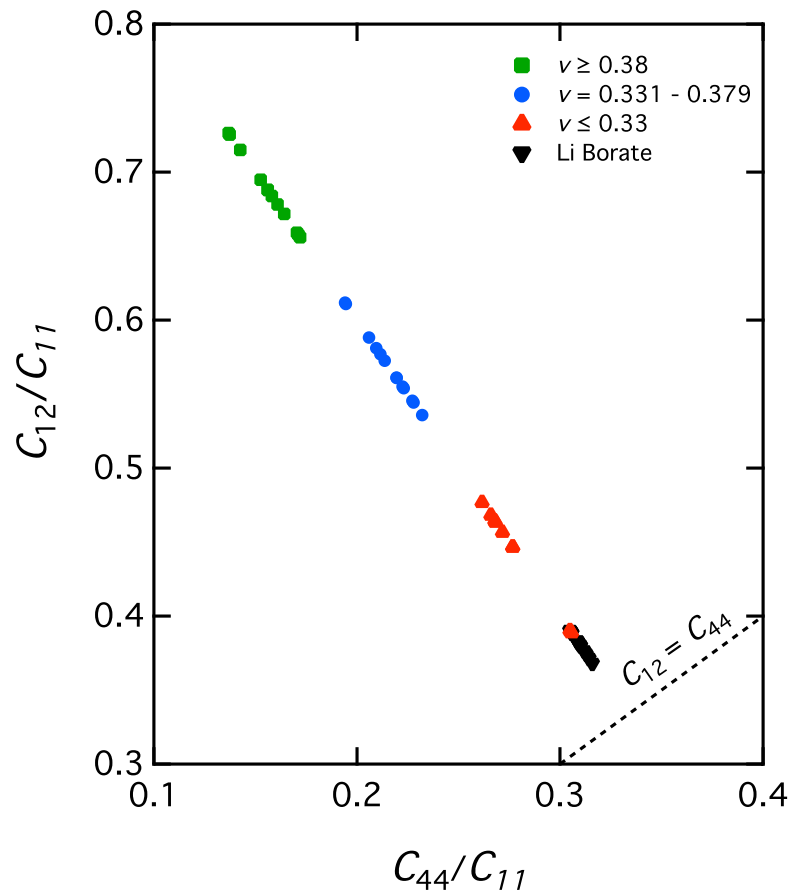
Figure 5.1. Blackman diagram for metallic glasses in Table I, grouped according to their Poisson's ratio, ν, and for Li borate glasses in Table 5.2.

Comparison of this figure with Figure 4.1 in Chapter 4 reveals an equivalency between the extent of plastic strain and the magnitude of ν; plastic and high ν alloys congregate at low values of C_{44}/C_{11} and high C_{12}/C_{11} with the opposite true for brittle metallic and oxide glasses. The strong groupings in Figure 5.1 result from mathematical relationships between moduli and demonstrate that the defined boundaries are justified for the glasses in Table 5.1 and 5.2.

5.3. Results

5.3.1. Correlation between shear and Young's modulus

It is known in solid materials that G and E can typically be related by $G=0.375E$ [48]. It has additionally been demonstrated that proportionality exists between G and E in polycrystalline metals specifically, where the relationship $G=0.39E$ was fitted to data for a

range of face centered cubic (FCC), body centered cubic (BCC) and hexagonal close packed (HCP) metals [49]. A theoretical consideration of the proportionality constant, b, by use of a simple two-body central-force interatomic potential showed that b had values of 0.396 and 0.367 for FCC and BCC metals respectively, indicating that subtle differences may in fact exist [49]. In Figure 5.2 G has been plotted versus E for the BMGs in Table 5.1, suggesting the relationship $G = 0.383E$.
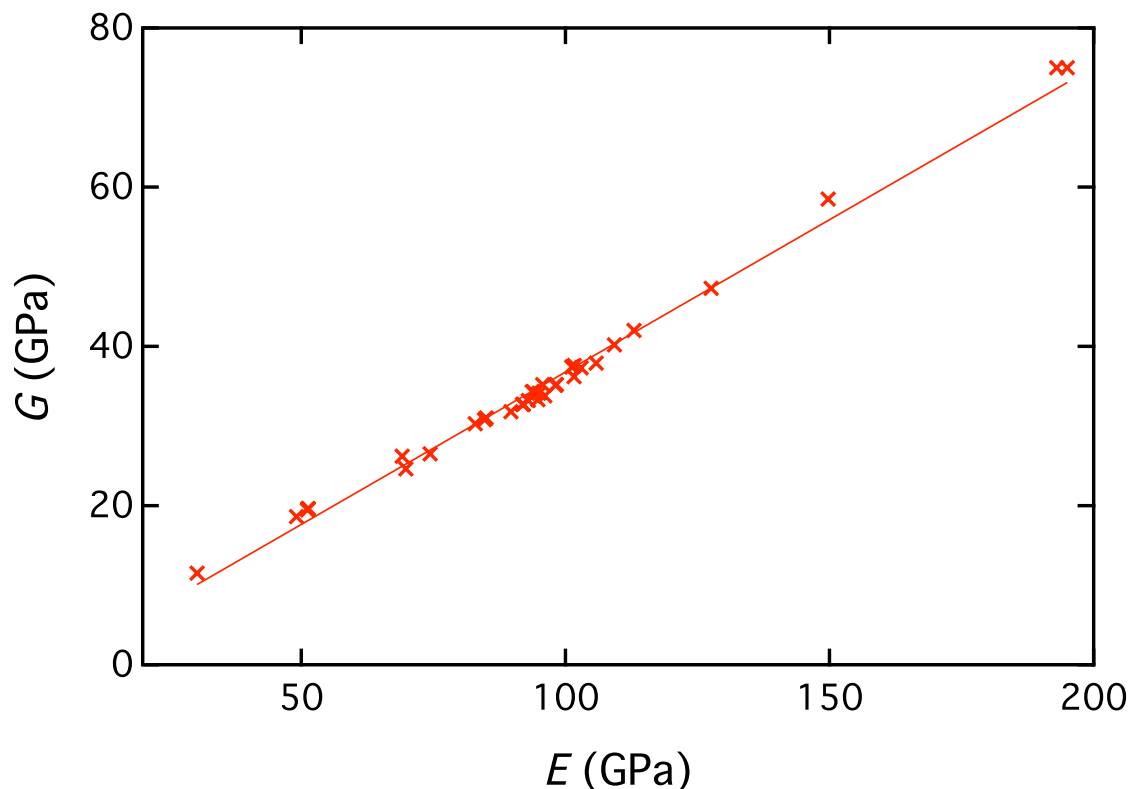
Figure 5.2. Variation in G as a function of E for the BMGs in Table 5.1. A straight line fit to the data yields the relationship $G = 0.383E$.

Such an expression appears suitable due to there being very strong correlation. However, given that $\nu = (E/2G)-1$, if the ratio G/E were the same for all glasses then ν would be constant. This is not true and so G/E must vary with ν. Figure 5.3 plots G versus E for the metallic groups in Table 5.1 and the Li borate series in Table 5.2.
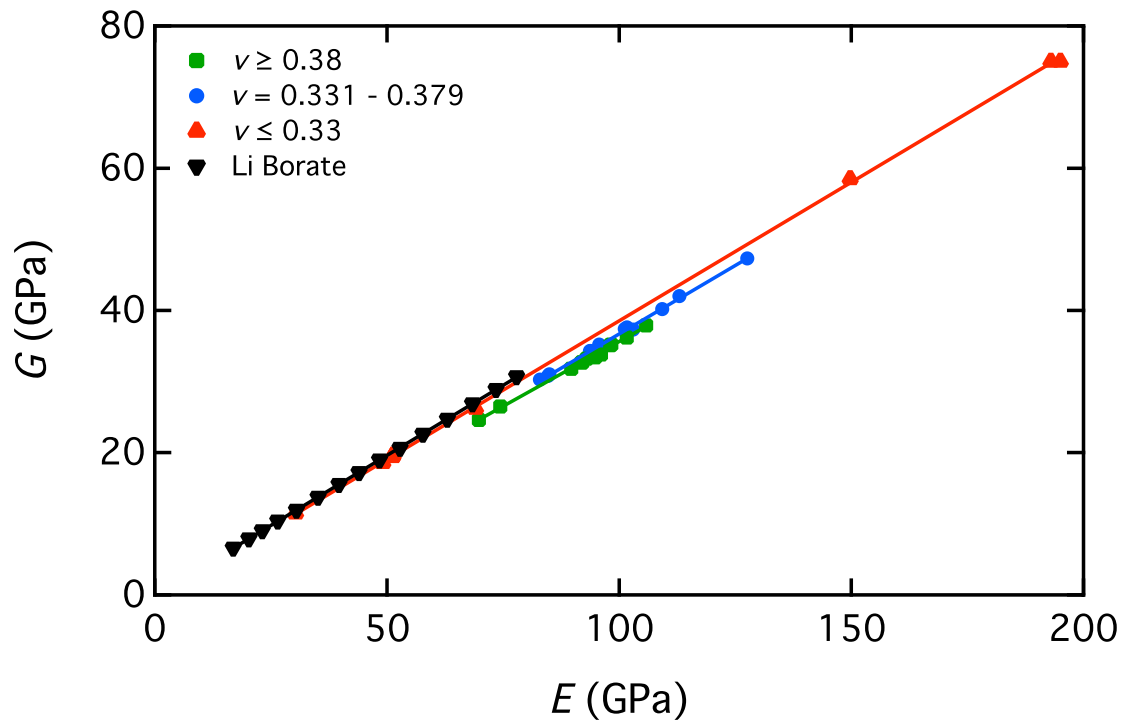
Figure 5.3. Plot of *G* versus *E* for the metallic glass groups in Table 5.1 and Li borate glasses in Table 5.2.

It can be seen here that subtle variation in gradient, *b*, may exist here; Table 5.3 reports *b* for each series and the correlation coefficient, *r*, which has a high value of at least 0.998 in all cases, indicating good data fitting. The value of *b* decreases as the tendency towards tougher behaviour is favoured; the Li borate group has the largest *b* while group III of the metallic glasses ($v \geq 0.38$) has the lowest.

Table 5.3. Gradient, b, correlation coefficient, r, and probability, p, from Figure 5.3 for the elastic groups: Li borate glasses, Group I ($v \leq 0.33$), Group II ($v = 0.331 - 0.379$) and Group III ($v \geq 0.38$).

Elastic group	b	r	p
Li borate	0.394 ± 0.0000	0.999	$<10^{-7}$
I	0.390 ± 0.0018	0.999	$<10^{-7}$
II	0.385 ± 0.0070	0.998	$<10^{-7}$
III	0.363 ± 0.0059	0.999	$<10^{-7}$

A regression analysis of this data has been performed to determine: 1) whether it is justifiable to fit a straight line to the data, and 2) given the apparent scatter, whether b varies enough to conclude that definite groups do exist. Regarding point 1, the probability of the null hypothesis, p, is calculated (that there is no correlation between the data in each group, and so the fitting of a straight line cannot occur) and, by convention, if $p > 0.05$ then the null hypothesis cannot be rejected. From Table 5.3 it is apparent that the null hypothesis can be rejected in all instances. To determine whether differences in b are meaningful, an analysis of covariance (ANCOVA) is typically applied to compare two data sets. This tests the null hypothesis that two data sets are not statistically different and if $p > 0.05$ then the hypothesis is not rejected. In Table 5.4 p only exceeds 0.05 when comparing Group I with both Li borates and Group II.

Table 5.4. Results of ANCOVA analysis for G versus E plots in Figure 5.2 for material groups: Li borate glasses, Group I ($v \leq 0.33$), Group II ($v = 0.331 - 0.379$) and Group III ($v \geq 0.38$).

Elastic groups	p
Li borate – I	0.46
Li borate – II	3.1×10^{-2}
Li borate –III	3.0×10^{-7}
I – II	0.29
I – III	3.1×10^{-3}
II - III	2.0×10^{-2}

The variation in *b* between each group can be considered real in most instances therefore and *G/E* is an indicator of the intrinsic toughness of a glass. Though *v* will be alloy dependent it is clear that by considering the glasses in Table 5.1 and Table 5.2, specific values of *b* do exist for each group.

5.3.2. Isomechanical groups

Whereas k_bT_m/Ω has been applied to construct isomechanical groups based on elastic moduli in the past [8], this has been done for materials that are non-glassy, where a breakdown in moduli occurs above T_m and mechanical rigidity is lost. For amorphous materials however, viscous flow can commence at T_g and so here we use this as the characteristic temperature instead of T_m. Atomic volume, Ω, is calculated by determining the molar volume, V_m, ($V_m = M_m/\rho$) and from Avogadro's number, N_v, ($\Omega = V_m/N_v$), resulting in the average atomic volume of one atom. Figure 5.4 plots k_bT_g/Ω versus *E*, *G* and *B* for the glass groups in Table 5.1 and Table 5.2, with data from the regression analysis in Table 5.5.
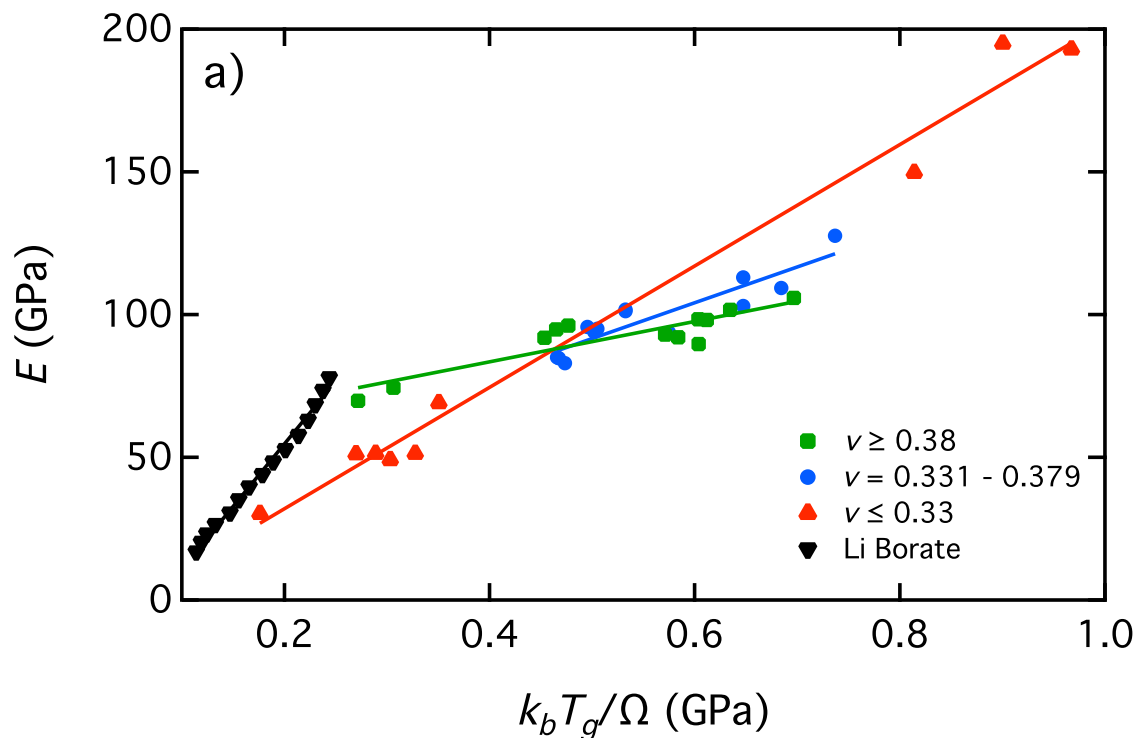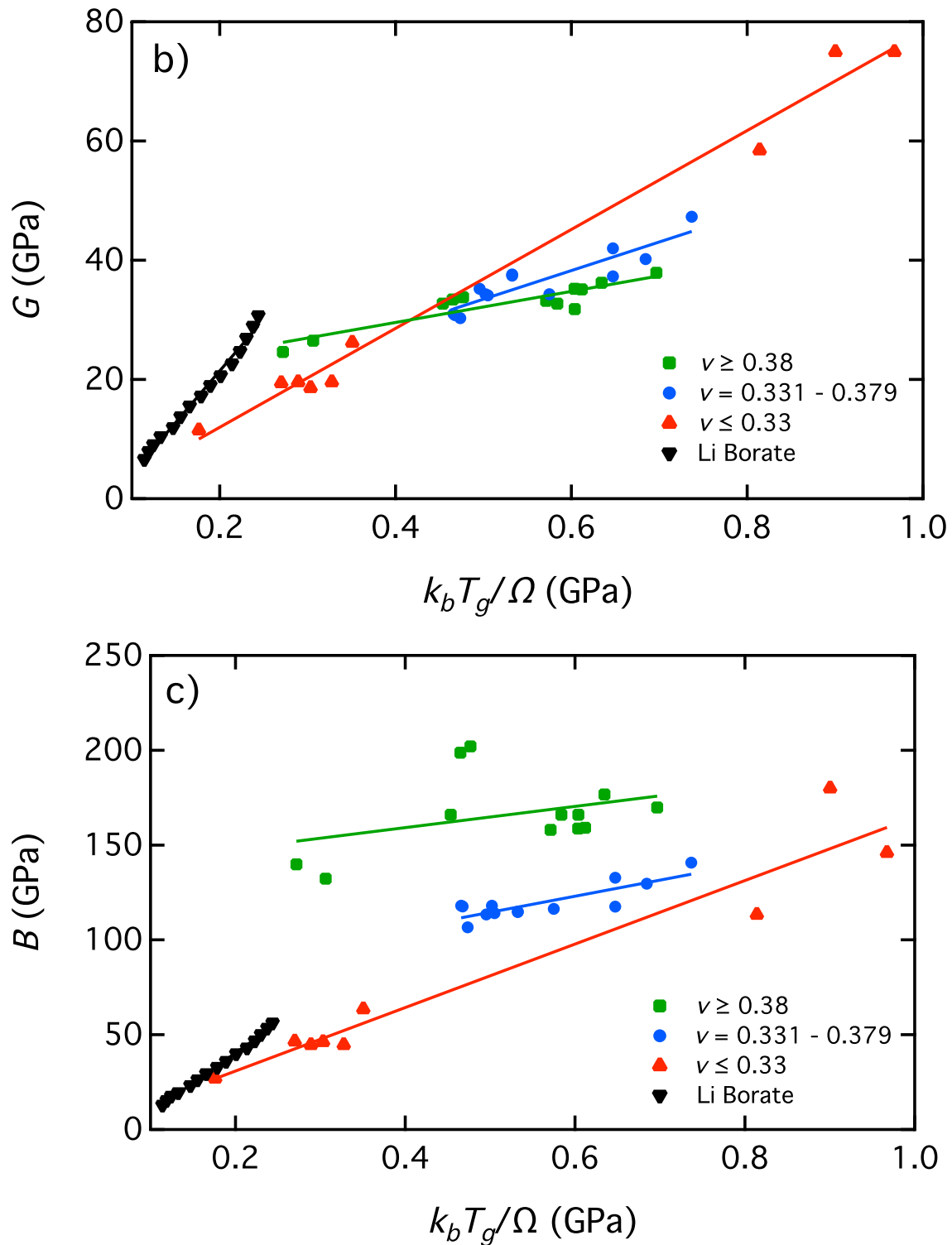
Figure 5.4. Plot of Young's modulus, *E*, (3a), shear modulus, *G*, (3b) and bulk modulus, *B*, (3c) versus k_bT_g/Ω, for the metallic glass groups in Table 5.1 and Li borate glasses in Table 5.2.

Table 5.5. Results of linear regression analysis for material groups: Li borate glasses, Group I ($v \leq 0.33$), Group II ($v = 0.331 - 0.379$) and Group III ($v \geq 0.38$). *c*, *b*, *r* and *p* are (respectively) the *y*-axis intercept, gradient, regression value and probability of the null hypothesis.

Elastic group	c (GPa)	b	r	p
Young's Modulus (E)				
Li borate	-33.0 ± 2.1	438.5 ± 11.6	0.995	$<10^{-7}$
I	-10.6 ± 5.5	212.6 ± 9.8	0.993	$<10^{-7}$
II	28.8 ± 9.8	125.6 ± 17.2	0.910	1.0×10^{-5}
III	55.1 ± 6.1	69.1 ± 13.1	0.892	5.0×10^{-5}
Shear modulus (G)				
Li borate	-13.1 ± 0.9	172.8 ± 4.8	0.995	$<10^{-7}$
I	-4.6 ± 2.0	83.0 ± 3.5	0.994	$<10^{-7}$
II	9.5 ± 4.0	48.0 ± 7.0	0.901	1.8×10^{-5}
III	19.1 ± 2.1	25.3 ± 4.5	0.903	3.0×10^{-5}
Bulk modulus (B)				
Li borate	-23.0 ± 1.1	316.6 ± 6.0	0.998	$<10^{-7}$
I	-2.7 ± 10.2	167.4 ± 18.0	0.962	1.5×10^{-5}
II	72.1 ± 9.6	84.9 ± 17.0	0.834	2.0×10^{-4}
III	136.9 ± 24.4	63.0 ± 52.1	0.363	0.19

It can be seen that it is possible to fit a straight line to each plot for each group of material (as $p < 0.05$) apart from B for Group III, where $p = 0.19$ and so the null hypothesis cannot be rejected in this instance. Table 5.6 presents results of the ANCOVA analysis for comparing metallic glass groups.

Table 5.6. Results of ANCOVA analysis between material groups: Li borate glasses, Group I ($v \leq 0.33$), Group II ($v = 0.331 - 0.379$) and Group III ($v \geq 0.38$).

Elastic group	p
Young's Modulus (E)	
Li borate – I	4.0×10^{-7}
Li borate – II	$<10^{-7}$
Li borate –III	$<10^{-7}$
I - II	7.0×10^{-4}
I - III	1.5×10^{-7}
II - III	6.8×10^{-3}
Shear modulus (G)	
Li borate – I	$<10^{-7}$
Li borate – II	$<10^{-7}$
Li borate –III	$<10^{-7}$
I - II	4.0×10^{-4}
I - III	3.0×10^{-3}
II - III	5.0×10^{-3}
Bulk modulus (B)	
Li borate – I	7.7×10^{-3}
Li borate – II	$<10^{-7}$
Li borate –III	2.9×10^{-3}
I - II	1.8×10^{-2}
I - III	0.46
II - III	0.30

From this data p is well below 0.05 when comparing all systems with regard to E and G, so it is possible to define these classes as distinct isomechanical groups. For B, p is below 0.05 in all instances apart from when comparing Group I and II with Group III. The issue here results from it not being possible to fit a straight line which accurately describes the trend for Group III, resulting in a low r of 0.363. Due to the scatter in Group III then, primarily caused by the two Pt-based alloys, less distinct isomechanical groups exist when considering B though it is

clear that the Li borates, Group I and Group II can all be statistically separated from one another.

For *E*, *G* and *B*, the value of *b* decreases as the tendency towards tougher behavior increases; this behaviour is shown in Figure 5.5 in comparison to other materials. It can be seen that when *G* is taken as the material parameter, *b* was determined as 20 for BCC alkali metals and 95 for oxides. Here we find *b* = 25 for Group III and *b* = 83 for Group I.
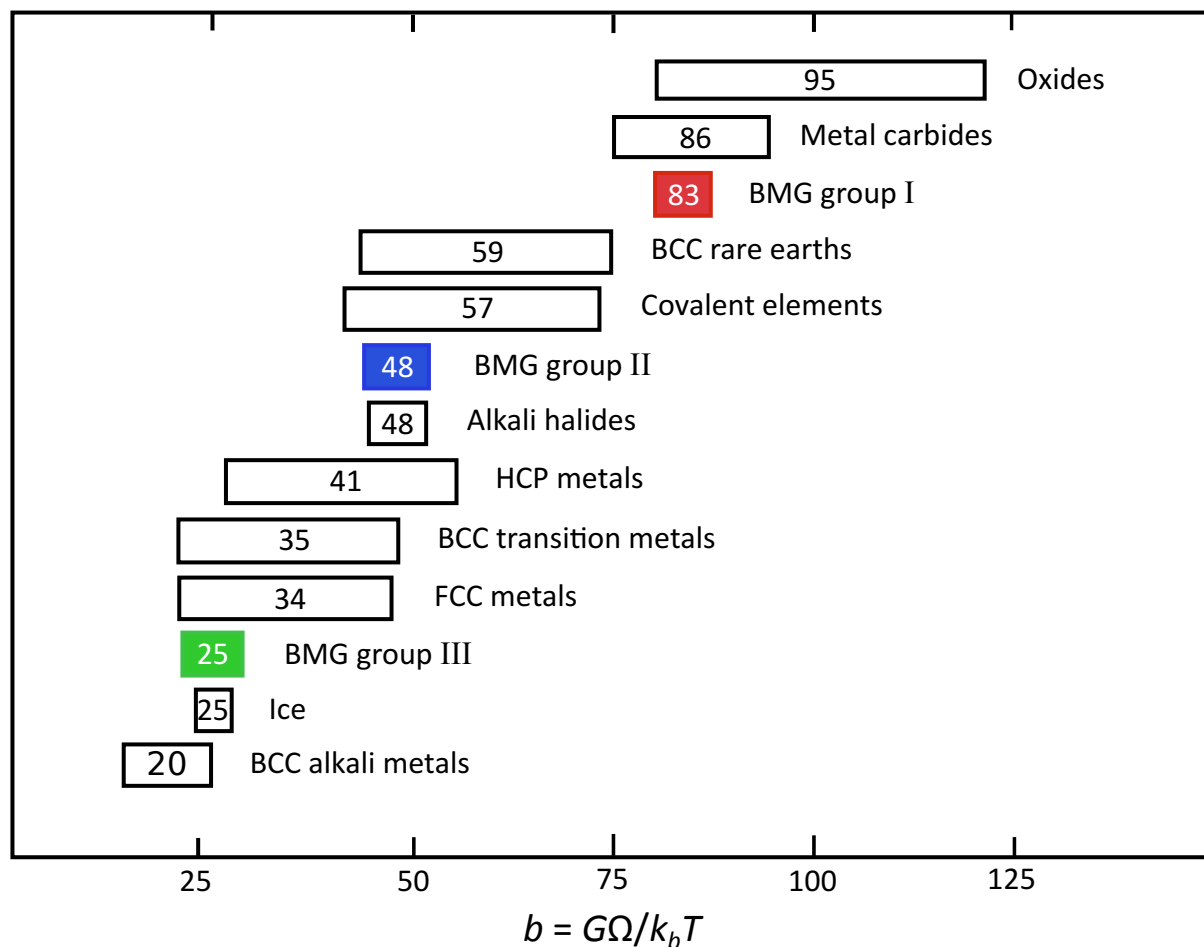

$$b = G\Omega/k_b T$$

Figure 5.5. Comparison of *b* with values reported in [8] for isomechanical groups of various materials (width of the bar indicates spread in data).

The analysis performed here agrees with low *b* corresponding to intrinsically more deformable materials, as alkali metals are known to be more resistant to crack propagation than oxides and it is noted that a large range in *b* exists within metallic glass, comparable to that shown between malleable alkali metals and brittle oxides.

5.4. Discussion

An isomechanical group is defined as a group of materials exhibiting similar transport and mechanical behaviour. These arise due to distinct differences in both structure and bonding. It would be anticipated that materials with pronounced differences in atomic interaction (covalent, ionic, wan der Waals etc.) and crystal structure should lie in different groups, and this justifies why the covalently bonded Li borates can be readily separated from each metallic glass group with respect to E, G and B. It is remarkable then that metallic glasses, which are all generally described by the same structural model i.e. the packing of short-range ordered clusters, and all with metallic bonding, should be present in distinct isomechanical groups. Additionally, the very large range of b with respect to G as the material property is comparable to the difference between alkali metals and oxides (see Figure 5.5). There must therefore exist fundamental differences in atomic packing and metallic bonding of metallic glasses that belong to the different groups.

Non-directional inter-atomic bonding permits rapid relaxation of a stress concentrator since atomic rearrangement readily occurs. Highly directional bonding however, such as covalent bonds in oxide glasses, are much stiffer with strong angularity and a concurrent inability for ease of rearrangement. We have previously used a Blackman diagram [4] to demonstrate that those metallic glasses with largest positive deviation from zero Cauchy pressure, indicating more non-directional bonding, are also the most ductile. Brittle and non-metallic glasses are located much closer to zero Cauchy pressure, or deviate negatively from it, indicating a strong angular component to the bonds. As seen in Figure 5.1 these relationships hold when grouping materials according to v also. These thoughts appear to be in agreement with Chen [15], who suggested that decreasing v may be attributable to a tendency for directional interatomic bonds due to atomic ordering or s-d hybrid bonding in transition metals.

Those alloys with largest v, present in Group III, are generally metal-metalloid glasses, where it is considered that there is strong tendency for directional bonding due to the metalloid influence; this would appear to be at odds with what is being suggested here. Interestingly however, elemental Pd, Pt, and Au are all known to exhibit large positive deviations form zero Cauchy pressure, suggesting that non-directional bonding is a feature of the element on which the glass is based. Moreover, their noticeably large B in comparison to BMGs in other groups would imply incompressibility of the electron gas [16], again suggesting a large number of delocalized electrons. The tight-bond cluster model [17,18] also states that it is the interaction between clusters that controls yielding rather than the short-range order. Therefore the tendency for more covalent-like bonding around a metalloid may not be affecting mechanical behavior since it is the non-directional bonding between noble

metal atoms in adjacent clusters that is critical. When considering differences in bonding between the isomechanical groups considered here then, it is apparent that it is the directionality, and resulting ease of atomic rearrangement, that may be causing differing deformation response.

A conceptual model of the structure of metallic glasses is widely held, involving the packing of SRO icosahedral clusters with a high efficiency, potentially giving rise to some medium range order (MRO) beyond nearest neighbours. By maximizing space filling, the Efficient Cluster Packing (ECP) model is capable of predicting bulk glass forming compositions [19]. The actual atomic scale structure is known to be more complex however, with there being the possibility for SRO units with different coordination numbers, incomplete clusters, atoms located outside of clusters ("glue" atoms) and, more generically, regions high in free volume. These defects have given rise to cluster and glue models [20] as well as the core – shell model [21], in which an elastically soft, loose packed region of clusters is surrounded by a constraining shell. The structure of metallic glasses is therefore diverse with local chemistry and thermal history [22] having an effect. Structure differences are yet to be studied directly as a function of v (or, equivalently, m) making determining the exact structural source of the isomechanical groups found here problematic.

A direct indicator of the extent of local topological strain can be calculated from b, through Egami's local topological instability condition (e.g. [23, 24]) for the dense random packing (DRP) of atoms. Here, for a change in coordination number (N_c) of 0.5 to occur, an 11 % volumetric strain, $\varepsilon_v^{T,crit}$, is required in the surroundings. Instability occurs, meaning the topological structure is not favored, and N_c may change, if the volumetric strain, ε_v^{T}, is above or below 11%, termed liquid-like and solid-like sites respectively. ε_v^{T} can be calculated at T_g from Equation 5.3, where R is the gas constant:

$$E = \frac{9RT_g(1-v)}{4V_m\left(\varepsilon_v^{T}\right)^2}$$

(5.3)

Since $k_b T_g/\Omega$ is equivalent to RT_g/V_m, the gradient of each isomechanical group, b, determined in this study can be used to calculate ε_v^{T} by equating Equation 5.1 with 5.3, when M is taken as E:

$$\varepsilon_v^{T} = \sqrt{\frac{9(1-v)}{4b}}$$

(5.4)

As isomechanical groups are defined by changes in *b*, Equation 5.4 provides a physical basis as to why isomechanical groups exist in BMGs. This calculation for each isomechanical group were performed using *b* from Table 5.5 and the average *v* for all the data in each group (0.276, 0.307, 0.361 and 0.407 for Li borates, Group I, Group II and Group III respectively); the results can be seen in Table 5.7.

Table 5.7. Volumetric strain, ε_v^T, and fraction of liquid-like sites, *f*, calculated from Equations 5.4 and 5.5.

Elastic group	ε_v^T	*f*
Li borates	6.1 %	11.9 %
I	8.6 %	26.7 %
II	10.7 %	37.5 %
III	13.9 %	49.4 %

ε_v^T increases with the tendency for toughness, and, concurrently, with *m*. Liquid-like sites are associated with ε_v^T values greater than 11 %, and are considered to be unstable [23]; ε_v^T has a value of 13.9 % for Group III and 6.1 % for the Li borates. The fraction of liquid-like sites that exceeds the 11% threshold, *f*, can then be determined through the complementary error function ($CE(y_c) = f$) of Equation 5.5:

$$y_c = \varepsilon_v^{T,crit} / \sqrt{2} \left\langle \left(\varepsilon_v^T \right)^2 \right\rangle^{\frac{1}{2}} \tag{5.5}$$

In Table 5.7 *f* can be seen to increase in higher *m* groups; a direct link appears to exist then between the extent of liquid-like structure (as defined in the topological instability condition), a large *m* and a resultant ability to exhibit tough behavior, embodied by a high *v*. The actual value of *f* at room temperature would be expected to be lower than the values determined in Table 5.7. The trend however will remain the same, with *f* being higher in the more fragile groups. Through the application of the topological instability condition, it can be seen that the structural characteristic that may be varying, and so giving rise to the observation of different isomechanical groups in BMGs determined here, is the liquid-like fraction of sites, where volumetric strain is high, causing structural instability.

It is known that potential energy landscapes (PELs) of fragile glass formers contain a more diverse range of inherent states (IS) in comparison to strong glass formers – this is shown schematically in Figure 5.6.
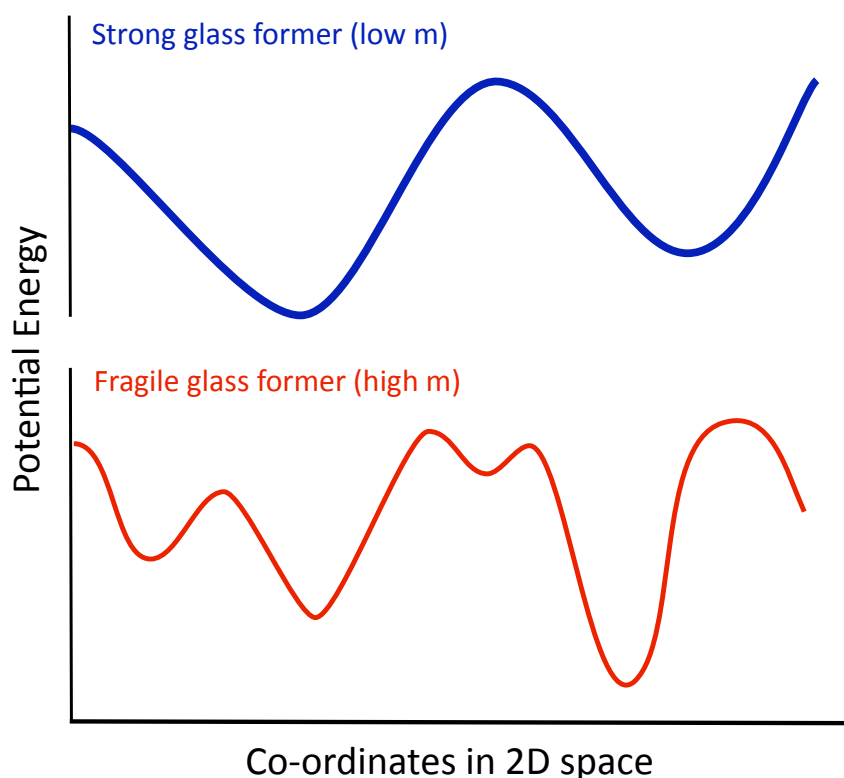

Figure 5.6. Schematic representation of energy landscapes in strong and fragile glasses. Note that barriers between energy wells correspond to α relaxations; inherent states associated with β relaxation events are not shown (Note: α events correspond to mechanical and thermal relaxation at the yield point and glass transition respectively, while β events involve the oscillation and movement of atoms over small distances).

Debenedetti *et al*. [25] point out that the constant activation energy for viscous flow resulting from Arrhenius viscosity-temperature dependence in strong glass formers e.g. SiO_2, would suggest a constant flow mechanism, where equivalent inherent states are sampled as the temperature approaches T_g. Fragile glass formers exhibit a greater range of IS, compared to what is essentially a single basin when the activation energy for flow is constant, suggestive of a greater number of IS as *m* increases. This may account for why the boson peak in fragile glasses (in both metallic and non-metallic systems) is of a lower amplitude than that observed in strong glass formers as when there is a non-homogeneous atomic structure the transverse

phonons that are believed to be the source of the boson peak [26] are more likely to be scattered. Since G is determined by transverse phonon vibrations, and is known to be more sensitive to structure than B is (which is dependent on the electron gas density), it appears logical that the signal from the boson peak in fragile glasses would experience more interference, reducing its magnitude. This enhanced range of IS may be beneficial as under shear loading energy landscapes are known to re-align, reducing the magnitude of the energy barrier for a relaxation (yield) event [27]. If the structure is frozen into essentially a single basin with a large activation energy, such as for SiO_2, then it is unlikely the yield barrier is reached before brittle fracture occurs. A fragile glass with a range of inherent states will inevitably contain some sites in the landscape where the barrier is reduced, permitting more favourable conditions for yielding. As it is local elastic moduli that provide the activation barrier for relaxation (proportional to G_iV in the shoving model [28] where G_i is the instantaneous G and V is a temperature insensitive volume) it would be expected that a wide variation in structure would also vary the local elastic moduli.

With regard to the isomechanical groups determined here, it may be that a PEL with a more diverse range of metastable inherent states results in an enhanced range of possible structural configurations with differing tendencies for yield, and that this could be a structural aspect contributing to the observation of isomechanical groups. Understanding how this structural variation as a function of m is realized atomistically is not easily resolved, though the topological instability model suggests that volumetric strain and the resulting number of liquid-like sites could be important. That ε_v^T and f increases with m would additionally support the idea that a more diverse energy landscape should be present in fragile glasses. It may be anticipated that this results to some extent from a breakdown in the ordered packing of atoms, such as the previously mentioned incomplete icosahedra and regions high in free volume, which can interact with their surroundings, causing local fluctuations in modulus and tendency for yielding. As the tight-bond cluster model [18] suggests it is interactions between short-range ordered clusters that controls yielding rather than the atoms within them, this particular structural aspect may be critical i.e. how clusters fill space and the effect this has on inter-cluster bonding. We additionally note that this model seems to be supported by high energy x-ray scattering studies, where it was found that more strain is accommodated beyond nearest neighbor length scales than is within them during compressive loading below the yield point [29], suggesting that yielding is not controlled by short-range order configuration and bonding. Interactions beyond the nearest neighbour could more accurately determine the macroscopic elastic modulus also, as calculations based on short range interactions resulted in an over estimate [29]. Although further experimental work is required to understand and directly probe glass structure as a function of m, the presence of isomechanical groups within metallic glasses suggests real differences in both structure and bonding and implies that

metallic glasses may not all be characterizable by a single structural model or possessed of identical bonding.

5.5. Conclusion

The main findings of Chapter 5 can be summarised as follows:

• Isomechanical groups are classes of material with similar deformation and transport properties, resulting from similarities in both structure and bonding.

• By plotting elastic moduli versus the $k_b T_g/\Omega$ parameter it is apparent that isomechanical groups exist within BMGs when grouping them according to their intrinsic ability for toughness, which can be quantified via their Poisson's ratio. This result is found to be statistically valid in the case of E and G, with less defined groups existing when B is the modulus of interest. That isomechanical groups exist explains why BMGs span a large data range in the Blackman diagrams of Chapter 4.

• By comparing the coefficient constants of the different BMG groups with those of other material classes it is apparent that large differences in behaviour should be observed; this is known to be true since the fracture toughness of BMGs range from those of brittle oxide glasses to tough Pd- and Pt-based alloys.

• The fundamental structure and bonding characteristics of BMGs must be non-similar for isomechanical groups to exist – it is suggested that bond directionality is one source of this, with there being more non-directional bonding (i.e. non-central forces) in the toughest BMGs and bonds and a strong angular nature in the brittle group.

• Variation in structure between the groups is not simple to resolve. Because intrinsic ability for permanent deformation correlates with fragility however it is possible to consider variation in structure as a function of this. This is performed in two ways: 1) the fraction of liquid-like sites, as mathematically determined from Egami's topological instability model, which is higher in the tougher groups and 2) through a qualitative discussion in the tendency for fragile glasses to exhibit a more diverse potential energy landscape. Both these aspects may be expected to lead to a more diverse structure in fragile glasses and, by application of the tight-bond cluster model, this structural inhomogeneity may be accommodated between short range ordered units.

- Finally, the presence of isomechanical groups within BMGs suggests that there may be subtle differences in relationships between physical trends of BMGs in different groups, and so they may not necessarily all be characterizable by a single mathematical formulae, model or rule.

5.6. References

[1]   J. J. Lewandowski, W. H. Wang, and A. L. Greer, Philos. Mag. Lett. **85**, 77 (2005).

[2]   J. D. Plummer, I. A. Figueroa, R. J. Hand, H. A. Davies, and I. Todd, J.Non-Cryst. Solids **355**, 335 (2009).

[3]   Y. Zhang and A. L. Greer, J. Alloy & Comp. **434**, 2 (2007).

[4]   J. D. Plummer and I. Todd, Appl. Phys. Lett. **98**, 021907 (2011).

[5]   M. Born, J. Chem. Phys. **7**, 591 (1939).

[6]   M. D. Demetriou, M. E. Launey, G. Garrett, J. J. Schramm, D. C. Hofmann, W. L. Johnson and R. O. Ritchie, Nature Mater. **10**, 123 (2011).

[7]   A. M. Brown and M. F. Ashby, Acta Metall. **28**, 1085 (1980).

[8]   H. J. Frost and M. F. Ashby, *Deformation-mechanism Maps* (Pergammon Press, Oxford, 1982)

[9]   B. Derby, Phys. Rev. B **76**, 054126 (2007).

[10]   U. F. Kocks, A. S. Argon and M. F. Ashby, *Thermodynamics and kinetics of slip*, (Pergammon Press, Oxford, 1975).

[11]   W. L. Johnson and K. Samwer, Phys. Rev. Lett. **95**, 195501 (2005).

[12]   M. Jiang and L. Dai, Phys. Rev. B **76**, 054204 (2007).

[13]   M. Kodama and S. Kojima, J. Therm. Analy. & Calorim. **69**, 961 (2002).

[14]   J. D. Plummer, R. Goodall, I. A. Figueroa, and I. Todd, J. Non-Cryst. Solids **357**, 814 (2011).

[15]   H. S. Chen, J. Appl. Phys. **49**, 1 (1978).

[16]   J. Gilman, *Electronic basis of the strength of metals* (Cambridge University Press, Cambridge, 1973).

[17]   C. Fan, P. K. Liaw, V. Haas, J. J. Wall, H. Choo, A. Inoue and C. T. Liu, Phys. Rev. B **74**, 014205 (2006).

[18]   C. Fan, P. K. Liaw and C. T. Liu, Intermet. **17**, 86 (2009).

[19]   D. B. Miracle, Acta. Mater. **54**, 16 (2006).

[20]   C. Dong, Q. Wang, J. B. Qiang, Y. M. Wang, N. Jiang, G. Han, Y. H. Li, J. Wu and J. H. Xia, J. Phys. D: Appl. Phys. **40**, R273 (2007).

[21]   J. C. Ye, J. Lu, C. T. Liu, Q. Wang and Y. Yang, Nature Mater. **9**, 619 (2010).

[22]   Y. Q. Cheng, A. J. Cao and E. Ma, Acta Mater. **57**, 3253 (2009).

[23]   T. Egami, S. J. Poon, Z. Zhang and V. Keppens, Phys. Rev. B **76**, 024203 (2007).

[24]   T. Egami, J. Alloy & Comp. **509S**, S82 (2011).

[25]   P.G. Debenedetti, F.H. Stillinger, Nature **410**, 259 (2001).

[26]   H. Shintani and H. Tanaka, Nature Mater. **7**, 870 (2008).

[27]   D. L. Melandro and D. J. Lacks, J. Chem. Phys. **110**, 4593 (1999)

[28]   J. C. Dyre, N. B. Olsen, and T. Christensen, Phys. Rev. B **53**, 2171 (1996).

[29]   T. C. Hufnagel and R. T. Ott, Phys. Rev. B **73**, 064204 (2006).

[30]   V. Ponnambalam, S. J. Poon, and G. J. Shiflet, J. Mater. Res. **19**, 3046 (2004); **19**, 1320 (2004).

[31]   W. H. Wang, J. Non-Cryst. Solids **351**, 1481 _2005_; J. Appl. Phys. **99**, 1 (2006).

[32]   L. Battezzati, Mater. Trans. **46**, 2915 (2005).

[33]   L. N. Hu, X. F. Bian, W. M. Wang, G. R. Liu, and Y. B. Jia, J. Phys. Chem. B **109**, 13737 (2005).

[34]   D. N. Perera, J. Phys.: Condens. Matter **11**, 3807 (1999).

[35]   V. N. Novikov and A. P. Sokolov, Phys. Rev. B **74**, 064203 (2006).

[36]   B. Zhang, M. X. Pan, Q. Zhao, and W. H. Wang, Appl. Phys. Lett. **85**, 61 (2004).

[37]   Y. Kawamura, T. Nakamura, H. Kato, H. Mano, and A. Inoue, Mater. Sci. Eng., A **304**, 674 (2001).

[38]   D. H. Xu, G. Duan, and W. L. Johnson, Acta Mater. **52**, 3493 (2004).

[39]   J. Lu, G. Ravichandran, and W. L. Johnson, Acta Mater. **51**, 3429 (2003).

[40]   H. Bruck, T. Christman, A. J. Rosakis, and W. L. Johnson, Scr. Metall. Mater. **30**, 429 (1994); also F. Szuecs, C. P. Kim, and W. L. Johnson, Acta Mater. **49**, 1507 (2001).

[41]   Y. Zhang, D. Q. Zhao, R. J. Wang, and W. H. Wang, Acta Mater. **51** (1971) (2003); also W. H. Wang, C. Dong, and C. H. Shek, Mater. Sci. Eng., R **44**, 45 (2004).

[42]   Y. Zhao, X. F. Bian, K. B. Yin, J. K. Zhou, J. Y. Zhang, and X. X. Hou, Physica B **349**, 327 (2004).

[43]   Y. X. Wei, B. Zhang, R. J. Wang, M. X. Pan, D. Q. Zhao, and W. H. Wang, Scr. Mater. **54**, 599 (2006).

[44]   B. Golding, B. G. Bagley, and F. S. L. Hsu, Phys. Rev. Lett. **29**, 68 (1972).

[45]   J. Schroers, B. Lohwongwatana, A. Peker, and W. L. Johnson, Appl. Phys. Lett. **87**, 061912 (2005).

[46]   H. S. Chen, J. T. Krause, and E. Coleman, J. Non-Cryst. Solids **18**, 157 (1975).

[47]   J. Schroers and W. L. Johnson, Appl. Phys. Lett. **84**, 3666 (2004); also Phys. Rev. Lett. **93**, 255506 (2004).

[48]   C. Zwikker, Physical Properties of Solid Materials, Pergamon Press, London, 1954, p. 90.

[49]   H. M. Ledbetter, Mat. Sci. Eng. A **27**, 133-136 (1977).

6. Mechanical heterogeneity in as-cast bulk metallic glass rods

6.1. Introduction

The mechanism through which bulk metallic glasses (BMGs) yield involves the co-operative shearing of a local atomic environment, proposed to be of the order of 100 atoms, termed shear transformation zones (STZs) [1]. The shear modulus, G, is believed to provide the principal barrier to this event, although, based on models for shear in an amorphous granular material where a small dilatational strain is exerted on the surroundings, the bulk modulus, B also would be expected to provide a contribution to the activation energy [2]. A band of reduced viscosity subsequently propagates from the STZ, allowing for plastic deformation, before void formation occurs in the band [3], developing into a crack and causing failure. As plasticity is mediated by both the nucleation of a shear band at an STZ and its subsequent propagation, its attainment in BMGs requires that both these stages of plastic deformation are understood, and that they may be controlled.

A local reduction in atomic bond density creates a more fertile site for STZ nucleation. This is the principle central to the idea of Poon *et al*. [4] which suggests that brittle behaviour, indicated by a low Poisson ratio, ν, can be alleviated by a low ratio of local shear modulus to global modulus, $G^*/\langle G \rangle$. Similarly, Cheng *et al*. [5] conceptually separated the elemental (G_e) and configurational (G_c) contribution to elastic moduli in BMGs, and believed that brittle alloy systems, such as those based on Fe, Mg, Ce etc., require significant local reductions in G to encourage multiple STZ nucleation. One might suggest that basing the prediction or explanation of plastic strain in BMGs on measured global elastic moduli, such as by sound wave measurement techniques, averages local perturbations in modulus, and so sensitivity to the dependence of mechanical behaviour on the ability for a local structure to co-operatively collapse is lost.

A soft surface layer has been reported for a 2 mm diameter rod of $Cu_{50}Zr_{50}$ in the as-cast condition [6]. Instrumented nanoindentation, performed along a traverse from the edge of the casting towards the centre, revealed a 13% drop in elastic modulus between the two ends of the line which was ascribed to the differing cooling conditions at the centre and edge during copper-mould casting of BMG rods generating more atomic defects at the surface as compared to the centre-line. The local moduli of this sample vary between the edge and centre of the rod, and so a quantification of these moduli by standard techniques will not provide sensitivity to the composite nature of the rod, with respect to atomic environments.

Nanoindentation allows the structural response of a material to be investigated in a controlled manner, typically without the risk of failure in the case of more brittle materials. It

has been implemented to study the deformation characteristics and tendency for shear banding in BMGs [7-8] and enables the probing of a small region, where the generated shear stress ahead of the indenter is sufficient to induce shear banding, without influencing the surrounding bulk. This has led to the development of theory relating to shear band activity as a function of loading rate [7] and temperature [8], through an analysis of the extent of serrated flow, with the corresponding "pop-in" events (a rapid increase in depth with little or no increase in load) indicating the activation of a shear band. In this chapter nanoindentation is used to investigate and probe the extent of hardness and elastic modulus variation across as-cast and annealed BMG rods. This is performed as a function of section diameter and with BMG composition, characterised by the fragility index, m, which quantifies the rate of change of viscosity as the glass transition temperature, T_g, is approached. With this in mind, one BMG from each isomechanical group in Chapter 5 is studied so to understand this effect with respect to both m and ability to permanently deform.

6.2. Experimental

$Pd_{77.5}Si_{16.5}Cu_6$, $Zr_{65}Cu_{15}Al_{10}Ni_{10}$ and $Ce_{70}Al_{10}Cu_{10}Ni_{10}$ were selected for this study owing to their range of fragility index values (21, 30 and 52 respectively) and their differing propensities to demonstrate plastic flow; selected properties can be found in Table 6.1. As a result of this variation in properties they each belong to the separate isomechanical groups defined in Chapter 5. Figure 6.1 shows their placement on a Blackman diagram

Table 6.1. Selected properties for the alloys studied; elastic moduli (E, G and B), glass transition temperature, T_g, plastic strain, ε_p, and fragility index, m.

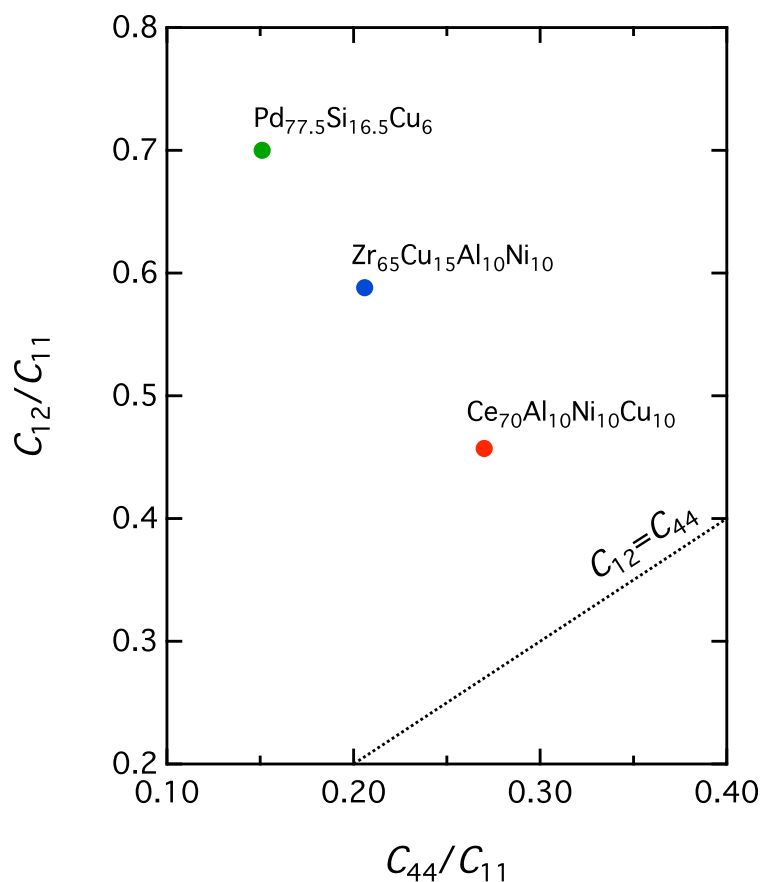| Alloy	E (GPa)	G (GPa)	B (GPa)	T_g (K)	ε_p (%)	m	*ref.*
$Pd_{77.5}Si_{16.5}Cu_6$	88.8	31.5	167	635	10.4	52	2,9
$Zr_{65}Cu_{15}Al_{10}Ni_{10}$	83.0	30.3	106.7	653	0.12	30	2,9
$Ce_{70}Al_{10}Ni_{10}Cu_{10}$	30.3	11.5	27	359	0	21	2,10

Figure 6.1. Blackman diagram representation of the alloys studied.

10 g ingots of each alloy were generated by arc melting high purity constituents ($\geq$ 99.6 %) in an environment evacuated to 5×10^{-3} Pa and then backfilled with 1/3 of an atmosphere of argon. A Ti "getter" was melted prior to sample melting to favour the creation of a localised high vacuum, and ingots were flipped and re-melted four times to ensure chemical homogeneity and complete melting. An *in-situ* copper mould suction casting facility enabled the production of amorphous rods, all from the same ingot for a single alloy, with a range of diameters (1 mm – 4 mm). Their glassy structure was analyzed by x-ray diffraction using CuKα radiation; thin slices were cut from the rod enabling the probing of the structure through the entire cross-section. Diameters up to the largest over which each BMG composition could be cast and remain fully amorphous, within the limits of determination by the x-ray diffraction technique, were used in this study; 3 mm for $Pd_{77.5}Si_{16.5}Cu_6$, 4 mm for $Zr_{65}Cu_{15}Al_{10}Ni_{10}$ and 1 mm for $Ce_{70}Al_{10}Cu_{10}Ni_{10}$. It would be anticipated that $Ce_{70}Al_{10}Cu_{10}Ni_{10}$ may display the largest glassy diameter, as it is, on the basis of measured fragility index, the strongest glass former. The inability to generate larger sections is considered to originate from sensitivity to impurities acting as heterogeneous

nucleation agents; the large negative enthalpy of formation of Ce_2O_3 (-1823 kJ/mol [11]) will drive the reaction of Ce with dissolved oxygen, increasing the number density of nucleation sites, with these potentially acting to promote crystal formation and thereby reducing the glass forming ability of the alloy. Whilst the large negative enthalpy of formation of rare-earth oxides can act as oxygen scavengers when added in small amounts to base glass forming alloys, improving critical diameters [12], as $Ce_{70}Al_{10}Cu_{10}Ni_{10}$ is the glass forming composition it may exhibit strong sensitivity to impurities with respect to glass formation. After casting, BMG rods were sectioned on a slow speed precision diamond cut-off saw and cold mounted in resin parallel to the cut surface for subsequent grinding and polishing, giving a high quality mirrored finish. Samples of the largest diameter cast for each alloy were heat treated in a high vacuum furnace (5×10^{-4} Pa) for 5 hours at 0.6 of the glass transition temperature ($0.6T_g$).

Nanoindentation was performed on a Hysitron Nanomechanical Tester, fitted with a Berkovitch diamond tip, using an applied load of 6 mN with a load, hold and unload segment time of 5 seconds each, obtaining hardness, H_v, and reduced modulus, E_r, data. H_v is defined as the maximum applied load divided by the resulting indent area and E_r is computed from Equation 6.1 [13], where, respectively, E and E_i are the elastic modulus of the sample and indenter, and v and v_i the Poisson's ratio of the sample and indenter.

$$\frac{1}{E_r} = \frac{\left(1 - v^2\right)}{E} + \frac{\left(1 - v_i^2\right)}{E_i}$$

(6.1)

E_r thus provides a measure of the elastic modulus, though it includes a contribution from the elastic properties of the indenter. H_v and E_r profiles were obtained for the cross-section of each diameter rod by performing indentation traverses from the edge of the rods to the centre at 10 μm steps for the first 450-500 μm and then in groups of four steps at 100 μm intervals. This method permits increased data acquisition in the region of interest (i.e. the rod surface). Three parallel traverse lines were used with a spacing of 10 μm between them so to obtain an average H_v and E_r for each location, aiding reduced spread in the results.

6.3. Results

Figure 6.2 shows the results of the XRD scans performed for the annealed samples of each composition. It should be noted that the annealed rods were the largest diameter specimens that could be cast in the fully amorphous state. Additionally, samples of various

diameters were cast as a single rod (i.e. in a die with stepped die) and so, by inference, the smaller diameter samples were also fully amorphous.
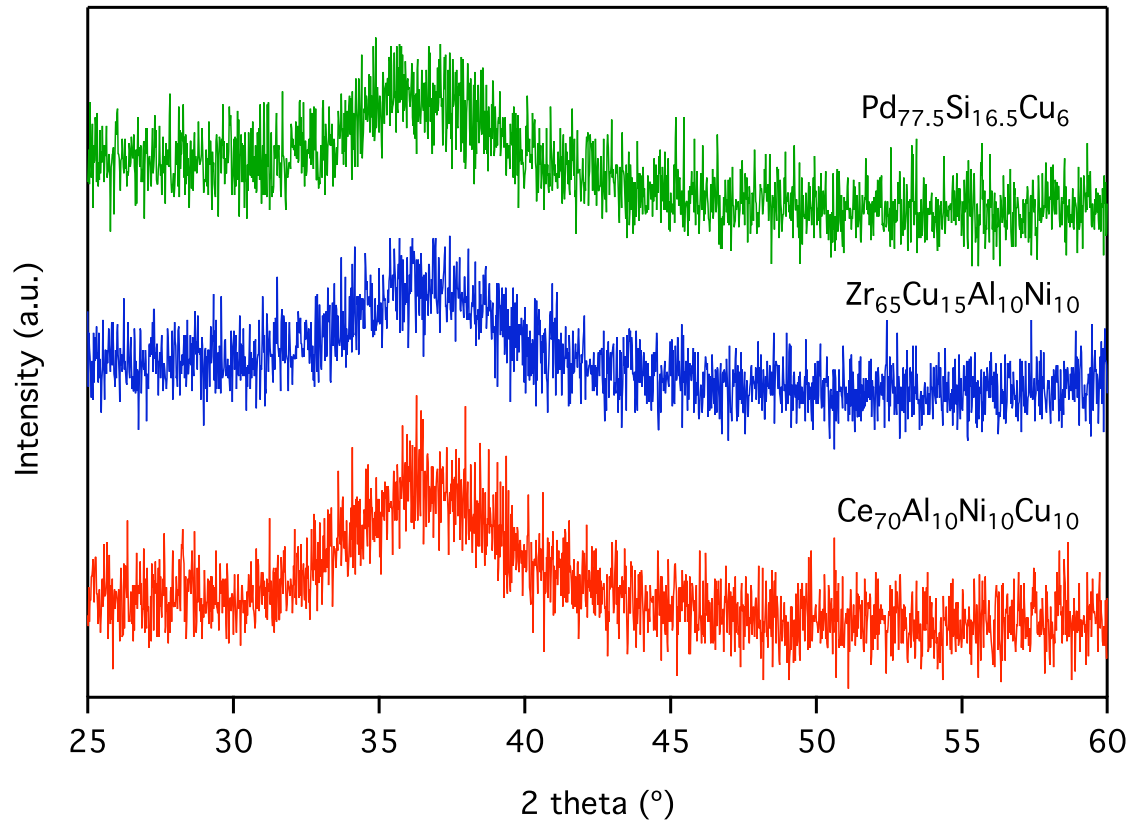

Figure 6.2. XRD scans for annealed specimens of each composition.

The unloading portion of indentation curves can be used to extract data pertaining to H_v and E_r [13]. For the samples tested here, the resulting reduced elastic modulus and hardness traverses can be seen in Figure 6.3 and 6.4 respectively. Reducing sample diameter induces a reduction in H_v and E_r across the whole traverse, i.e. the statistical average of all measurements decreases as rod diameter decreases; this is considered, and hereafter called, a global softening effect, as it would be expected that it would be perceived as such in conventional mechanical tests on macroscopic specimens. Whilst pronounced surface softening can be seen in some of the traverses, it is not apparent in all; the magnitude of the effect decreases with increasing sample size, and subsequently disappears beyond a critical size.
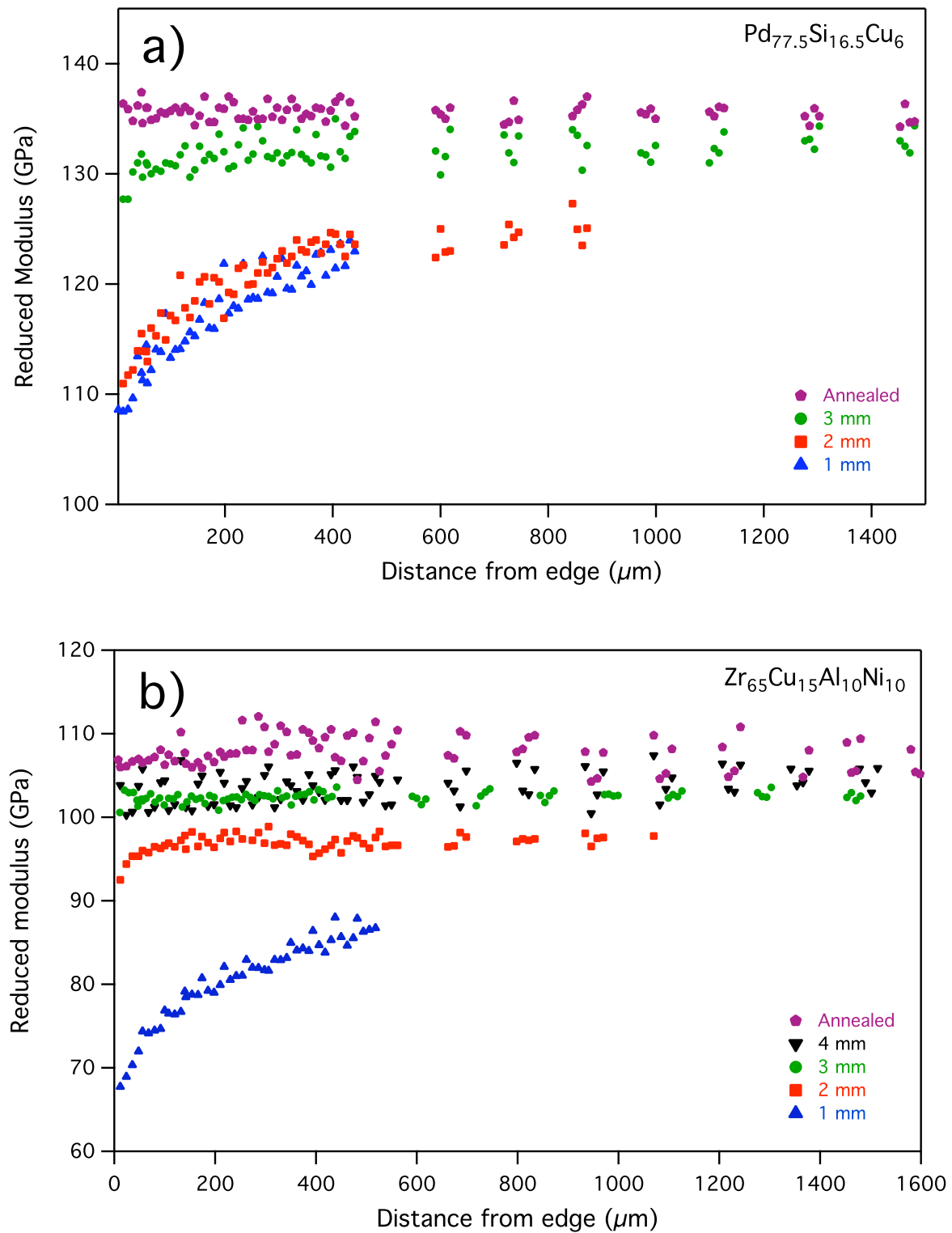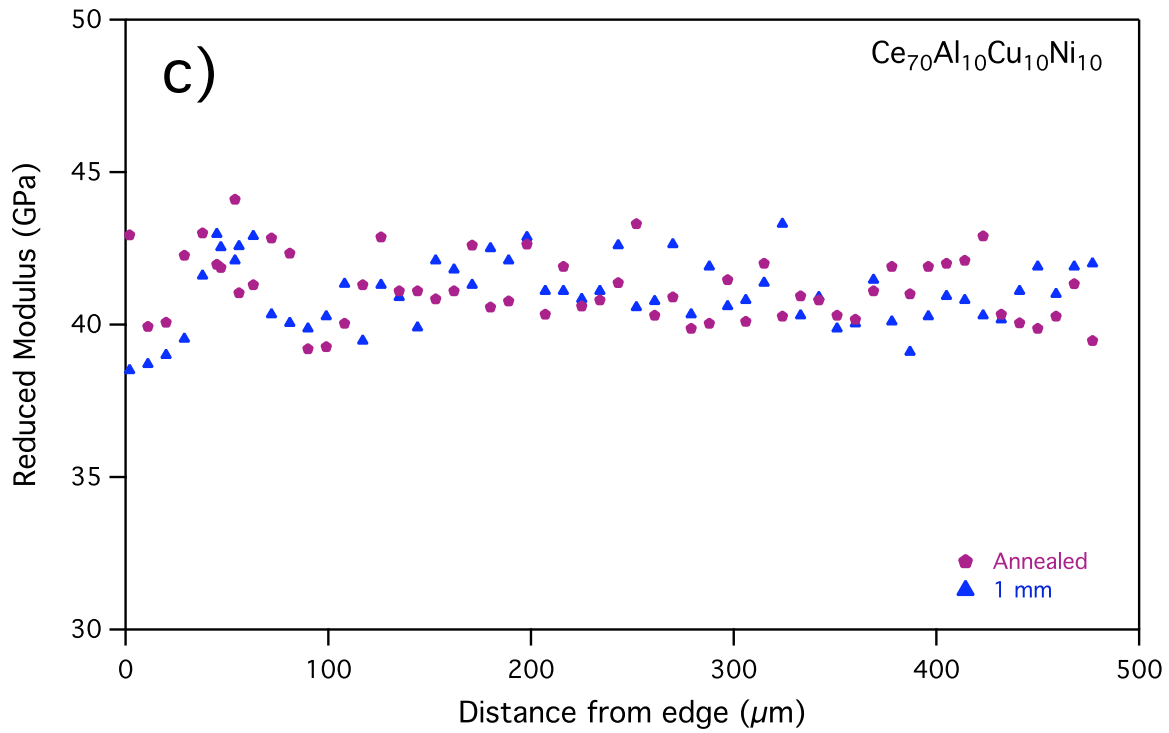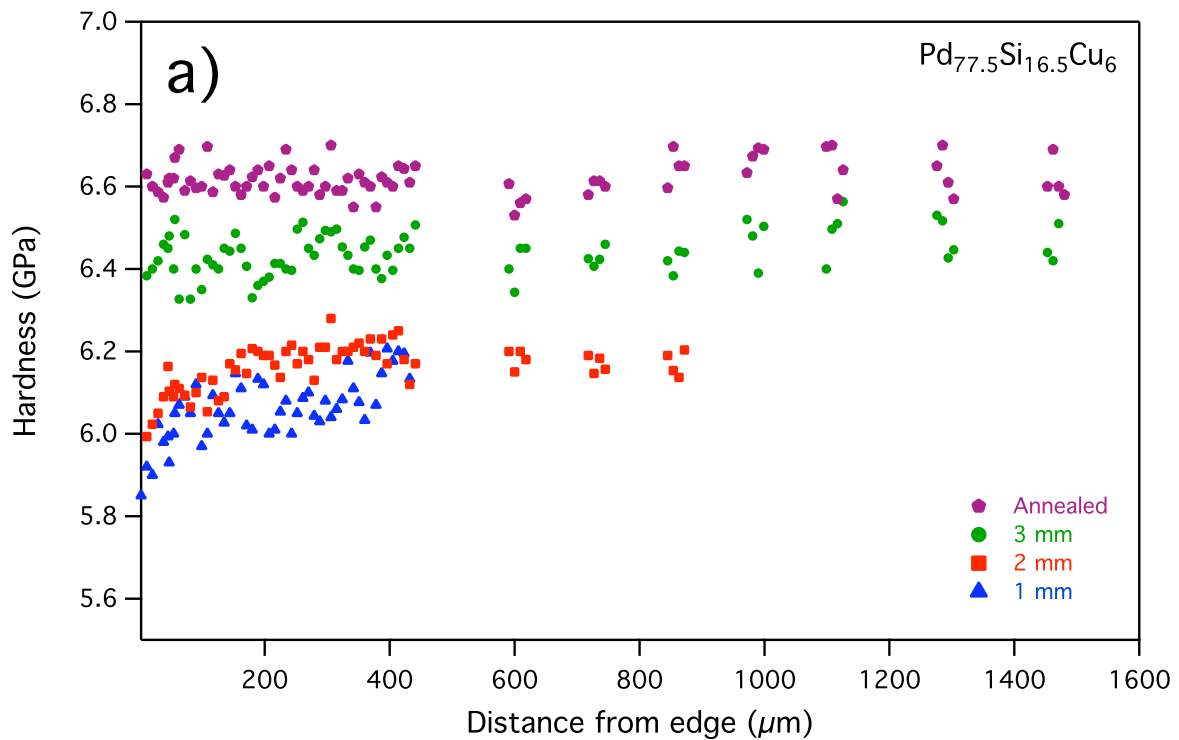
Figure 6.3. Reduced Modulus, E_r, profiles from the edge of as-cast BMG rods towards the centre for (a) $Pd_{77.5}Si_{16.5}Cu_6$, (b) $Zr_{65}Cu_{15}Al_{10}Ni_{10}$ and (c) $Ce_{70}Al_{10}Cu_{10}Ni_{10}$. Rod diameter indicated on graph.
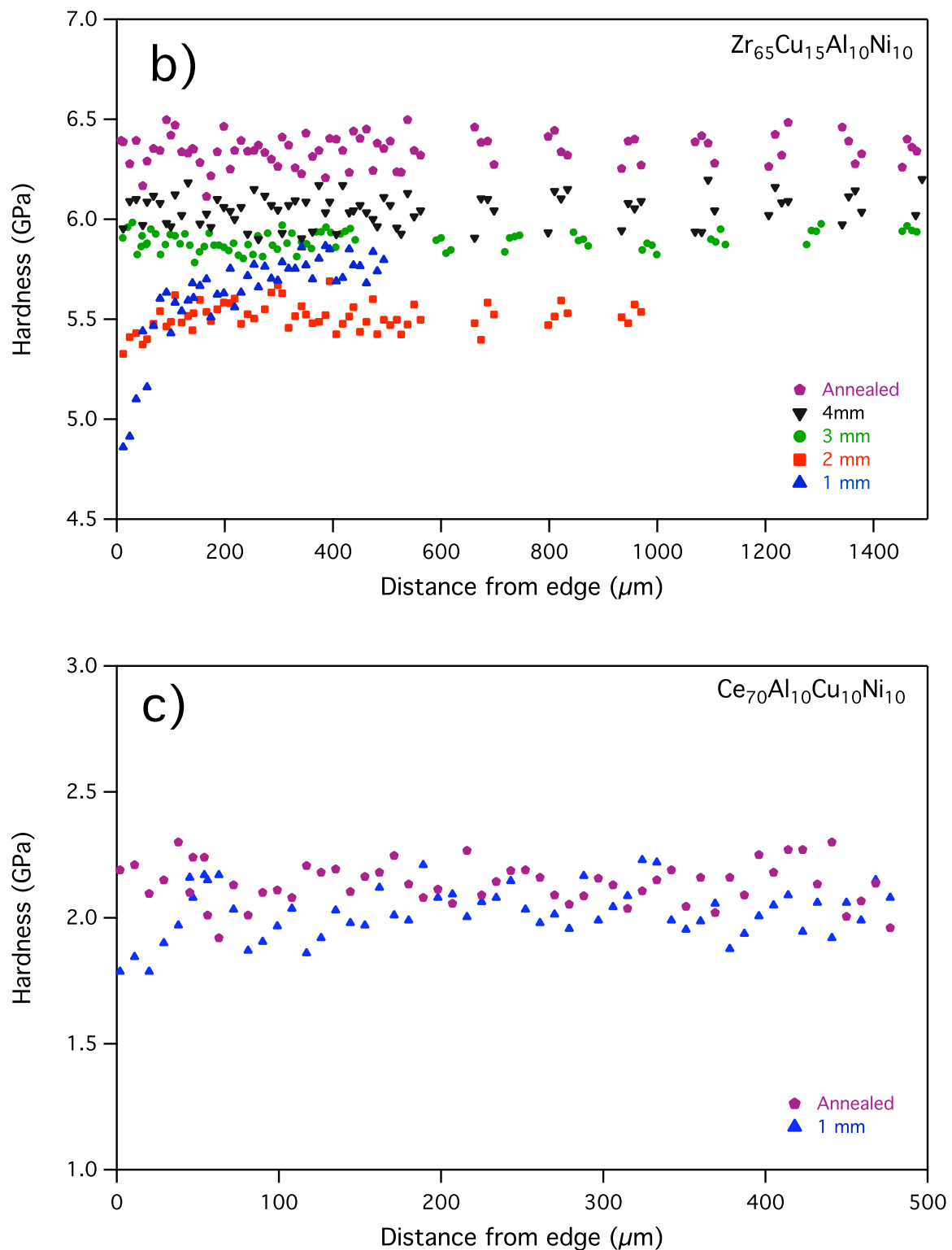
Figure 6.4. Hardness, H_v, profiles from the edge of as-cast BMG rods towards the centre for (a) $Pd_{77.5}Si_{16.5}Cu_6$, (b) $Zr_{65}Cu_{15}Al_{10}Ni_{10}$ and (c) $Ce_{70}Al_{10}Cu_{10}Ni_{10}$. Rod diameter indicated on graph.

In order to compare the relative magnitudes of the softening effect between the alloys, E_r is used in place of H_v. Work softening of BMGs [14] is anticipated to potentially influence H_v, the extent of which will be a function of the local structure and is thus not constant for each indentation. This may be the origin of increased scatter in H_v as compared to E_r (see Figure 6.3 and 6.4). Data for the surface reduction in E_r is contained in Table 6.2 where, in an attempt to reduce the variation to a simple quantitative parameter, the edge result is divided by that obtained in the centre, enabling direct comparison without the relative magnitude of the values influencing the analysis.

Table 6.2. Comparison of relative surface drop-off in reduced modulus, E_r.

Alloy	Rod diameter (mm)	$\dfrac{E_{r(edge)}}{E_{r(centre)}}$
$Pd_{77.5}Si_{16.5}Cu_6$	1	0.87
	2	0.88
	3	0.96
$Zr_{65}Cu_{15}Al_{10}Ni_{10}$	1	0.77
	2	0.95
	3	1.00
	4	1.00
$Ce_{70}Al_{10}Ni_{10}Cu_{10}$	1	0.94

The Pd-based glass shows an almost identical effect in the 1 mm and 2 mm rods with a reduction of 13% and 12% respectively in E_r at the edge versus that of the centre-line. Although the Zr-based glass shows the largest drop-off of 23% for 1 mm diameter samples, this reduces to just 5% when the sample diameter increases to 2 mm. $Zr_{65}Cu_{15}Al_{10}Ni_{10}$ therefore has increased sensitivity to diameter with regard to the magnitude of the surface phenomenon. Lastly, the Ce-based alloy shows only a slight decrease in E_r of 6% at the surface, the lowest for all the 1 mm specimens. It can be seen that the more fragile Pd-based BMG can most favourably retain a surface reduction effect, while the ability to do this is much reduced for the least fragile Ce-based alloy.

Typical load/unload curves at varying locations and rod size can be seen in Figure 6.5.
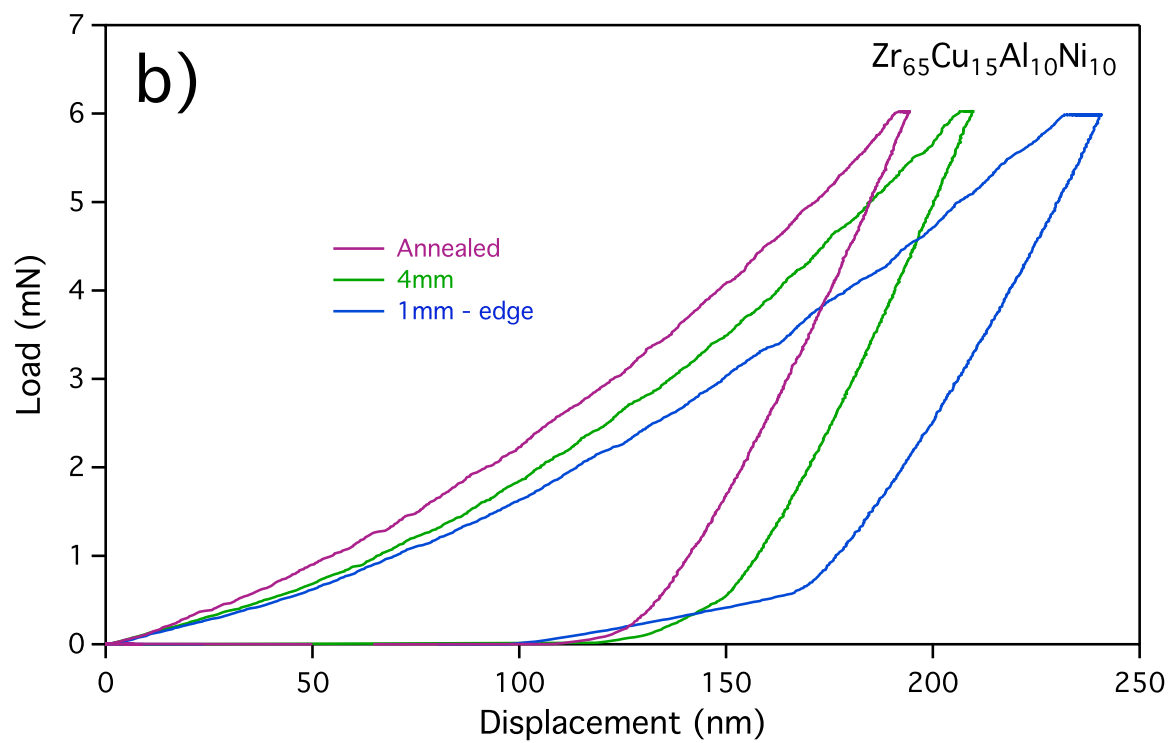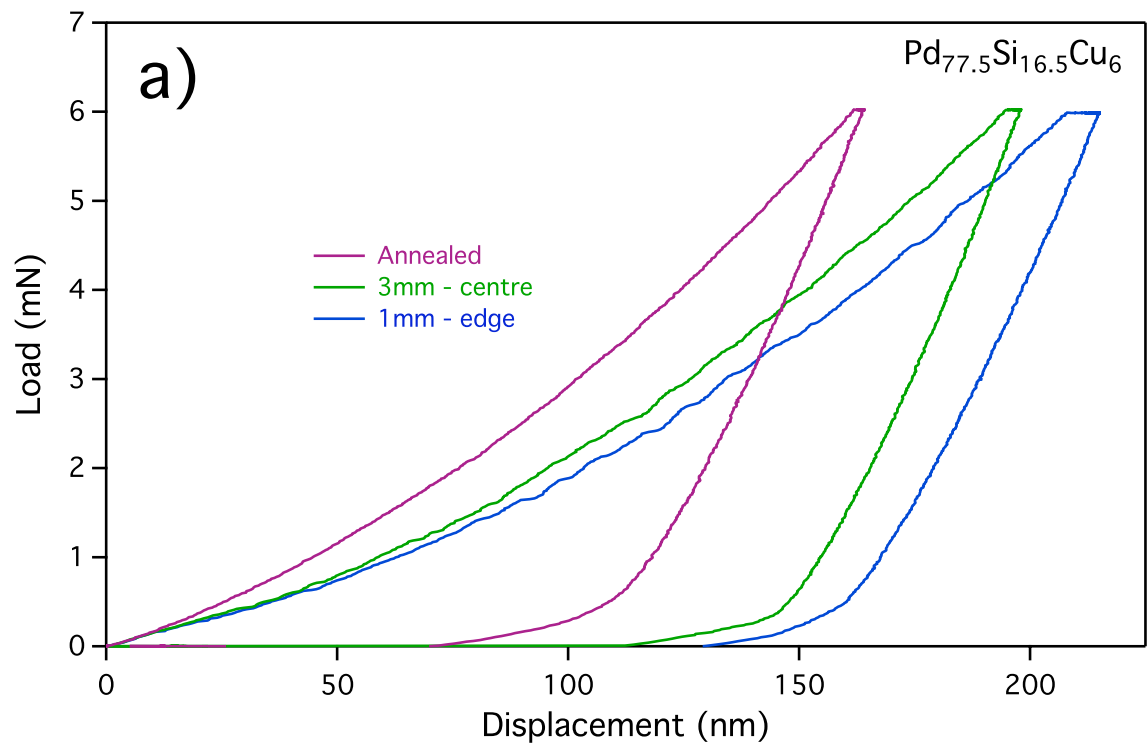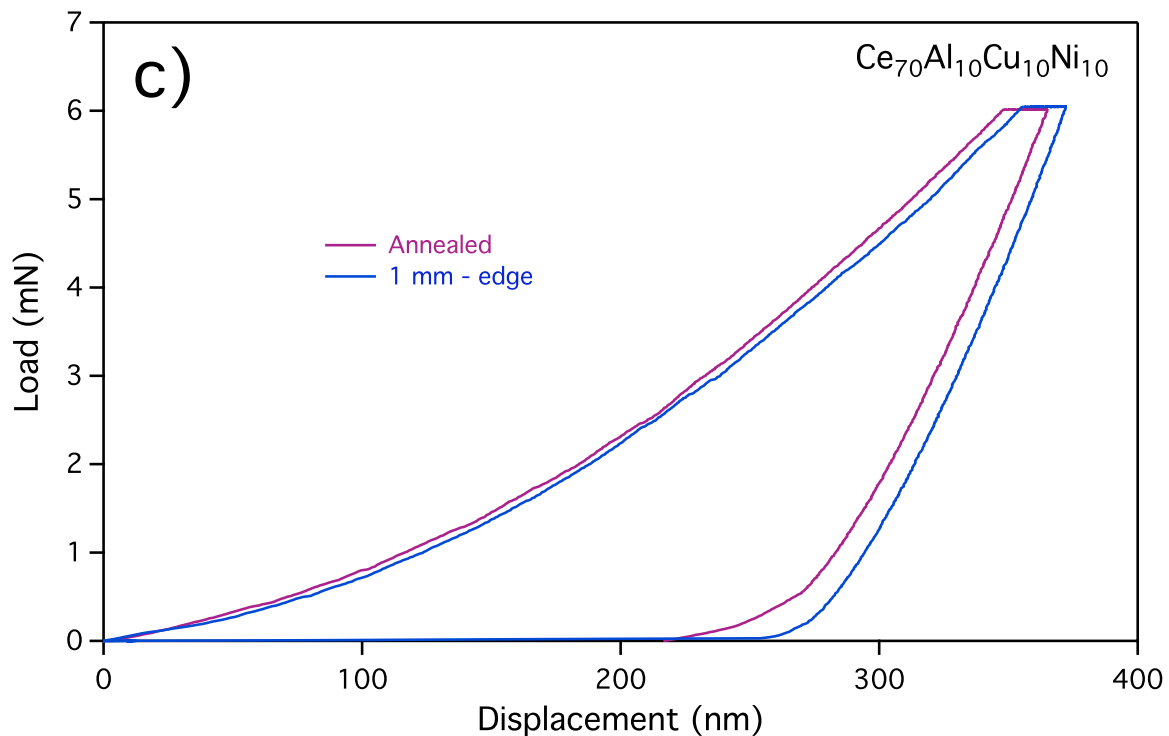
Figure 6.5. Load/unload curves for (a) $Pd_{77.5}Si_{16.5}Cu_6$, (b) $Zr_{65}Cu_{15}Al_{10}Ni_{10}$ and (c) $Ce_{70}Al_{10}Cu_{10}Ni_{10}$. Rod diameter indicated on graph.

The loading curves for the $Pd_{77.5}Si_{16.5}Cu_6$ and $Zr_{65}Cu_{15}Al_{10}Ni_{10}$ samples feature a number of pop-ins, indicating that shear systems have been activated. Serrated flow is more prevalent at the edge of the 1 mm rods than at the centre of both the 3 mm and 4 mm samples for $Pd_{77.5}Si_{16.5}Cu_6$ and $Zr_{65}Cu_{15}Al_{10}Ni_{10}$ respectively. Pop-in events are more restricted in the annealed samples of the Pd-based and Zr-based alloys and in as-cast and annealed $Ce_{70}Al_{10}Cu_{10}Ni_{10}$. Maximum indenter penetration depth is visible in $Pd_{77.5}Si_{16.5}Cu_6$ and $Zr_{65}Cu_{15}Al_{10}Ni_{10}$ specimens with lowest diameter and, during the load hold, some creep-like phenomena are enhanced at the edge of the smallest samples for each alloy. Depth penetration is restricted in the annealed alloys. These results show a variation in hardness as a function of indenter location, rod size and whether or not they have received an annealing treatment; the smaller the diameter of the sample, and the closer to the surface, the softer the structure is and the more shear band activity is generated.

6.4. Discussion

Liu *et al*. derived an expression to relate defect concentration to cooling rate, where proportionality between the two was suggested [6]. As a result of the higher cooling rate at the surface of BMGs as compared to the centre, it was considered that surface softening of BMGs is universal and is thus present in all copper-die suction cast rods. The data presented here suggests differently and that the extent of surface softening is dependent on two factors: 1) sample size, and 2) glass fragility index. With regard to sample size, the magnitude of the surface softening in the Pd and Zr-based alloys is seen to decrease with increasing sample size, despite the cooling rate generally being higher at the surface of each casting. As the radial distance over which heat is extracted increases however, the surface will experience a slower cooling rate, allowing for more atomic movement and structural relaxation. A greater *in-situ* annealing effect also takes place in larger diameter samples, where the surface is held at elevated temperatures, which is sufficient for atomic relaxation, for longer time periods. This results in the magnitude of surface softening decreasing in the Pd and Zr-based glasses as sample diameter is increased.

The concept of a potential energy landscape (PEL) defines a multi dimensional surface, where the energy of available structural states (defined with regard to position, orientation and vibration co-ordinates) is given, and minima in the energy landscape are thus representative of different atomic co-ordinations, or inherent states (IS). The crystalline state can be considered the lowest energy configuration minima (or basin) in a PEL, with glassy states having minima in energy very close to the crystalline potential. PELs of strong glass formers contain less "features" corresponding to a reduced number of local environments that can be sampled in a glassy structure [15-17]. This is illustrated schematically in Figure 5.6. A wide range of local minima exist in the PEL of a high *m* (fragile) glass however. To illustrate this point, amorphous silica follows a near Arrhenius viscosity temperature dependence, indicating an almost constant activation energy across the temperature range for viscous flow [17], and it is this that distinguishes it as a strong glass former, as compared to a fragile system where the activation energy rapidly increases as T_g is approached. This implies that the atomic movements that are required for flow are the same at all temperatures in amorphous silica, and so the energy landscape can be expected to consist of minima of approximately equal depth. When a strong glass forming BMG is cast, the lack of different IS means the structure at the surface is more similar to that in the centre. Therefore, despite the surface experiencing a higher cooling rate, a limited number of IS are permitted and so the structure has to conform to similar configurations to those in the rod centre. Fragile glasses however have a number of features in their PEL, and so a greater range of metastable atomic configurations. Thus, when the surface is rapidly cooled it stabilises into different energy

minima than in the slower cooled centre. This may explain why the fragile Pd-based alloy was most able to retain a low modulus surface layer up to a 3mm rod diameter, and so fragile glasses are most effective at exhibiting surface softening.

The observation of increased pop-in phenomena in Figure 6.5 occurs in the lowest H_v and E_r structural states i.e. at the edge of the samples that surface soften as compared to the annealed states, where more structural relaxation has occurred. Since all samples tested for any given alloy were from the same ingot, compositional variation is not the source of the different mechanical response, and so it is the structural aspect that is dominating behaviour. Since the activation energy of a shear event in a glassy substance, be it thermal or mechanical, is dependent on G, the enhanced tendency to shear banding originates from a reduction in elastic moduli. This may be explained by invoking arguments regarding the extent of local atomic connectivity. Atomic rearrangement requires that bond breaking and subsequent re-formation occur; the local co-ordination number will have an influence on this as it will dictate the number of bonds that must be broken. Minima in PELs correspond to stable co-ordination numbers, with higher energy states representing less favourable environments that contribute more elastic energy to a shear process [18]. Rapid surface cooling freezes the structure into these less stable states [17] (with increased propensity in fragile systems as previously mentioned) resulting in an improved tendency for shear banding at these locations, realised as a transfer between minima in the energy landscape.

A measure of G for the data in Figure 6.3 would permit an understanding of the activation barrier to STZ nucleation, and to subsequent plastic strain. This will only be a function of structural state as it is a reasonable assumption that the chemical contribution is unaffected by indentation location, i.e. the cast rods are chemically homogeneous. Plotting G versus E for the range of BMGs in Table 5.1 yields a strong linear relationship ($G = 0.383E$ - see Figure 5.2), allowing G to be estimated directly from E in BMGs, irrespective of their differing v. This value of proportionality between G and E is in accordance with that of 0.39, which has previously been found in polycrystalline metals [20]. For the E_r data determined in this study, difficulties exist in calculating the absolute E using Equation 6.1 as v varies with thermal history, and so will differ with location in the samples. However, using Figure 5.2 some measure of the shear modulus, $G^{\bullet}$, can be determined from E_r. This value is not comparable with G due to the elastic contribution from the indenter and the fact that the local v at each location cannot be determined. However, it does permit a measure of the configurational G to be deduced, due to the elemental contribution being constant for each location, based on the assumption of chemical homogeneity. Then, $G^{\bullet}$ within a 1 mm rod and across the whole as-cast state for an alloy are representative of changes in G. The range can be characterised by dividing the maximum value by the minimum, to give a value illustrative of the structural variation in G:

$$\left(\frac{G^{\bullet}_{edge}}{G^{\bullet}_{centre}}\right)_{(1mm)} \tag{6.2}$$

$$\left(\frac{G^{\bullet}_{min}}{G^{\bullet}_{max}}\right) \tag{6.3}$$

The values in Table 6.3 demonstrate the differences in $G^{\bullet}$ that are encountered within cast BMG rods, due to surface and global softening and represent significant differences in $G^{\bullet}$ as a function of the cast state.

Table 6.3. Comparison of magnitude of change in $G^{\bullet}$ across all as-cast diameters ($G^{\bullet}_{min}/G^{\bullet}_{max}$) and due to surface effects in the 1 mm rods of each alloy.

Alloy	$\left(\dfrac{G^{\bullet}_{min}}{G^{\bullet}_{max}}\right)$	$\left(\dfrac{G^{\bullet}_{(edge)}}{G^{\bullet}_{(centre)}}\right)_{(1mm)}$
$Pd_{77.5}Si_{16.5}Cu_6$	0.60	0.87
$Zr_{65}Cu_{15}Al_{10}Ni_{10}$	0.61	0.77
$Ce_{70}Al_{10}Ni_{10}Cu_{10}$	0.94	0.94

Rather than using the annealed samples for $G^{\bullet}_{max}$, the centre of the largest diameter as-cast sample is taken to highlight the magnitude of the difference in G across as-cast states instead of in those that have undergone secondary processing. As an example, $Pd_{77.5}Si_{16.5}Cu_6$ shows a 13% difference between the centre and edge of a 1 mm rod and a 40% difference between the edge of the 1 mm rod and the centre of the 3 mm sample. This range of G values helps to explain why shear bands are less activated when the structural state tends towards being fully relaxed, visible as reduced pop-ins in the annealed and centre region of the larger diameter sample loading curves of $Pd_{77.5}Si_{16.5}Cu_6$ and $Zr_{65}Cu_{15}Al_{10}Ni_{10}$ in Figure 6.5. $G^{\bullet}$ determined here is on a larger structural scale than that proposed for G^* [4] and G_c [5], though, by using nanoindentation it is possible to obtain an indication of local values that are not sample averages, and reflects a higher degree of resolution as a result of the intrinsic nature of the nanoindentation test itself. This continuous structural variation means that under certain circumstances BMG rods should be considered a composite of differing local structures, and

so do not posses a single *G*, *B* and *E*; moduli determined by techniques such as sound wave velocities are a global average.

The plastic zone size, r_p, of a material represents the plastic region generated ahead of a crack tip when the applied stress exceeds the yield point, σ_y, of the material. It can be considered the length scale over which stable shear banding is possible in BMGs [21]. In the case of plane stress, where K_{1C} is fracture toughness:

$$r_p = \frac{K_{1C}^2}{2\pi\sigma_y^2}$$

$$(6.4)$$

Then, as shear yield stress, $\tau_y = \sigma_y/2$ and $G = \tau_y/\gamma_c$, where γ_c is the critical shear strain for BMGs (0.0267) [1], the following relationship relates r_p to G:

$$r_p = \frac{K_{1C}^2}{8\pi G^2 \gamma_c^2}$$

$$(6.5)$$

As with $G^{\bullet}$, pronounced variation in r_p is expected as a result of its inverse dependence on G^2; this illustrates the structural diversity, and therefore range of mechanical response, that is possible from a single alloy (global softening) and within a cast rod (surface softening). The analysis presented here, with regard to variation in $G^{\bullet}$ and r_p, demonstrates the structural sensitivity of BMGs to thermal history (i.e. cooling conditions). Replication of mechanical data between researchers is therefore problematic due to variations in experimental technique and intrinsic cooling conditions of the casting arrangement resulting in different structures. As more structural states may be present in fragile glass formers (see Figure 5.6) it may be these alloys that are most sensitive to their preparation route and might exhibit the largest range in plastic response.

Reported in [22] is that shot-peening induced residual compressive surface stresses and a soft surface in a Ti-based BMG, resulting in an $H_{v(edge)}/H_{v(centre)}$ value of 0.88. Plasticity increased to an average of 11% (and a maximum of 22%) from an average of 6% in the non-peened state. A soft surface may have benefitted this, due to a reduced energy barrier to STZ activation in the surface region, as is shown in Figure 6.5, which could enhance macroscopic plasticity. The results of the present study show $H_{v(edge)}/H_{v(centre)}$ for 1 mm $Pd_{77.5}Si_{16.5}Cu_6$ and $Zr_{65}Cu_{15}Al_{10}Ni_{10}$ are 0.94 and 0.78 (see Figure 6.4a and 6.4b) respectively and so are in broad agreement with the observations made for the shot-peened sample, though it must be considered that the extent of work softening may not be consistent at each site, as previously mentioned. Surface softening in as-cast components might then have an effect on macroscopic plasticity.

Finally, it has been demonstrated that anisotropy exists in melt spun ribbons, where the majority of cooling occurs through the copper wheel and so is highly directional. As the soft surface structure studied here results from differential cooling across a sample, it may permit some anisotropy, particularly in the instance of the Pd-based alloy. This would be an interesting point for future investigation.

6.5. Conclusion

The major findings of Chapter 6 are summarised as follows:

- Surface softening is found to not be a universal phenomenon in copper-mould cast BMGs, as its magnitude continuously decreases with increasing diameter, resulting in its absence in rods beyond a critical size. This is attributed to longer *in-situ* annealing times at higher temperatures in large diameter samples activating more atomic relaxation events. The effect is also believed to be more prevalent in fragile glasses.

- Fundamental differences in atomic structure are to be expected between each alloy studied as they belong to different isomechanical groups. Enhanced diversity in the potential energy landscape of fragile glasses may permit a large range of different atomic sites, to be present at room temperature, and so fragile glasses may be the most likely to show the surface softening effect.

- Samples that surface soften contain different local structures at the centre and edge, each with differing tendencies for STZ nucleation, resulting from reduced atomic connectivity and a resulting decrease in G. By extracting a measure of the shear modulus, $G^{\bullet}$, for each indent location, a range of values is found across a single rod, illustrated by a 33% difference between the centre and edge of 1 mm $Zr_{65}Cu_{15}Al_{10}Ni_{10}$. This causes increased shear band nucleation, identifiable as more pop-ins in the loading curves at the edge of 1 mm rods in comparison to the more relaxed larger diameter and annealed structural states and may result from more energetic energy minima at these sites in the energy landscape.

- The range in $G^{\bullet}$ and r_p reflects the varied mechanical performance that is possible within a single alloy system, and the potential sensitivity of mechanical performance to preparation history.

- Finally, studying BMG properties as a function of isomechanical group occupied, or position on a Blackman diagram may be capable of explaining differences in the empirical observation of properties of BMGs.

6.6. References

[1]   W. L. Johnson and K. Samwer, Phys. Rev. Lett. **95**, 195501 (2005).

[2]   M. Jiang and L. Dai, Phys. Rev. B **76**, 5 (2007).

[3]   S. Pauly, M. H. Lee, D. H. Kim, K. B. Kim, D. J. Sordelet and J. Eckert, J. Appl. Phys. **106**, 103518 (2009).

[4]   S. J. Poon, A. Zhu and G. J. Shiflet, Appl. Phys. Lett. **92**, 261902 (2008).

[5]   Y. Q. Cheng, A.J. Cao and E. Ma, Acta Mat. **57**, 3253 (2009).

[6]   Y. Liu, H. Bei, C. T. Liu and E. P. George, Appl. Phys. Lett. **90**, 71909 (2007).

[7]   C. A. Schuh and T. G. Nieh, Acta Mat. 51, **87** (2003).

[8]   C. A. Schuh, A. C. Lund and T. G. Nieh, Acta Mat. **52**, 5879 (2004).

[9]   J. D. Plummer, I. A. Figueroa, R. J. Hand, H. A. Davies and I. Todd, J. Non-Cryst. Solids **355**, 335 (2009).

[10]   Y. Liu, H. Wu, C. T. Liu, Z. Zhang and V. Keppens, Appl. Phys. Lett. **93**, 151915 (2008).

[11]   G. V. Raynor, Metallurgical Thermochemistry, Pergammon Press, 5 (1979).

[12]   I. A. Figueroa, H. A. Davies and I. Todd, Phil. Mag. **89**, 27 (2009).

[13]   W. C. Oliver and G. M. Pharr, J. Mater. Res. **7**, 6 (1992).

[14]   H. Bei, S. Xei and E. P. George, Phys. Rev. Lett. **96**, 105503 (2006).

[15]   C. A. Angell, Science **267**, 1924 (1995).

[16]   R. J. Speedy, J. Phys. Chem. B **103**, 4060 (1999).

[17]   P. G. Debenedetti and F. H. Stillinger, Nature **410**, 259 (2001).

[18]   M. Miller and P. Liaw, Bulk Metallic Glass, Springer, 2008, p. 41.

[19]   J. J. Lewandowski, W. H. Wang and A. L. Greer, Phil. Mag. Lett. **85**, 77 (2005).

[20]   H. M. Ledbetter, Mater. Sci. Eng. **27**, 133 (1977).

[21]   D. C. Hoffmann, J. Y. Suh, A. Wiest, G. Duan, M. L. Lind, M. D. Demetriou and W. L. Johnson, Nature, **451** (2008).

[22]   Y. Zhang, W. H. Wang and A. L. Greer, Nature. **5**, 857 (2006).

7. Length scales that control plastic deformation in bulk metallic glass

Forward to Chapter 7

The data collection presented in this chapter was performed in collaboration with Dr Paul Quinn at the I18 beamline at Diamond Light Source. The computational processing of the raw data was performed by both PQ and JDP, and the analysis and discussion of the data is entirely that of JDP.

7.1. Introduction

Understanding the influence of structure on properties is one of the core aims of materials science, with critical length scales ranging from a few angstrom up to the macro-scale potentially influencing experimental outcome. In bulk metallic glasses (BMGs) however, the lack of a periodic structure makes identifying the specific units that determine physical properties problematic and, instead, more conceptual ideas such as potential energy landscapes (PELs) are often applied, such as were used in Chapters 5 and 6. Attempts have been made to understand these complex interrelations in BMGs, particularly via the use of molecular dynamic simulations [1-3]. For example, Cheng *et al.* [3] correlated a high fraction of incomplete icosahedra with an ability to demonstrate large plastic strain in compressive loading, and relationships also exist with the glass transition temperature and yield strength. Rigorous experimental data, linking what is observed in the laboratory to the specific atomistic units that determine physical behaviour, remains elusive however, particularly with regard to plastic flow, which is mediated by shear transformation zones (STZs) and shear bands.

In Chapter 6 a trend was demonstrated between cooling rate, hardness (H_v) and reduced modulus (E_r) by nanoindentation, performed along a traverse on the cross-section of as-cast monolithic BMG rods. In $Zr_{65}Cu_{15}Ni_{10}Al_{10}$, H_v and E_r were both found to be lower in the more rapidly cooled edge region of a 1 mm rod, as compared to the centre, while an annealed sample showed the largest values. E_r could be linked to some measure of an extracted shear modulus (termed $G^{\bullet}$), variation in which was believed to be causing the differing propensities for shear banding. This chapter aims to understand the structure unit that is causing this non-identical mechanical behavior with thermal history. This is done by

probing nearest-neighbour atomic environments via extended absorption fine edge structure (EXAFS) in the $Zr_{65}Cu_{15}Ni_{10}Al_{10}$ alloy.

EXAFS explores the nearest neighbour configurations in materials. It makes use of the high energy x-rays provided by a synchrotron to excite core electrons, emitting them as photoelectrons, the energy and intensity of which are subsequently measured. Information regarding atomic separation distances and coordination number can then be determined due to interactions between the emitted photoelectrons that have been emitted with those that are backscattered by the surrounding atoms. EXAFS is thus most applicable to the study of nearest neighbours as these interactions cause significant noise in the data at longer length scales. More details regarding EXAFS are provided in Chapter 3.

7.2. Experimental procedure

The edge and centre regions of the as-cast 1 mm rod were selected for this study, as well as the annealed 4 mm rod (5 hours at $0.6T_g$), because of their large degree of inhomogeneity in mechanical response. Sections were cut from the same rods which were studied by nanoindentation in Chapter 6. Additionally, to provide a more extreme processing condition, a 15 micron thick ribbon of $Zr_{65}Cu_{15}Ni_{10}Al_{10}$ was produced by melt spinning. The ingot was loaded into a quartz crucible, with a 0.5 mm diameter orifice at the injection end, and the chamber was pumped down to 10^{-3} Pa and then backfilled with 2/3 atmosphere of helium. The sample was melted in an induction coil and a helium overpressure applied, injecting the melt onto a copper wheel rotating at 45 ms^{-1}. Sections were cut from the monolithic rods for EXAFS, and were mechanically thinned by a grinding and polishing route.

EXAFS studies were performed on the I18 microfocus beamline at Diamond Light Source, where an incident beam diameter of approximately 10 microns was used, providing similar resolution to the nanoindentation data collected in Chapter 6. The I18 beamline has an energy range of 2 – 20.7 KeV making it possible to scan the Zr, Cu and Ni k-edges (17.9976 KeV, 8.9789 KeV and 8.3328 KeV respectively) but not the Al k-edge (1.5596 KeV) since it is below the available energy range. This also justifies the use of the $Zr_{65}Cu_{15}Ni_{10}Al_{10}$ alloy for this study rather than $Pd_{77.5}Si_{16.5}Cu_6$ or $Ce_{70}Al_{10}Cu_{10}Ni_{10}$, since Pd, Si and Ce are not detectable. 4 scans were performed for each absorption edge at the same site, which were averaged together to improve signal quality. The Athena software developed by Prof. B. Ravel, which runs the IFEFFIT program [47], was used for data analysis (details of which are given in Chapter 3).

7.3. Results

Figure 7.1 presents k-space scans for Zr, Cu and Ni. It can be seen that signal noise dominates at k vales greater than 7 Å^{-1}. This was believed to be due to surface roughness of the mechanical thinning technique used and due to some beam wobble during experimentation. Focused ion beam (FIB) is another possible thinning technique for the preparation of EXAFS samples. However, FIB can impart severe deformation into the sample [5], potentially increasing defect concentration; this technique could therefore influence the results observed and so was not used.
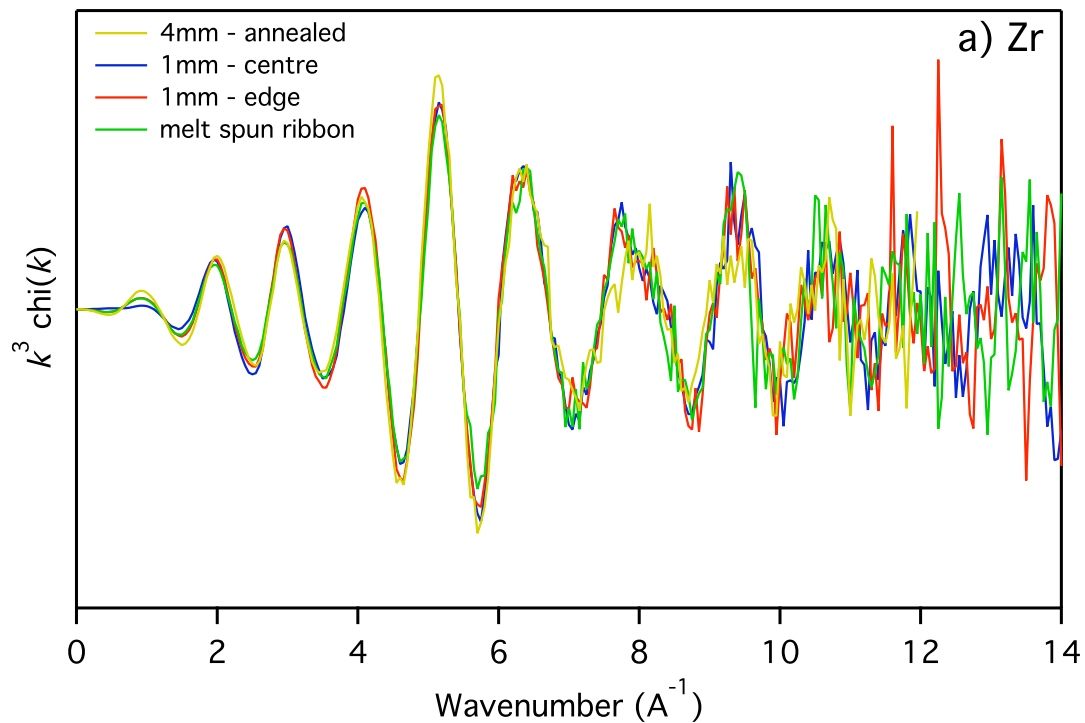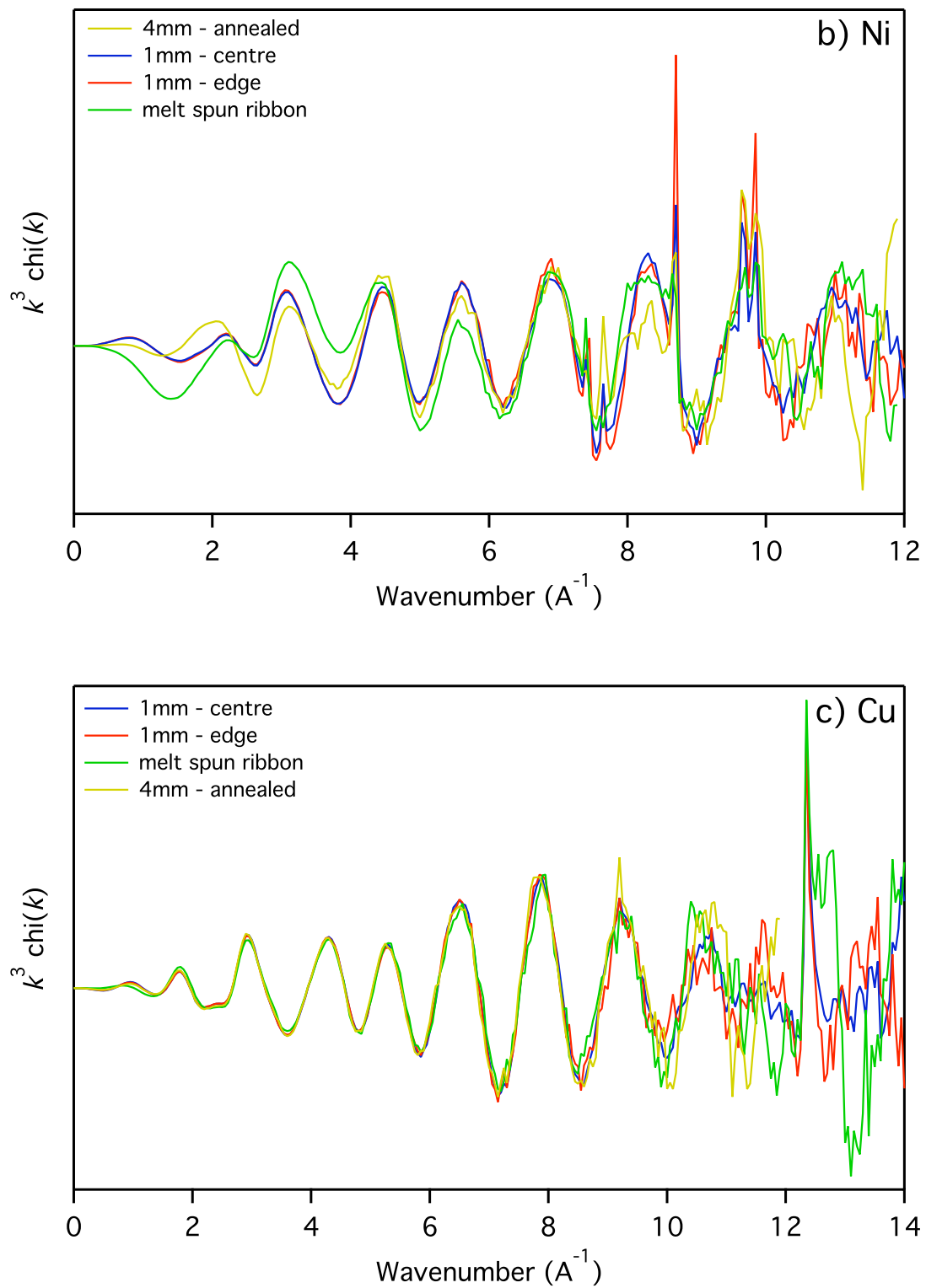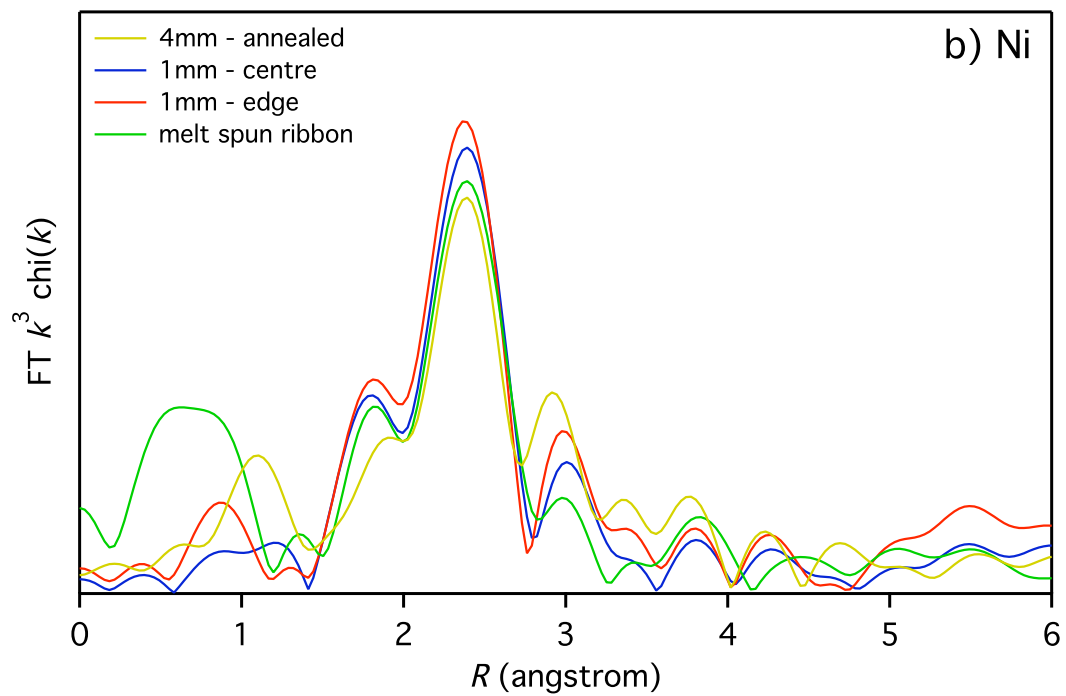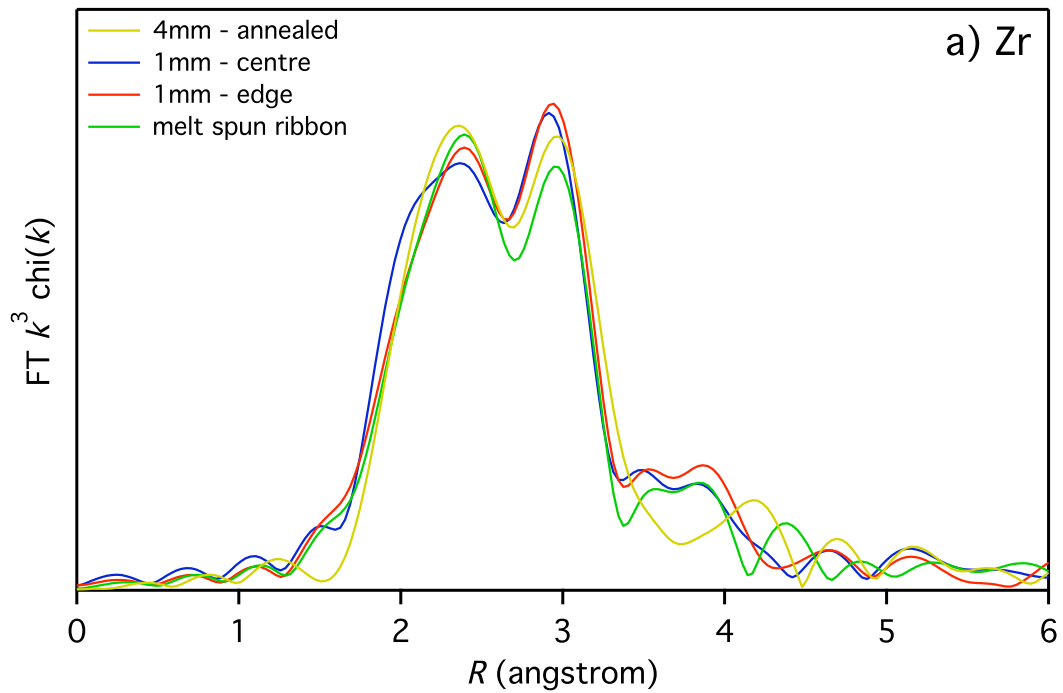
Figure 7.1. k-space scans determined by EXAFS for a) Zr, b) Ni and c) Cu in the $Zr_{65}Cu_{15}Ni_{10}Al_{10}$ BMG.

Radial distribution functions (RDFs) can be seen in Figure 7.2, obtained by forward Fourier transform of the data in Figure 7.1.
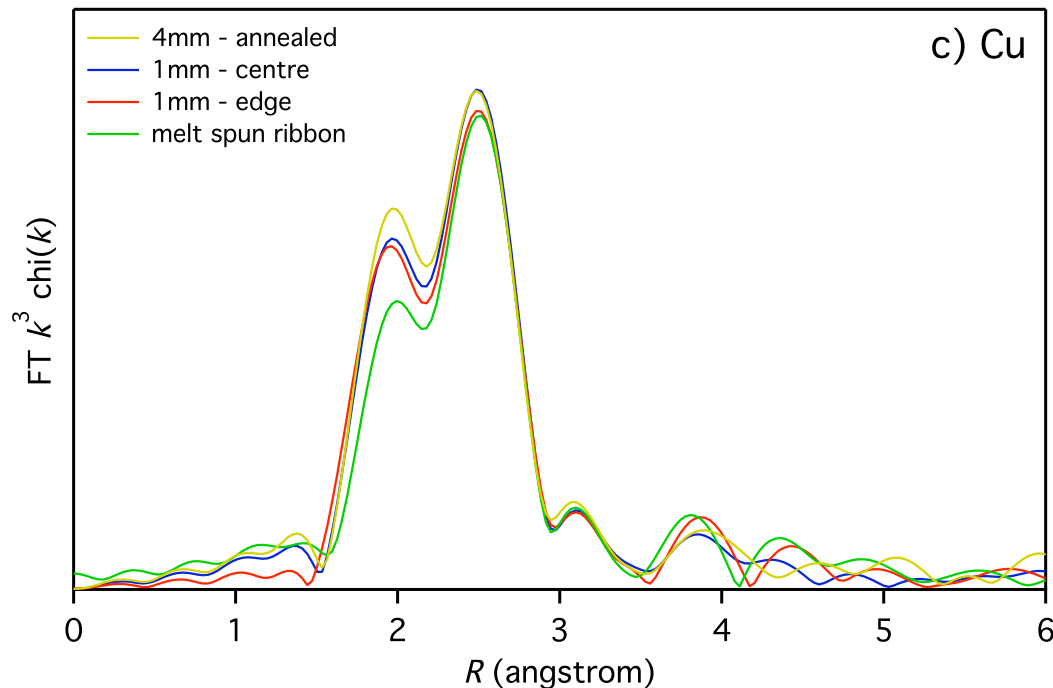
Figure 7.2. Radial distribution functions determined by EXAFS scans for a) Zr, b) Ni and c) Cu in the $Zr_{65}Cu_{15}Ni_{10}Al_{10}$ BMG. (FT represents Fourier Transform).

It is apparent in this data that no systematic changes in atomic pair separation distances can be observed as a function of thermal history, and in each case the observed shifts in peak do not exceed 0.1 angstrom. Because of the significant noise in the data, modification of the background subtraction is ongoing, though does not appear to yield any specific trends, in terms of a systematic change in atomic separation distances being a function of thermal history. Bearing this in mind, it could be inferred from the results shown in Figures 7.1 and 7.2 that short range ordering in $Zr_{65}Cu_{15}Ni_{10}Al_{10}$ may be insensitive to thermal processing, at least in respect to the samples studied here. This suggests that the variable mechanical response seen in Chapter 6 is not due to nearest neighbour length scales.

7.4. Discussion

It may at first seem surprising that little or no change in local atomic environment is observed, given the large variation in thermal history experienced by the specimens; melt spinning generates cooling rates of the order 10^6 K/s, while suction casting of a 4 mm rod using the University of Sheffield facility gives a centre-line cooling rate of the order 10^2 K/s, as determined from dendrite arm spacing in an Al-4.5 wt% Cu alloy [6]. There is a known sensitivity of metallic glass structure to thermal history [7], particularly with regard to

relaxation of atomic environments. This change in structure may be embodied as a reduction in free volume (as per the concept of Cohen *et al.* [8]) or changes in bond lengths (Egami *et al.* [9,10]), where some bonds lengthen and some shorten as atoms rearrange about their sites, adopting lower energy inherent states (IS) in the PEL. Applying either convention to describe relaxation mechanisms, it would be anticipated that structure changes occur, which would be apparent as shifts in peak positions or, as Dmowski *et al.* [11] have seen, peak sharpening caused by long and short bonds relaxing out. Neither of these can be seen in Figure 7.2 however, and two possibilities exist to explain this: 1) variation in thermal history between samples was insufficient to alter the atomic structure, or 2) structure variation is accommodated over longer length scales than were probed here. Regarding point 1, and as will be discussed shortly, non-uniform mechanical properties were reported in the samples studied and so diversity in atomic structure must exist. Changes in the structure outside of nearest-neighbours may be the preferred mechanism for accommodating atomic relaxation therefore, and so the sensitivity of the atomic structure of the BMG studied to its thermal history is not dependent on bond length within a cluster. The tight-bond cluster model [12,13] suggests that free volume is accommodated between clusters in BMGs, which are bonded by much weaker forces than those within a cluster (see Figure 2.7). How relaxation is accommodated in the atomic environments between clusters appears to be a critical parameter then, which could originate from changes in a number of factors, including: 1) how clusters are packed (such as in the Efficient Cluster Packing model [14]), 2) the presence of "glue" atoms between clusters [15], 3) the extent of bond connectivity between clusters [13], and 4) the presence of liquid-like regions [3], where disorder would be anticipated to be greater.

Based on Figure 7.1 and 7.2, and the non-uniform mechanical properties previously reported, it would appear that length scales beyond nearest-neighbours control mechanical behaviour in BMGs. Hufnagel *et al.* [16] found in a $Zr_{57}Ti_5Cu_{20}Ni_8Al_{10}$ alloy that during compressive loading below the yield point, greater elastic strain was accommodated between clusters than was within them. Interactions beyond nearest neighbours could more accurately determine the macroscopic elastic moduli also; calculations based on short-range interactions resulted in an over estimate. As the activation energy for yielding in amorphous materials is proportional to *G*, length scales beyond nearest-neighbours seem to determine the onset of yield. The tight-bond cluster model [13] goes on to suggest that cluster sliding and rotation are the mechanisms by which STZs are activated and Delogu [17,18] took a similar approach in molecular dynamics simulations, where yielding occurred by cluster rotation. If the environment between clusters in the more rapidly cooled samples are located in more unstable IS, then cluster movement may be less constrained by the surroundings, justifying the greater tendency for yielding shown previously.

The length scales that control plastic yielding and flow therefore appear to be larger than those of nearest-neighbours. It has been shown that dilatation occurs in shear bands in BMGs, evident from a marked decrease in hardness when nano indents were performed across a single shear band. In soil mechanics, for granular materials, it is known that in a dilatant shear band the number of particles that can be accommodated in the width of the band is equal to approximately 6-20 [19]. Such a rule was capable of explaining the observation of dilatation during the shearing of crystals in a semi-solid melt [20]. In BMGs shear bands are reported to be 10-20 nm thick and solute centered clusters are approximately 3 atomic diameters wide [21]. Assuming an atomic radius of 0.26 nm, this gives a shear band width of 12-26 clusters, assuming a width of 10 and 20 nm respectively. Such values suggest that it is cluster reorientation that is responsible for plastic yield and flow in BMGs, and so it may indeed be the inter-cluster bonding that controls mechanical behaviour, as per the tight-bond model [13]. Further experimental work is required to characterise BMG structure outside of solute centered clusters, as a function of both cooling rate and plastic strain.

The presence of isomechanical groups in BMGs shown in Chapter 5 signifies that significant differences in both structure and bonding exist, as a function of their Poisson's ratio. As the evidence presented here, from both the literature and in Figure 7.2, suggests that is it not intra-cluster interactions that determine mechanical behaviour, the structural component of BMGs that most influences intrinsic toughness, contributing to the presence of isomechanical groups, may be the inter-cluster environment. In amorphous silicon, Demkowicz and Argon [22,23] have demonstrated by simulation that plastic flow is permitted in a liquid-like region which surrounds more ordered solid-like environments, distinguished from each other by similarity in radial distribution functions to molten and solid silicon respectively. That a liquid-like structure (defined as the fraction of incomplete icosahedra) may promote plastic strain was suggested [3], and links between fragile glass formers, with respect to the kinetic glass fragility index (m), (and which can be linked to structure disorder in the solid state through the non-ergodicity factor, α) plastic strain and proximity to the Born mechanical instability criterion, considers a liquid-like structure to be critical for developing large plastic strains (as demonstrated in Chapter 4). This may therefore exist between clusters, where atoms are located in higher energy IS, favouring atomic rearrangement. A number of questions remain as to the structural units and length scales that determine mechanical behaviour in BMGs, with there being a clear need for more conclusive experimental evidence to support or challenge the current theoretical models.

7.5. Conclusion

The main findings of Chapter 5 can be summarised as follows:

- EXAFS was used to probe local atomic structure in samples of the $Zr_{65}Cu_{15}Ni_{10}Al_{10}$ BMG with various thermal histories, which showed large mechanical inhomogeneity, including tendency for mechanical yielding, in Chapter 6.

- It is found that limited or no systematic structure variation exists within the nearest-neighbours as the thermal history of each sample is changed, ranging from a melt spun ribbon to an annealed 4 mm diameter rod. Significant noise is present in the data however and so data processing is ongoing – however, this too does not suggest large or systematic change in nearest-neighbour length scales.

- Given the mechanical inhomogeneity shown in Chapter 6, and the sensitivity of glass structure to thermal history, it is unlikely that identical structures exist in all samples. Diversity may exist at larger length scales therefore, in the atomic environment surrounding clusters.

- Mechanical yielding of BMGs may therefore involve the rearrangement of clusters, either by shear or by rotation, which are constrained by the inter-cluster region. It would appear then length scales beyond nearest neighbour control plastic yielding in BMGs.

7.6. References

[1]   Y. Q. Cheng, H. W. Sheng and E. Ma, Phys. Rev. B **78**, 014207 (2008).

[2]   Y. Q. Cheng, E. Ma and H. W. Sheng, Phys. Rev. Lett. **102**, 245501 (2009).

[3]   Y. Q. Cheng, A. J. Cao and E. Ma, Acta Mater. **57**, 3253 (2009).

[4]   http://cars9.uchicago.edu/ifeffit (Accessed 1/10/2011).

[5]   J. P. McCaffrey, M. W. Phaneuf and L. D. Madsen, Ultramicroscopy **87**, 97-104 (2001).

[6]   P. A. Carroll PhD thesis, University of Sheffield, May 2003.

[7]   K. M. Flores, D. Suh, R. H. Dauskardt, P. Asoka-Kumar, P. A. Sterne and R. H. Howell, J. Mater. Res. **17**, 5 (2002).

[8]   M. H. Cohen and D. Turnbull, J. Chem. Phys. **31**, 1164-1169 (1959).

[9]   T. Egami, JOM **62**, 70-75 (2010).

[10]   T. Egami, Prog. Mat Sci. **56**, 637-653 (2011).

[11]   W. Dmowski, W. Fan, M. L. Morrison, P. K. Liaw and T. Egami, Mat. Sci. Eng. A **471**, 125-129 (2007).

[12]   C. Fan, P. K. Liaw, V. Haas, J. J. Wall, H. Choo, A. Inoue and C. T. Liu, Phys. Rev. B **74**, 014205 (2006).

[13]   C. Fan, P. K. Liaw and C. T. Liu, Intermet. **17**, 86-87 (2009).

[14]   D. B. Miracle, Nature Mater. **3**, 697-702 (2004).

[15]   C. Dong, Q. Wang, J. B. Qiang, Y. M. Wang, N. Jiang, G. Han, Y. H. Li, J. Wu and J. H. Xia, J. Phys. D: Appl. Phys. **40**, 273-291 (2007).

[16]   T. C. Hufnagel and R. T. Ott, Phys. Rev. B **73**, 064204 (2006).

[17]   F. Delogu, Chem. Phys. **386**, 101-104 (2011).

[18]   F. Delogu, Acta Mater. **59**, 5961-5969 (2011).

[19]   K. H. Roscoe, Geotechnique **20**, 129-170 (1970).

[20]   C. M. Gourlay and A. K. Dahle, Nature Lett. **445**, 70-73 (2007).

[21]   Y. Zhang and A. L. Greer, Appl. Phys. Lett. **89**, 071907 (2006).

[22]   M. J. Demkowicz and A. S. Argon, Phys. Rev. Lett. **93**, 025505 (2004).

[23]   M. J. Demkowicz and A. S. Argon, Phys. Rev. B **72**, 245206 (2005).

8. Summary and conclusions

The headings in this section bring together and summarise the individual conclusions of Chapters 4 – 7, rather than re-stating the individual findings of each chapter.

8.1. Correlation between elastic moduli and tendency for permanent deformation

The observation of Lewandowski *et al.*, that high fracture energy correlates with a low ratio of shear to bulk modulus (G/B), is examined via a Blackman diagram for a representative group of bulk metallic glasses (BMGs), which plots C_{12}/C_{11} versus C_{44}/C_{11}. As a result of the assumption of isotropy in BMGs, all alloys on this plot are located on a straight line. From this plot it is found that deformable alloys, indicated by large plasticity in compression, are located at largest C_{12}/C_{11} and lowest C_{44}/C_{11}. Moving down the data set towards low C_{12}/C_{11} and high C_{44}/C_{11}, there is a strong tendency for a reduction in compressibility in BMGs, with brittle alloys found at the lowest points. The trend can be extended to oxide glass formers, which represent the lowest bound points on the data line. A Blackman diagram thus appears to be an effective tool for considering deformability in both metallic and oxide glasses.

Frost and Ashby define an isomechanical group as a group of materials with similar deformation and diffusion behaviour. An analysis is performed to determine whether isomechanical groups exist in three classes of BMGs, grouped according to their Poisson's ratio, v, which is known to be an indicator for intrinsic toughness. This is done by plotting Young's modulus (E), shear modulus (G) and bulk modulus (B) against the ratio $k_b T_g/\Omega$ (where k_b, T_g and Ω are the Boltzmann constant, glass transition temperature and atomic volume respectively) for each alloy and then fitting a straight line through the data for each group. An analysis of covariance (ANCOVA) reveals that strong isomechanical groups exist when considering E and G, but less defined ones exist for B, as a result of the deformable Pt-based alloys lying outside the trend of the other alloys in their group. The gradient of each group, b, when considering G as the modulus of interest, is compared to a variety of other isomechanical groups for different materials, and it is found that b determined for the groups defined here fit in with the general trend that a low b indicates large permanent deformability.

Blackman diagrams and an analysis for the presence of isomechanical groups in BMGs have demonstrated the usefulness of elastic moduli as indicators of ability to plastically deform. As it has been shown that elastic moduli can be predicted with a reasonable degree of accuracy (resulting from their being single phase and essentially

isotropic), they have been found here, and elsewhere, to be an effective tool for consideration when both designing deformable BMGs and when analysing their mechanical response.

8.2. Physical origins of variable deformation response

Two limiting physical conditions are imposed on a Blackman diagram, being 1) proximity to the Born instability condition (defined as the point at which shear moduli tend to zero) and, 2) deviation from zero Cauchy pressure, represented by the relationship $C_{12}=C_{44}$. From the Blackman diagram presented in Chapter 4, the most plastic alloys were located closest to the Born instability criterion and exhibited largest positive deviations from zero Cauchy pressure, with the reverse true of brittle BMGs and oxide glasses. It is additionally found that fragile glass formers are closest to the Born criterion and so correlate with being the most plastic BMGs. Based on these findings it is apparent that non-directional bonding and liquid-like behaviour (when quantified by m) may be two characteristics of deformable glasses.

Between different isomechanical groups, fundamental differences in structure and bonding are known to exist; isomechanical groups defined in the past show obvious differences with respect to these features, making it clear why they exist e.g. they have different crystal structures. However, Figure 5.5 shows that the isomechanical groups found here show large differences in b, when compared to other groups, and so significant variation in structure and bonding must exist. Given that BMGs are all generally considered as having metallic bonding, with their structure being conceptually described by atomic and cluster packing ideas, the physical origins as to why isomechanical groups exist is not simple to derive. As shown in Chapter 4, bond directionality may be one factor contributing to this. With respect to structure, the link between fragile glass formers being more deformable (and therefore an increasing m scales with a decreasing b) and their potential energy landscapes (PELs) exhibiting a greater number of inherent states in comparison with strong glass formers, is exploited to try to elucidate structure differences. This behaviour in the liquid state can be linked to the solid state as m correlates with the non-ergodicity parameter, α, and so allows for greater structure diversity and heterogeneity. Moreover, a greater fraction of liquid-like sites suggests that atomic scale disorder may be favourable, as the inherent states occupied in PELs may be of higher energy, promoting a relaxation (yield) event. Glass structure has yet to be considered as a function of m and so understanding the structural variation directly, and beyond qualitative ideas such as PELs, remains a challenge.

Fragile glasses show a lower melt viscosity than strong glass formers, permitting more rapid atomic diffusion during cooling from the melt. Because of this it is generally observed that fragile glasses are not the best glass formers, with limited critical diameters.

Pd-based alloys are an exception to this, since they display some of the lowest critical cooling rates for glass formation, though critical diameters are limited if the melt is not fluxed prior to casting, so to remove impurities that can act as heterogeneous nucleation sites. Despite this, because fragile glasses are the most deformable, a significant challenge exists in generating large sections of malleable monolithic BMGs and it may be difficult to generate cost effective solutions also, as Pd- and Pt-based alloys remain expensive.

8.3. Experimental evidence for tendency for differences in atomic structure

The previous observation of differential cooling rates during suction casting of a BMG, leading to variation in hardness and modulus along a rod cross section is investigated here as a function of rod diameter and *m*. It is found that the observation of a soft surface is favoured in small diameter castings and that global hardness increases with sample size. These observations could be linked to faster cooling limiting in-situ atomic relaxation, potentially leading to a greater tendency for shear band nucleation as a result of reduced *G*. It was also found that a low modulus and low hardness surface was most prevalent in fragile glass formers and this was considered to result from the potential for a greater range of structural configurations in fragile glasses, as more inherent states exist in the PEL. High *m* glasses can therefore more readily respond to variations in cooling rate, with respect to freezing in different structural configurations. This appears to support the notion that enhanced structure diversity may exist in the lowest *b* isomechanical group.

To understand how the mechanical inhomogeneity in the Zr-based alloy reported in Chapter 6 was structurally accommodated extended x-ray absorption fine edge structure (EXAFS) was utilised at Diamond Light Source. Although samples studied ranged from an annealed 4 mm diameter rod to a melt spun ribbon, no significant changes in nearest neighbour environments were observed despite the large variation in thermal history. Given the sensitivity of mechanical behaviour to cooling rate demonstrated in Chapter 6, this result suggests that yielding in BMGs is controlled over longer length scales than nearest neighbours, potentially by cluster reorientation. This finding appears to be supported by other high energy x-ray experiments, and by the tight-bond cluster model. The structure diversity suggested in Chapter 4 (resulting from the distinct isomechanical groups) may be accommodated therefore between short range ordered clusters rather than within them, and so length scales beyond nearest neighbour appear to control mechanical yielding. This results appears to be in accordance with previous studies though actual experimental evidence is limited.

9. Further work

The following bodies of work are proposed as being suitable for furthering some of the conclusions drawn in this project:

- Create a reliable and consistent data set for approximately 20 bulk metallic glasses (BMGs) for thermal transition temperatures, density, elastic moduli, mechanical properties in compression and fracture toughness. By this being performed by the same researcher and using identical experimental procedure and equipment, it will enable the more reliable analysis of generalities in BMG behaviour, such as was done in Chapters 4 and 5. Trends shown in the Blackman diagrams and the presence of the isomechanical groups could be reanalysed.

- Take a BMG belonging to the intermediate isomechanical group (and, concurrently, an intermediate plastic deformer on the Blackman diagram) and selectively alloy it so to promote and reduce intrinsic toughness based on predicted elastic properties e.g. G/B, C_{12}/C_{11} and C_{44}/C_{11}. By pushing the alloy up or down the data line on a Blackman diagram a concurrent variation in plasticity should be observed.

- Repeat the nanoindentation traverse study for other BMG compositions with varying fragility index values, m.

- Consider whether the soft surface of some as-cast BMGs causes anisotropy in their elastic tensor, and if this transfers over to orientation dependence during macroscopic compression testing.

- Perform EXAFS on a sectioned fracture plane of a BMG that has undergone large compressive plasticity, so to see if the known dilatation is accommodated on the nearest-neighbour length scale.

- For the previous point, and the alloy studied in Chapter 7, use high energy neutron diffraction to determine whether variation exists on length scales longer than nearest neighbour.

10. Publications and conference presentations

10.1. Publications

J.D. Plummer, I.A. Figueroa, R.J. Hand, H.A. Davies & I. Todd, *Elastic properties of some bulk metallic glasses*, Journal of Non-Crystalline Solids 355, 2009.

J.D. Plummer, I.A Figueroa, R. Goodall & I. Todd, *A study of mechanical homogeneity in as-cast bulk metallic glass by nanoindentation*, Journal of Non-Crystalline Solids 357, 2011.

J.D. Plummer & I. Todd, *Implications of elastic constants, fragility, and bonding on permanent deformation in metallic glass*, Applied Physics Letters 98, 2011.

A. Cunliffe, J.D. Plummer, I.A. Figueroa & I. Todd, *Glass formation in a high entropy alloy system by design*, Intermetallics 23, 2012.

J.D. Plummer & I. Todd, *Isomechanical groups in bulk metallic glasses*, Philosophical Magazine, in-press, 2012.

J.D. Plummer, I.A. Figueroa & I. Todd, *Phase stability, microstructure and mechanical properties of Li containing Mg-based bulk metallic glass composites*, Materials Science and Engineering A, in-press, 2012.

10.2. Conference presentations

(Presenting author, *Oral presentation (poster presentation otherwise))

*J.D Plummer, I.A. Figueroa, R.J. Hand, H.A. Davies & I. Todd, *Influence of elastic moduli on glass forming ability and plasticity of bulk metallic glasses*, Society of Glass Technology Annual Meeting, Cambridge 2008.

J.D. Plummer, I.A. Figueroa, R.J. Hand, H.A. Davies & I. Todd, *Elastic moduli – mechanical property relationships in bulk metallic glasses*, TMS, San Francisco 2009.

*J.D. Plummer, I.A. Figueroa, H.A. Davies & I. Todd, *Amorphous alloys at the University of Sheffield*, IMMPETUS Colloquium, Sheffield 2010.

J.D. Plummer, I.A Figueroa, R. Goodall & I. Todd, *Characterisation of free volume in bulk metallic glass*, CAMTEC II – Symposium on Fine-Scale Mechanical Characterisation and Behaviour, Cambridge 2010.

*J.D. Plummer, I.A Figueroa, R. Goodall & I. Todd, *Mechanical inhomogeneity in as-cast bulk metallic glass*, TMS, San Diego 2011.

*S.S. Chen, J.D. Plummer & I. Todd, *Enhanced plasticity of a Zr-Cu-Ni-Al bulk metallic glass by micro Nb additions*, TMS, San Diego 2011.

*J.D. Plummer, I.A. Figueroa & I. Todd, *Effect of Li on microstructure and mechanical properties of an Mg-based bulk metallic glass*, TMS, San Diego 2011.

*J.D. Plummer, A.J. Cunliffe, I.A. Figueroa & I. Todd, *Glass formation in a high entropy alloy*, Bulk Metallic Glass VIII, Hong Kong 2011.

J.D. Plummer, P. Quinn, I.A Figueroa, R. Goodall & I. Todd, *A mechanical and structural study of the composite nature of as-cast monolithic bulk metallic glasses*, 18th International Symposium on Metastable, Amorphous and Nanostructured Materials, Gijon 2011.

*J.D. Plummer & I. Todd, *Analysis and grouping of the deformation response of bulk metallic glasses using elastic constants*, 18th International Symposium on Metastable, Amorphous and Nanostructured Materials, Gijon 2011.